Technetium retention and migration in clay systems in presence of iron

Inaugural dissertation
of the Faculty of Science,
University of Bern

presented by

Ping, Chen

from Jiangxi, China

Supervisor of the doctoral thesis:
Prof. Dr. Sergey V. Churakov, University of Bern
Dr. Luc Robert Van Loon, Paul Scherrer Institut

Technetium retention and migration in clay systems in presence of iron

Inaugural dissertation
of the Faculty of Science,
University of Bern

presented by

Ping, Chen

from Jiangxi, China

Supervisor of the doctoral thesis:
Prof. Dr. Sergey V. Churakov, University of Bern
Dr. Luc Robert Van Loon, Paul Scherrer Institut

Accepted by the Faculty of Science.

Bern, 2nd Oct, 2023

The Dean
Prof. Dr. Marco Herwegh

Acknowledgement

It is a supper long journey for me to completing my dissertation. Throughout the journey, I have overcome numerous challenges and learned a lot by heart. Here, I would like to sincerely express my thanks to all the people who have hoped me.

Firstly, I would like to give my gratitude to Luc Van Loon and Sergey Churakov, who initiated and supervised my PhD project, and guided me writing paper with great patience. Thank you both for all the effort you did to me. Moreover many thanks have to give to Maria Marques, who guide me the Fe sorption experiment and teach me modeling skill with her aboundant experience and profound knowledge. A great special thank has to give to Peter alt-Epping, who teach me transport modeling skill over and over again with great patience. The same sincere thanks have to give to Martin Glaus and Wilfried Pfingsten, who also give me a lot help. Prof Dr Thorsten Schäfer is thanked for playing the role of external referee and his pertinent remarks.

Many thanks also to Petar Bunic and Sabrina Frick, who attentively and patiently shared all their experience and skill for diffusion experiments. Dr Mirjam Wolffers is thank for helping the XRD measurement. I would also like to thank Koch Steffen and Reich Tobias from University of Mainz, whose corporation in Tc transport modeling in opalinus clay do me a great favor.

Special thanks to my colleagues, Bin Ma, Guoqing Geng, Yanting Qian, Yanhua Chen, fulvio DI Lorenzo, Rene and Georgia Cametti for their all kinds of help and companion. I would like to extent my gratitude to my friends and family for everything they did for me, especially Song Xue and Cong Wang. Without their companion I could not successfully finished my PhD with heath mindset.

Great thank is given to the China Scholarship Council (CSC) for their financial support.

TABLE OF CONTENTS

Summary

Technetium is a redox sensitive radionuclide. Due to its high fission yield in nuclear reactors, its long half-life and radiotoxicity, and its high mobility, retention and migration of ^{99}Tc in environment is of great importance for the safety assessment of radioactive waste disposal. Significant mobility difference has been measured for technetium in different oxidation states. Clay rich formations are considered as favorable host rocks in the repository concept for the deep geological disposal of High Level radioactive Waste (HLW). Montmorillonite, illite, kaolinite and chlorite are the major components of clay rocks. Therefore, a mechanistic understanding of Tc interaction with clay minerals is important for increasing the confidence in the safety assessment of nuclear waste disposal. The repository concept is based on the multi-barrier system, in which HLW and/or spent fuel are solidified, contained in iron casks and finally emplaced in tunnels in a deep underground geological formation. The omnipresence of iron and its strong redox activity make iron being an important redox agent in the environment. In addition to the iron present in host rocks, the corrosion of engineered barriers, e.g. steel disposal casks, is another considerable source of iron in the repository nearfield. Therefore, the presence of iron in clay minerals may affect Tc migration in clay minerals. In this study, a through-diffusion technique, developed by Luc Van Loon (Van Loon et al., 2003), was used to investigate Tc migration in compacted illite, in which the diffusion set-up was a compacted illite sandwiched between two stainless steel filters. The impact of two types of Fe(II) on Tc migration was studied, Fe(II) sorbed on the surface of illite and Fe(II) added as pyrite. In order to make a comprehensive interpretation of Tc diffusion in compacted illite in the presence of Fe(II), the Fe(II) sorption behavior on illite was investigated in detail. The diffusion of TcO_4^- in natural illite was also studied, together with its behaviour in the filters used in the sandwich set-up. The latter is necessary to properly model the diffusion data. With this knowledge, a reactive transport modeling of Tc diffusion in Opalinus Clay was performed. In a first step, a simple model was used in which only diffusion and redox reactions with solid surface complexed Fe(II) were considered. This model was further improved by including the reactivity of Fe-bearing phases.

Aqueous Fe, Fe-minerals, surface complexed Fe and structural Fe show a different activity toward redox sensitive nuclides, especially Tc. Thus, a quantitative description of Fe(II) sorption on clay minerals such as illite, is important to understand its subsequent influence on reactions with redox sensitive radionuclides. In this study, the sorption of Fe(II) on illite was investigated in batch experiments, including sorption as a function of pH (sorption edge) and sorption as a function of concentration (sorption isotherms) under anoxic condition. A 2 SPNE SC/CE (2 sites protolysis non-electrostatic surface complexation/cation exchange) sorption model extended to account for surface oxidation of sorbed Fe(II) was used to model the sorption data with the geochemical modeling code PHREEQC. Three models (A, B, C) with an increasing level of complexity were tested. The model A, in which only Fe(II) interacts with illite, does not satisfactorily fit the experimental data. This model was modified by including oxidation of surface complexes (Model B) and precipitation of iron bearing phases (Model C). The modified models showed that most of the sorbed Fe(II) was oxidized at pH below 6.5. At pH above 6.5, the oxidized surface complexes either react with water, forming surface iron hydroxides or precipitating as hematite, although the presence of these mineral phases could not be confirmed by X-ray diffraction measurements. These sorption processes might be coupled with the behavior of redox sensitive radionuclides in future reactive transport research.

In order to study the role of iron on technetium migration, a through-diffusion technique was employed to

investigate the diffusion of Tc in compacted illite in presence of Fe(II) under oxic and anoxic conditions. The sorption studies described above were used to help pre-loading the illite with Fe(II) by sorption. The other Fe was introduced to the system by mixing illite with pyrite grains. Because the stainless filters are necessary to confine clay in diffusion experiments, the diffusion parameters of Tc in stainless filter were measured for the first time. The COMSOL Multiphysics software was used to simulate the diffusion process. Under oxidizing conditions, Tc is transported in its anionic form, i.e. as TcO_4^-, and a similar effective diffusion coefficient was obtained for Tc diffusion in the filters and in illite. Fe(II) has a significant effect on the Tc diffusion behavior. The effective diffusion coefficient of Tc in Fe-loaded illite was approximately one order of magnitude smaller than in "Fe-free" illite. Analysis of the Tc distribution along the diffusion path suggested that most Tc was retarded in the filters, and only a small part reaches the clay phase. A delocalized redox reaction was proposed to explain this observation, in which means that electrons from the oxidation of the preloaded Fe(II) in the central part of the cell are transferred to the filter via the walls of the steel diffusion cell. Tc reacts with the electrons in the filter at a relative slow rate, which results in most of the Tc retarded in the filter, while some small amounts of it may diffuse through the clay.

A reactive transport modeling of Tc diffusion in Opalinus Clay (OPA) was performed in cooperation with the University of Mainz. Diffusion of ^{99}Tc in OPA was studied under an inert argon and under air atmosphere. In a first step, a model was proposed that couple pyrite dissolution, diffusion, and redox reactions in PFLOTRAN. The model results showed that the final immobilized Tc is affected by the dissolution rate of pyrite, the equilibrium constant of redox reactions of Tc with surface complexed Fe, and the diffusion coefficient of TcO_4^-, which means that all these processes play an important role on the migration and immobilization of Tc. Under argon atmosphere, TcO_4^- diffuses into the OPA clay column and is partially reduced into surface complexed Tc (IV) by pyrite or dissolved pyrite. Under air atmosphere, the presence of O_2 competitively consume Fe^{2+} and pyrite, result in no Tc retarded in the beginning zone, where O_2 is available.

This study provide us with a better understanding of Tc transport in clay rich rocks. Repository evolution scenarios assume that iron casks may corrode and fail after exposure to ground water after a long time. The corroded iron diffuses in the ground water and sorbs on surface sites of clay minerals such as illite and montmorillonite. It is expected that Fe will occupy so called strong and weak sorption sites on the edges of clay minerals, and on planar sites by cation exchange. Some of the adsorbed iron at edge sites may be oxidized by structural iron and influences its redox activity towards redox sensitive nuclides, for instance Tc in our study, which will migrate in pore water after iron casks failure. Opalinus Clay is the selected host rock for a repository for radioactive waste in Switzerland. It is a reducing sediment that contains substantial amounts of Fe(II), mainly present as siderite and pyrite. Based on the observed migration behavior of Tc in Fe-loaded illite and in Opalinus Clay, it is expected that ^{99}Tc released from the waste as TcO_4^- will migrate in the OPA but will be quickly reduced by the Fe(II) present in OPA and therefore Tc will be immobilized.

1 Introduction

1.1 Concept of repository

Since the discovery of nuclear reactions in 20th century, nuclear energy has many application in the civilian and military sectors, such as nuclear weapons in military (Knorr, 2015), nuclear power in energy (Yun et al., 2021), non-destructive test in industry (IAEA, 2020), nuclear thermal propulsion in aerospace (Gabrielli and Herdrich, 2015), medicine (Ziessman et al., 2013) and some other fields. The big challenge in the peaceful use and sustainable development of nuclear energy is the issue of huge amounts of radioactive waste, especially the high level radioactive waste (HLW) and spent fuel (SF) from nuclear power plants (IAEA, 2022). Many exotic concepts have been proposed, such as disposal in space (Burns et al., 1978; Coopersmith, 1999) or in the deep sea (Calmet, 1989), in ice sheets (Philberth, 1977), melting within a rock (Heuze, 1981; Logan, 1974) or conversion (transmutation) into stable nuclides (NRC, 1996). But disposal in a deep geological repository is the only internationally widely accepted and practicable option for the safe disposal of HLW and SF. For instance, the construction of a repository is in progress in Olkiluoto in Finland. In 2022, the excavation of the first five final disposal tunnels has been completed (POSIVA, 2022). The license application for building a repository in Forsmark has been submitted in Sweden (Litmanen et al., 2017). In many other countries, field and laboratory investigations are ongoing for characterizing potential host rocks (Meuse/Haute-Marne underground research laboratory in France (Plúa et al., 2021; Zhang et al., 2010), Nizhnekansky Rock Massif in Russia (Neuvazhaev et al., 2020; Rodionova et al., 2019; Rozov et al., 2019), and many other sites in China (Wang et al., 2018), Switzerland (ANSI, 2018a, b), and other countries (Faybishenko and Swift, 2016).

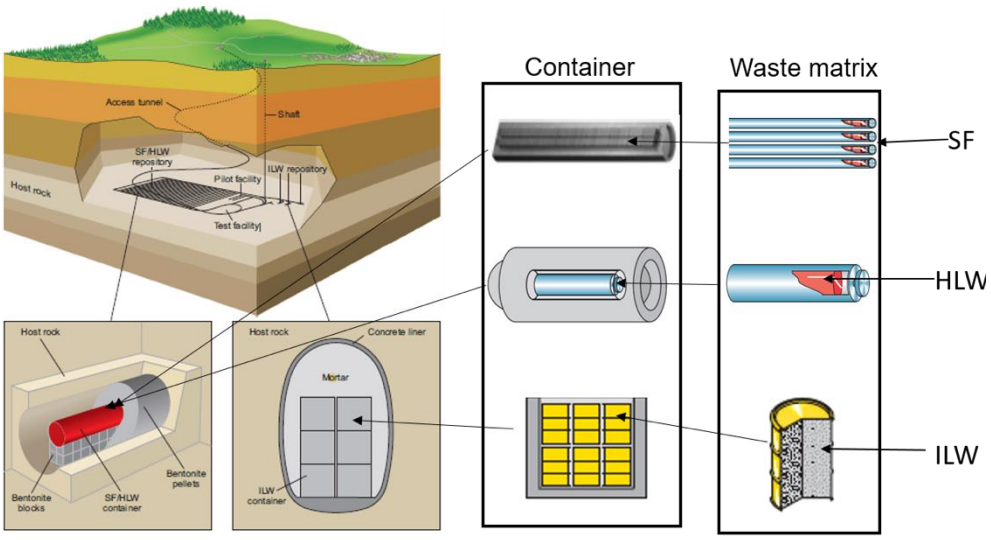

Figure 1: Conceptual a repository of Switzerland. (Picture taken from Nagra) (Nagra, 2008).

The sophisticated concepts of waste disposal rely on a multi-barrier system, which consists of natural and engineering barriers. The multi-barrier conceptual design of a repository in Switzerland (Nagra, 2008) is shown

in Fig 1. The HLW is solidified by glass, or the SF itself forming the waste matrix, which is usually the first barrier. Then the waste matrix is encapsulated in iron casks. These casks are the second barrier. They are further emplaced in tunnels, which are excavated in geological formations at a depth of several hundreds of meters. Bentonite is used as backfill materials to fulfil the gap between the canisters and the host rock in the tunnels. These backfill materials form the third barrier. All the earlier mentioned barriers are the so called ‘‘engineered barriers’’. The host rock (i.e. granite, salt or claystone) is the last barrier, usually called the ‘‘natural barrier’’. Steel casks are designed to isolate and contain the radionuclides for at least 10’000 years. After this period, the canisters are assumed to fail due to corrosion by ground water. From this moment on, long-lived radioactive nuclides will be released from the waste matrix and will migrate in the backfill materials and host rocks, and finally will reach the biosphere. Major radiological impact of HLW after thousands of years comes from minor actinides (MAs; isotopes of Np, Am, and Cm) and some long-lived fission products (LLFPs; ^{79}Se, ^{93}Zr, ^{99}Tc, ^{107}Pd, ^{129}I, and ^{135}Cs) (Organisation for Economic Co-Operation and Development). Therefore, comprehensive investigations of migration/retention of these nuclides in the backfill materials and host rock, are an important issue in the safety assessment of a repository. Technetium-99 (^{99}Tc) is one of the important safety relevant nuclides, due to its significant inventory in HLW and SF, its long half-life (2.13 x 10^5 years), its high mobility in oxidizing conditions, and its radiotoxicity. Its chemistry will be discussed in detail in section 1.2.

Clay formations (rocks) are one of the favorable host rocks, because of its low hydraulic conductivity, its high retention potential for radionuclides and its omnipresence in the form of large geological formations. Examples of such clay layers are Opalinus Clay (Nagra, 2002), the Callovian-Oxfordian Argillite (Dupuis and Gonnot, 2013). and the Boom Clay (Gens et al., 2003), selected in Switzerland, France and Belgium, respectively. A great effort was devoted to research on clays and clay minerals, especially on its properties toward confining radionuclides (such as nuclides Np, Am, and Cm^{79}Se, ^{93}Zr, ^{99}Tc, ^{107}Pd, ^{129}I, and ^{135}Cs) (Fan et al., 2009; Fan et al., 2014a; Fan et al., 2014b; Li et al., 2017; Pan et al., 2017; Powell et al., 2006; Schmeide and Bernhard, 2010; Wu et al., 2018; Xu et al., 2014; Zhao et al., 2017a; Zhao et al., 2017b) in clays. Clay rocks are a mixture of clay minerals such as illite, smectite, kaolinite and some other secondary phases like calcite and quartz. Table 1 shows the average mineralogical composition of Opalinus Clay from the Mont Terri Underground Research Laboratory in Switzerland (Nagra, 2002). The properties of clay minerals may have a significant influence on performance of repository in confining radionuclides.

Table 1: Mineralogical composition of the Opalinus clay (Nagra 2002).

Mineral phase	Amount in wt. %
calcite	13 ± 8
dolomite/ankerite	n.a.
quartz	14 ± 4
albite	1 ± 1
potassium feldspar (K-spar)	1 ± 1.6
siderite	3 ± 1.8
pyrite	1.1 ± 0.5
organic carbon	0.8 ± 0.5
illite	23 ± 2

illite/smectite mixed layers	11 ± 2
chlorite	10 ± 2
kaolinite	22 ± 2

uncertainty in "amount" is standard deviation (1 sigma).
n.a.: not analysed

Smectite, chlorite, montmorillonite and illite (Bergaya and Lagaly, 2013) consist of tetrahedral and octahedral sheets as shown in Fig. 2. This structural arrangement is referred to as 2:1 phyllosilicates. Substitution of Al^{3+} for Si^{4+} in tetrahedral sites or substitution of Al^{3+} by divalent Mg^{2+} or Fe^{2+} in octahedral sites result in a permanent surface charge of clay particles. This permanent structural charge is compensated by cations in the interlayer space between 2:1 layers. In illite, K^+ is the main charge compensating cation in the interlayer, leading to a collapse of the interlayers, which largely influences the retention properties of illite towards radionuclides (Benedicto et al., 2014).

Iron is a ubiquitous reducing agent in nature and Fe(II) was shown to be an active reductant in the environment for redox sensitive nuclides (Huang et al., 2021). Its impact on the long-term fate of ^{99}Tc will be studied in this work.

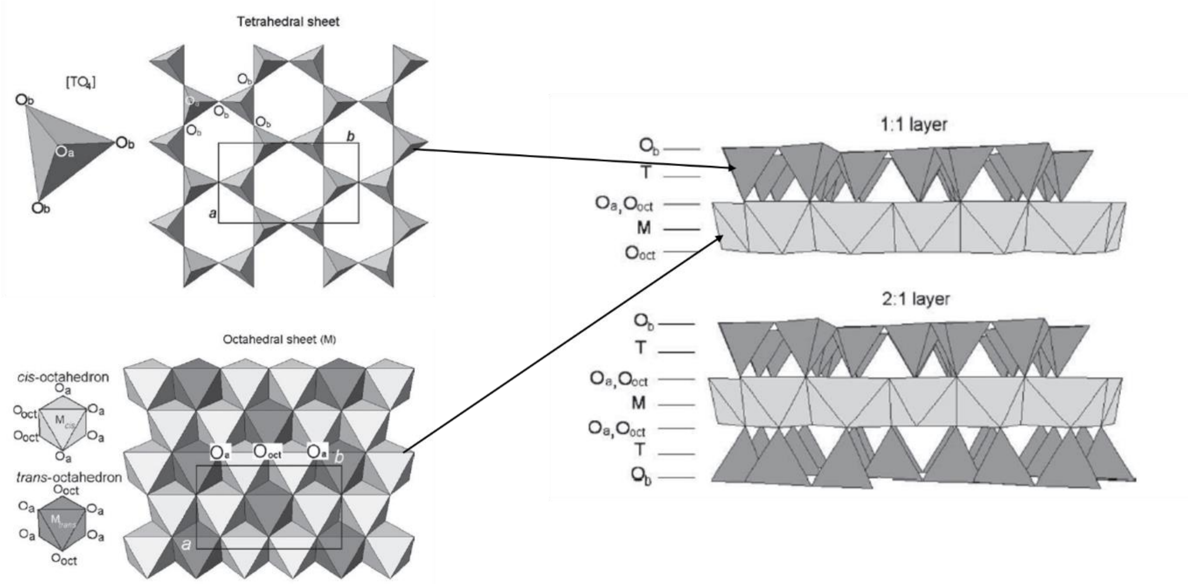

Figure 2: Model of the layered structure of clay minerals. O_a, O_b, and O_{oct} refer to tetrahedral basal, tetrahedral apical, and octahedral anionic positions, respectively. M and T indicate the octahedral and tetrahedral cations, respectively (Bergaya and Lagaly, 2013).

1.2 Tc chemistry and the role of Fe in the environment

^{99}Tc is one of the dose-determining radionuclides in the disposal of HLW, especially because of its long half-life and its potential high mobility. Tc is a chemical element with 45 isotopes, which are produced by nuclear reactions. Among these, the long-lived isotopes are ^{97}Tc (2.6×10^6 a), ^{98}Tc (4.2×10^6 a) and ^{99}Tc (2.13×10^5 a). ^{99}Tc is the dominant isotope present in the nuclear fuel cycle because of its high fission product yield (6.03%) and long half-life (Desmet and Myttenaere, 1986). It decays via β-emission to stable Ruthenium-99, emitting β-particles with an energy of 0.293 MeV (Tro, 2008). It is glossy silver- colored when present in its metal form, but is more

often produced in its most reactive forms as a sponge or powder (Greenwood and Earnshaw, 2012; Stwertka, 2002). Unlike its neighbors, Nb and Mo, Tc has a $[Kr]4d^5 5s^2$ electron configuration because one electron is promoted from the *d* to the *s* subshell (Siekierski and Burgess, 2002). Due to these higher shells, Tc has a higher stability in the higher oxidation states when compared to other transition metals. Its oxidation states range from -1 to +7, with the most common valences being Tc(VII) and Tc(IV) (Colton and Peacock, 1962). Tc is a redox sensitive element and its solubility and mobility in the subsurface strongly depend on its oxidation state (Icenhower et al., 2010). Its most stable oxidation state is Tc(VII), with pertechnetate TcO_4^- the prevailing chemical species. TcO_4^- hardly reacts with negatively charged mineral surfaces and is therefore highly mobile under oxidizing conditions. Poorly soluble Tc(IV) is formed if reducing species are present in the environment, such as iron (oxyhydr)oxides, iron sulfides, iron-bearing minerals, sulfide minerals and organic matter or microorganism (Huang et al., 2021).

Fe(II) is one of most important reductants in the environment. It is present in Fe(II)-bearing minerals such as magnetite, siderite and pyrite, in oxides within granite and in Fe(III) oxides, for instance ferrihydrite, goethite, hematite. All these minerals have the potential to reduce Tc(VII), but the availability and the steric distribution of the electron donors make a big difference. The speciation of iron was demonstrated to play a significant role in reactions with redox sensitive nuclides. For instance, the following affinity series for heterogeneous Tc(VII) reduction by different Fe(II) species was observed: aqueous Fe(II) ≈ adsorbed Fe(II) in phyllosilicates < structural Fe(II) in phyllosilicates < Fe(II) adsorbed on Fe(III) oxides (Peretyazhko et al., 2008). Thus Tc(VII) is sluggishly reduced by aqueous Fe(II), although the reducing activity of aqueous Fe(II) is high and the Fe(II)-to-Tc electron transfer is thermodynamically feasible (Cui and Eriksen, 1996). A relatively fast reduction of TcO_4^- to the hydrated Tc dioxide was observed when Fe(II) is incorporated into Fe(III) minerals (hematite and goethite) (Peretyazhko et al., 2008; Skomurski et al., 2010). Fe(II)-bearing minerals are known to reduce Tc(VII) to hydrous TcO_2-like phases (McBeth et al., 2011). In the study of Brookshaw et al. (2015), TcO_4^-, UO_2^{2+} and NpO_2^+ could be removed from solution by microbially reduced biotite and chlorite, and the reactivity was associated with redox cycling of the small fraction of Fe in these minerals (Brookshaw et al., 2015). Tc(IV) was found to be incorporated into a hematite structure because of the similar ion radii of Tc(IV) and Fe(III) in a sixfold coordination (Skomurski et al., 2010), which makes Tc(IV) more stable when subject to reoxidation. Pyrite is a minor component in clayrocks such as Opalinus Clay (Nagra, 2002), and has been recognized as a good sorbent for Tc(IV) (Bruggeman et al., 2007). The exact reaction mechanisms, however, are not well-understood so far. Therefore, in order to get a better understanding of the Tc-behavior in clay rocks, it is necessary to investigate the role of Fe in redox reactions and its role in the migration of Tc. Such studies would result in a better quantitative description of Tc behavior and would provide important input for the safety assessment of a deep geological repository.

1.3 Object of project

Once the steel casks encapsulating the waste fail due to corrosion, the radioactive waste will be in contact with pore water and radionuclides can be into aqueous solution and can migrate through the engineered barriers and the host rocks and eventually reach the biosphere. Thus, the objective of this project is to simulate a scenario in which Tc is released from the waste package and migrates through the clay rock. The thesis is organized in three parts:

1) Fe(II) sorption mechanism on illite. Fe(II) is the corrosion product of steel casks used to contain nuclear waste. Fe is also ubiquitously present in the environment either as dissolved aqueous complexes, or present in Fe-minerals, or adsorbed on clay surfaces (as surface complexes) or present as structurally incorporated Fe. The different Fe-species show different reactivities toward redox sensitive nuclides, especially towards Tc which is investigated in this work. The sorption of Fe(II) on illite was investigated in batch sorption experiments, including pH-dependent sorption (sorption edge) and concentration dependent sorption (sorption isotherms) measurements under anoxic condition. A 2 SPNE SC/CE (2 sites protolysis non-electrostatic surface complexation/cation exchange) sorption model extended to account for the surface oxidation of sorbed Fe(II) was used to model the sorption data with the geochemical modeling code PHREEQC.
2) Tc diffusion in compacted illite with and without reducing agents. Tc is a redox sensitive radionuclide. Being exposed to reducing conditions, the mobility of Tc decreases significantly. The mobility of Tc was studied in compacted illite using a through-diffusion experimental setup at oxic and anoxic condition and in presence of different Fe(II)-forms. Some of the illite samples were preloaded with Fe(II) (sorbed Fe(II)) and others were mixed with pyrite before compaction. Because stainless steel filters are used in the through-diffusion set-up, Tc-diffusion in the stainless filters was carried out to obtain the diffusion properties of Tc in the filter. After the diffusion experiment in compacted illite, the distribution of (retarded) Tc was measured by cutting the illite column and measuring the Tc activity in the slices after extraction with a strong acid.
3) Reactive transport modelling of Tc transport in Opalinus Clay. The model couples the redox and sorption reactions with diffusive transport of aqueous species in porous media. The parameters obtained from previous experiments, such as the porosity and diffusion coefficient of HTO through filters were used to constrain the diffusion cell. The species diffusion coefficient, equilibrium constant of reduction reaction and dissolution reaction rate constant of pyrite were taken into account to explain the distribution of Tc in Opalinus Clay.

The results obtained in this study provide a better understanding of the migration of Tc in illite-rich clay rocks, such as Opalinus Clay, the selected host rock for a deep geological repository in Switzerland. This work could be a reference for Tc mobility used in the repository safety assessment.

1.4 Outline of the thesis

This thesis consists of 3 papers, which are accepted or under review by peer reviewed journals. Chapter 1 provides a brief introduction of the research background, describes a repository concept for geological disposal of radioactive waste in argillaceous rocks, explains why Tc and illite are investigated and how the research is carried out. Chapter 2 addresses Fe(II) sorption mechanism studied by batch sorption experiments and sorption modeling. The results presented in this chapter have been published in Applied Geochemistry (Chen et al., 2022). The diffusion of Tc in compacted illite and the role of iron is explicitly described and discussed in chapter 3. This manuscript has been submitted to Applied Geochemistry (Chen et al. 2023a). Chapter 4 describes the transport modeling of Tc diffusion in Opalinus Clay. As a first step, a simple model was set up to explain Tc diffusion

experiments in Opalinus clay performed by a collaborator at the University of Mainz. The manuscript on diffusion of Tc in OPA will be submitted to Geochimica et Cosmochimica Acta (Chen et al. 2023b). Chapter 5 summarizes the main conclusions of this project and presents an outlook for future work.

References

Benedicto, A., Missana, T., Fernández, A.M., 2014. Interlayer collapse affects on cesium adsorption onto illite. Environmental Science & Technology 48, 4909-4915.

Bergaya, F., Lagaly, G., 2013. Handbook of clay science. Newnes.

Brookshaw, D.R., Pattrick, R.A., Bots, P., Law, G.T., Lloyd, J.R., Mosselmans, J.F.W., Vaughan, D.J., Dardenne, K., Morris, K., 2015. Redox interactions of Tc (VII), U (VI), and Np (V) with microbially reduced biotite and chlorite. Environmental Science & Technology 49, 13139-13148.

Bruggeman, C., Maes, A., Vancluysen, J., 2007. The identification of FeS2 as a sorption sink for Tc (IV). Physics and Chemistry of the Earth, Parts A/B/C 32, 573-580.

Burns, R., Causey, W., Galloway, W., Nelson, R., 1978. Nuclear Waste Disposal in Space. NASA Technical Paper 1225.

Calmet, D.P., 1989. Ocean disposal of radioactive waste. Status report. IAEA bulletin 31, 47-50.

Chen, P., Van Loon, L.R., Marques Ferneandes, M., Churakov, S., 2022. Sorption mechanism of Fe(II) on illite: Sorption and modelling. Applied geochemistry 143, 105389.

Chen, P., Van Loon, L.R., Glaus, M., Churakov, S., 2023a. Impact of Fe(II) on 99Tc diffusion behavior in illite. To be submited to Aplied Geochemistry.

Chen, P., Van Loon, L.R., Koch, S., Alt.Epping, P., Churakov, S., Reich, T., 2023b. Reactive transport modelling of TcO_4^- diffusion in clay with PFLOTRAN. To be submitted to Geochimica et Cosmochimica Acta.

Colton, R., Peacock, R., 1962. An outline of technetium chemistry. Quarterly Reviews, Chemical Society 16, 299-315.

Coopersmith, J., 1999. Disposal of high-level nuclear waste in space, AIAA Annual Technical Symposium.

Cui, D., Eriksen, T.E., 1996. Reduction of pertechnetate by ferrous iron in solution: Influence of sorbed and precipitated Fe (II). Environmental Science & Technology 30, 2259-2262.

Desmet, G., Myttenaere, C., 1986. Technetium in the Environment. Springer Science & Business Media.

Dupuis, M.-C., Gonnot, F.-M., 2013. The Cigeo project-Industrial centre of deep reversible storage of radioactive wastes in Meuse/Haute-Marne-the commissioner's file. Public debate from the 15 May to the 15 October 2013; Projet Cigeo Centre industriel de stockage reversible profond de dechets radioactifs en Meuse/Haute-Marne-le dossier du maitre d'ouvrage. Debat public du 15 mai au 15 octobre 2013.

ENSI, 2018a. Recommendations and notes resulting from the assessment of the nuclear waste disposal program and the 2016 research and development plan. Report 33/593, Eidgenössisches Nuklearsicherheitsinspektorat (ENSI), Brugg, Switzerland.

ENSI, 2018b. Statement on the 2016 nuclear waste disposal program of those responsible for the waste disposal. Eidgenössisches Nuklearsicherheitsinspektorat (ENSI), Brugg, Switzerland.

Fan, Q., Tan, X., Li, J., Wang, X., Wu, W., Montavon, G., 2009. Sorption of Eu (III) on attapulgite studied by batch, XPS, and EXAFS techniques. Environmental Science & Technology 43, 5776-5782.

Fan, Q., Tanaka, K., Sakaguchi, A., Kondo, H., Watanabe, N., Takahashi, Y., 2014a. Factors controlling radiocesium distribution in river sediments: Field and laboratory studies after the Fukushima Dai-ichi Nuclear Power Plant accident. Applied Geochemistry 48, 93-103.

Fan, Q., Tanaka, M., Tanaka, K., Sakaguchi, A., Takahashi, Y., 2014b. An EXAFS study on the effects of natural organic matter and the expandability of clay minerals on cesium adsorption and mobility. Geochimica et Cosmochimica Acta 135, 49-65.

Faybishenko, B., Swift, P., 2016. International approaches for deep geological disposal of nuclear waste: Geological challenges in radioactive waste isolation: Fifth worldwide review. Lawrence Berkeley National Laboratory.

Gabrielli, R.A., Herdrich, G., 2015. Review of nuclear thermal propulsion systems. Progress in Aerospace Sciences 79, 92-113.

Gens, R., Lalieux, P., De Preter, P., Dierckx, A., Bel, J., Boyazis, J.-P., Cool, W., 2003. The Second Safety Assessment and Feasibility Interim Report (SAFIR 2 Report) on HLW Disposal in Boom Clay: Overview of the Belgian Programme. MRS Online Proceedings Library 807, 469-474.

Greenwood, N.N., Earnshaw, A., 2012. Chemistry of the Elements. Elsevier.

Heuze, F.E., 1981. On the Geotechnical modeling of high-level nuclear waste disposal by rock melting. Lawrence Livermore Laboratory, University ofCalifornia , Livermore, California.

Huang, J., Jones, A., Waite, T.D., Chen, Y., Huang, X., Rosso, K.M., Kappler, A., Mansor, M., Tratnyek, P.G., Zhang, H., 2021. Fe (II) redox chemistry in the environment. Chemical Reviews 121, 8161-8233.

Icenhower, J.P., Qafoku, N.P., Zachara, J.M., Martin, W.J., 2010. The biogeochemistry of technetium: a review of the behavior of an artificial element in the natural environment. American Journal of Science 310, 721-752.

IAEA, 2020. An Introduction to Practical Industrial Tomography Techniques for Non-destructive Testing (NDT). INTERNATIONAL ATOMIC ENERGY AGENCY, Vienna.

IAEA, 2022. Status and Trends in Spent Fuel and Radioactive Waste Management, IAEA Nuclear Energy Series No. NW-T-1.14 (Rev. 1), INTERNATIONAL ATOMIC ENERGY AGENCY, Vienna.

Knorr, K.E., 2015. On the uses of military power in the nuclear age. Princeton University Press.

Li, P., Wu, H., Liang, J., Yin, Z., Pan, D., Fan, Q., Xu, D., Wu, W., 2017. Sorption of Eu (III) at feldspar/water interface: effects of pH, organic matter, counter ions, and temperature. Radiochimica Acta 105, 1049-1058.

Litmanen, T., Kari, M., Kojo, M., Solomon, B.D., 2017. Is there a Nordic model of final disposal of spent nuclear fuel? Governance insights from Finland and Sweden. Energy Research & Social Science 25, 19-30.

Logan, S.E., 1974. Deep self-burial of radioactive wastes by rock-melting capsules. Nuclear Technology 21, 111-124.

McBeth, J., Lloyd, J., Law, G., Livens, F., Burke, I., Morris, K., 2011. Redox interactions of technetium with iron-bearing minerals. Mineralogical Magazine 75, 2419-2430.

Nagra, 2002. Project Opalinus Clay: safety report: demonstration of disposal feasibility for spent fuel, vitrified high-level waste and long-lived intermediate-level waste (Entsorgungsnachweis). Nagra Technical Report NTB 02-05, Nagra, Wettingen, Switzerland.

Nagra, 2008, Entsorgungsprogramm 2008 der Entsorgungspflichtigen. Nagra Technical Report NTB 08-01, Nagra, Wettingen, Switzerland.

Neuvazhaev, G., Rastorguev, A., Morozov, O., Kapyrin, I., Grigorev, F., 2020. 3D hydrogeological modeling of Deep Geological Disposal in the Nizhnekansky Rock massif, EGU General Assembly Conference Abstracts, p. 21509.

NRC, 1996. Nuclear Wastes: Technologies for Separations and Transmutation. Committee on Separations Technology and Transmutations Systems, National Reseasrch Council. ISBN: 0-309-56195-7, National Academy Press, Washington D.C.

Organisation for Economic Co-Operation and Development, N.E.A., 75 - Paris (France) (2006). Advanced nuclear fuel cycles and radioactive waste management. Nuclear Energy Agency of the OECD (NEA): Organisation for Economic Co-Operation and Development - Nuclear Energy Agency.

Pan, D., Fan, F., Wang, Y., Li, P., Hu, P., Fan, Q., Wu, W., 2017. Retention of Eu (III) in muscovite environment: Batch and spectroscopic studies. Chemical Engineering Journal 330, 559-565.

Peretyazhko, T., Zachara, J.M., Heald, S.M., Jeon, B.-H., Kukkadapu, R.K., Liu, C., Moore, D., Resch, C.T., 2008. Heterogeneous reduction of Tc (VII) by Fe (II) at the solid–water interface. Geochimica et Cosmochimica Acta 72, 1521-1539.

Philberth, K., 1977. The disposal of radioactive waste in ice sheets. Journal of Glaciology 19, 607-617.

Plúa, C., Vu, M., Armand, G., Rutqvist, J., Birkholzer, J., Xu, H., Guo, R., Thatcher, K., Bond, A., Wang, W., 2021. A reliable numerical analysis for large-scale modelling of a high-level radioactive waste repository in the Callovo-Oxfordian claystone. International Journal of Rock Mechanics and Mining Sciences 140, 104574.

POSIVA, 2022. Excavation of the first five disposal tunnels completed. https://www.posiva.fi/en/index/news/pressreleasesstockexchangereleases/2022/excavationofthefirstfivedisposaltunnelscompleted.html.

Powell, B.A., Duff, M.C., Kaplan, D.I., Fjeld, R.A., Newville, M., Hunter, D.B., Bertsch, P.M., Coates, J.T., Eng, P., Rivers, M.L., 2006. Plutonium oxidation and subsequent reduction by Mn (IV) minerals in Yucca Mountain tuff. Environmental Science & Technology 40, 3508-3514.

Rodionova, A.A., Petrov, V.G., Vlasova, I.E., Kalmykov, S.N., Petrov, V.A., Poluektov, V.V., Hammer, J., 2019. The radionuclide distribution onto different mineral phases of the rocks of the exocontact zone of Nizhnekansky granitoid massif. Perspectives in Science 12, 100406.

Rozov, K., Rumynin, V., Nikulenkov, A., Leskova, P., 2019. Sorption of 137Cs, 90Sr, Se, 99Tc, 152 (154) Eu, 239 (240) Pu on fractured rocks of the Yeniseysky site (Nizhne-Kansky massif, Russia), E3S Web of Conferences. EDP Sciences, p. 10007.

Schmeide, K., Bernhard, G., 2010. Sorption of Np (V) and Np (IV) onto kaolinite: Effects of pH, ionic strength, carbonate and humic acid. Applied Geochemistry 25, 1238-1247.

Siekierski, S., Burgess, J., 2002. Concise chemistry of the elements. Elsevier.

Skomurski, F.N., Rosso, K.M., Krupka, K.M., McGrail, B.P., 2010. Technetium incorporation into hematite (α-Fe2O3). Environmental Science & Technology 44, 5855-5861.

Stwertka, A., 2002. A Guide to the Elements. Oxford University Press.

Tro, N., 2008. Periodic properties of the elements. Chemistry: A molecular approach, 1st ed. Upper Saddle River, NJ, USA: Prentice Hall, 355-357.

Van Loon, L., Soler, J., Bradbury, M., 2003. Diffusion of HTO, 36Cl− and 125I− in Opalinus Clay samples from Mont Terri: Effect of confining pressure. Journal of Contaminant Hydrology 61, 73-83.

Wang, J., Chen, L., Su, R., Zhao, X., 2018. The Beishan underground research laboratory for geological disposal of high-level radioactive waste in China: planning, site selection, site characterization and in situ tests. Journal of Rock Mechanics and Geotechnical Engineering 10, 411-435.

Wu, H., Qiang, S., Fan, Q., Zhao, X., Liu, P., Li, P., Liang, J., Wu, W., 2018. Exploring the relationship between Th (IV) adsorption and the structure alteration of phlogopite. Applied Clay Science 152, 295-302.

Xu, C., Athon, M., Ho, Y.-F., Chang, H.-S., Zhang, S., Kaplan, D.I., Schwehr, K.A., DiDonato, N., Hatcher, P.G., Santschi, P.H., 2014. Plutonium immobilization and remobilization by soil mineral and organic matter in the far-field of the Savannah River Site, US. Environmental Science & Technology 48, 3186-3195.

Yun, D., Lu, C., Zhou, Z., Wu, Y., Liu, W., Guo, S., Shi, T., Stubbins, J.F., 2021. Current state and prospect on the development of advanced nuclear fuel system materials: A review. Materials Reports: Energy 1, 100007.

Zhang, C.-L., Czaikowski, O., Rothfuchs, T., 2010. Thermo-hydro-mechanical behaviour of the Callovo-Oxfordian clay rock. Final report GRS- 266, Gesellschaft für Anlagen- und Reaktorsicherheit (GRS) mbH.

Zhao, X., Qiang, S., Wu, H., Yang, Y., Shao, D., Fang, L., Liang, J., Li, P., Fan, Q., 2017a. Exploring the sorption mechanism of Ni (II) on illite: batch sorption, modelling, EXAFS and extraction investigations. Scientific Reports 7, 1-12.

Zhao, X., Wang, Y., Wu, H., Fang, L., Liang, J., Fan, Q., Li, P., 2017b. Insights into the effect of humic acid on Ni (II) sorption mechanism on illite: Batch, XPS and EXAFS investigations. Journal of Molecular Liquids 248, 1030-1038.

Ziessman, H.A., O'Malley, J.P., Thrall, J.H., 2013. Nuclear medicine: the requisites e-book. Elsevier Health Sciences.

2 Sorption mechanism of Fe(II) on illite: sorption and modelling

Ping CHEN[a,b,*], Luc Robert Van Loon[a], Maria do Sameiro Marques Fernandes[a], Sergey Churakov[a,b]

[a] Paul Scherrer Institut, Laboratory for Waste Management, 5232, Villigen PSI, Swizterland

[b] Institute of Geological science, University of Bern, Switzerland

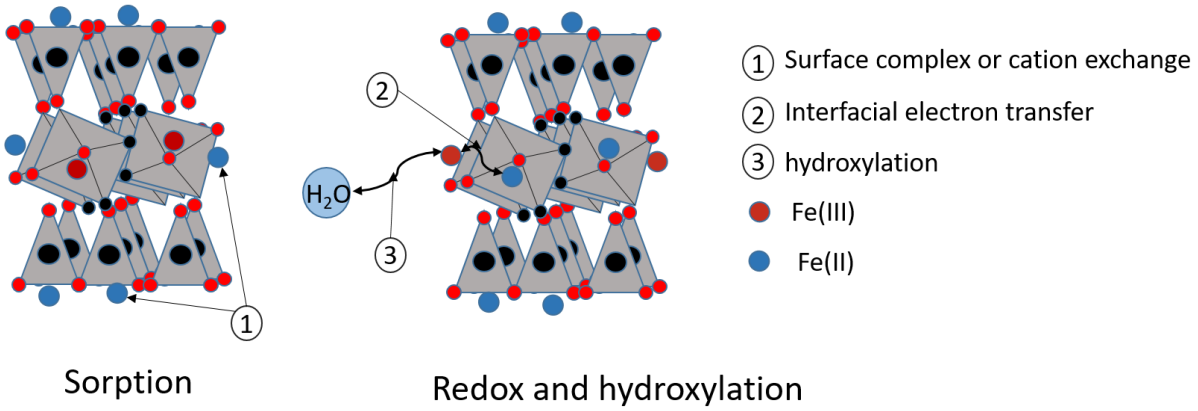

Abstract

Different countries consider clay formations as potential host rocks for the deep geological disposal of radioactive waste. Minor amounts of Fe(II), which is an important reducing agent in geochemical processes, are typically present in illite, which is one of the major clay minerals present in different argillaceous rocks. On the other hand, the corrosion of nuclear waste casks may act as sources of Fe(II) over time. The presence of Fe(II) in clay minerals may control the behavior of redox sensitive radionuclides such as ^{99}Tc, ^{75}Se and U, whose sorption, solubility and migration are largely affected by their redox state, which is affected by the redox potential in the environment. Thus, a quantitative description of Fe(II) sorption on clay minerals such as illite, is important to understand subsequent reactions with redox sensitive radionuclides. In this study, the sorption of Fe(II) on illite was investigated in batch experiments, including sorption edge and sorption isotherms measurements under anoxic condition. A 2 SPNE SC/CE (2 sites protolysis non-electrostatic surface complex/cation exchange) sorption model extended to account for the surface oxidation of sorbed Fe(II) was used to model the sorption data with the geochemical modeling code PHREEQC. Three models (A, B, C) with increasing level of complexity were tested. The model A, in which only Fe(II) interacts with illite, does not fit the experimental data satisfactorily. This model was modified to include oxidation of surface complexes (Model B) and precipitation of iron bearing phases (Model C). The modified models showed that most of the sorbed Fe(II) was oxidized at pH below 6.5. At pH above 6.5, the oxidized surface complexes either react with water forming surface iron hydroxides or precipitate as hematite, although presence of these could not be confirmed by X-ray diffraction measurements. These sorption processes could be used to couple with redox sensitive radionuclides in future reactive transport research.

Keywords: sorption edge, sorption isotherm, 2 SPNE SC/CE sorption model

2.1 Introduction

Different countries consider clay formations as potential host rocks for a deep geological disposal of

radioactive waste (Altmann, 2008; Andra, 2005; Lázár and Máthé, 2012; Nagra, 2002; Ondraf/Nirond, 2001). Clay minerals are important components of argillaceous rocks and backfill materials used in designs of waste repositories. Clay minerals may contain significant amounts of Fe (II) (Baeyens and Bradbury, 1997; Baeyens et al., 1985; Bradbury and Baeyens, 1999; Jaisi et al., 2005; Keeling et al., 2000; Kefas et al., 2007; Mogyorosi et al., 2003; Nayak and Singh, 2007; Poinssot et al., 1999), which is an important reducing agent in natural clays rocks. Iron containing clay minerals may control the long-term fate of redox sensitive radionuclides such as ^{75}Se and ^{99}Tc (De Cannière et al., 2010; Jaisi et al., 2009; Ma et al., 2019; Tsarev et al., 2016). Their speciation was demonstrated to play a significant role in reactions with redox sensitive nuclides. For instance, the following affinity series for heterogeneous Tc(VII) reduction by different Fe(II) species was observed: aqueous Fe(II) ≈ adsorbed Fe(II) in phyllosilicates < structural Fe(II) in phyllocilicates < Fe(II) adsorbed on Fe(III) oxides (Peretyazhko et al., 2008). Fe(II)-bearing minerals are known to reduce Tc(VII) to hydrous TcO_2-like phases (McBeth et al., 2011). In the study of Brookshaw et al., TcO_4^-, UO_2^{2+} and NpO_2^+ could be removed from solution by microbially reduced biotite and chlorite, and its reactivity was associated with redox cycling of the small fraction of Fe in these minerals (Brookshaw et al., 2015). On other hand, the corrosion of nuclear waste cannisters may act as a source of Fe(II) over time and not much is known about its behavior once it encounters the host clay rocks, in which clay minerals are the main component. Further, adding Fe(II) is a potential remediation technology for soils and sediments contaminated by redox sensitive nuclides. Therefore, it is important to have a comprehensive understanding of iron adsorption on clay minerals, and to develop quantitative sorption models, as part of models that describe and predict the long-term fate of redox sensitive nuclides for the safety assessment of radioactive waste repositories and/or remediation of polluted soils and sediments.

The redox properties of iron in clay minerals such as smectites (Gorski et al., 2012; Gorski et al., 2013; Hofstetter et al., 2006), nontronite (Jaisi et al., 2008; Neumann et al., 2013) and montmorillonite (Latta et al., 2017; Tsarev et al., 2016) have been widely investigated. Its redox behaviour in illite, especially the reactivity towards redox sensitive radionuclides, is largely unknown and needs a better understanding. In this study, a sorption edge and sorption isotherms were measured in batch experiments in order to obtain a comprehensive understanding of Fe(II) uptake mechanisms on illite. The two site protolysis non-electrostatic complexation and cation exchange (2SPNE SC/CE) sorption model, which was demonstrated to successfully and quantitatively explain the sorption mechanism of numerous cations (Bradbury and Baeyens, 2009a, b; Bradbury and Baeyens, 1997, 2005), was applied to model the sorption edge and sorption isotherm of Fe(II) on purified homoionic Na-illite with the help of PHREEQC. The model was further extended to take into account oxidation of surface complexes. Further XRD (X-ray diffraction) measurements were performed to verify whether precipitates were formed on the surface.

2.2 Materials and methods

2.2.1 Illite preparation

The illite used in this study was Illite du Puy (IDP) from Le Puy-en-Velay (France) (Gabis, 1958). Samples of illite were treated with a standard purification protocol described in Bradbury (Baeyens and Bradbury, 2004). The protocol described in Glaus et al. (2010) was applied to remove Ca-phases. The illite was equilibrated with a 1 M NaCl solution (solid to liquid ratio was 50 g/L) by stirring with a magnetic stirrer for 4 hours. The solution

was buffered at pH 3.5 by a formic acid/formate buffer. After settling down of the illite particles for 24 hours , the supernatant was replaced by a fresh 1 M NaCl electrolyte, and the procedure was repeated until no more Ca^{2+} could be extracted by this acid buffer (normally 7-8 times and verified by Ion Chromatography measurement of the supernatant). Then the suspension was washed with pure 1 M NaCl for 3 times to remove the residual acid buffer. After removing the NaCl by dialysing the suspension against de-ionized water, the illite was freeze-dried. The dried illite was stored under atmospheric conditions. All chemicals used were of suprapur grade quality.

2.2.2 Batch sorption

The illite suspension was prepared by adding about 3 g of pretreated illite (see section 2.1) to 100 mL of 0.1 M NaCl. All sorption experiments were performed in a glovebox under a controlled N_2 atmosphere (O_2 < 0.1 ppm) at 25 ± 1 °C. Before being transferred into the glovebox, the illite suspension and aqueous solutions were deoxygenated by heating to 60 °C and bubbling N_2 through the solutions for at least 2 hours. Tracer ^{55}Fe was purchased from Eckert & Ziegler Isotope Products, CA. Three $FeCl_2$ stock solutions (10^{-3} M, 10^{-4} M and 10^{-5} M) were prepared by dissolving given amounts of $FeCl_2 \bullet 4H_2O$ in 0.1 M NaCl solution. These stable $FeCl_2$ stock solutions together with ^{55}Fe tracer were first reduced in an electrochemical cell (Eh = -0.65 V vs SHE) as depicted in (Aeschbacher et al., 2010), to ensure all iron was in a reduced state, that is Fe(II). The cell consisted of a glass vessel closed with a teflon cover, a glassy carbon working electrode (Sigradur G, HTW, Germany), an Ag/AgCl reference electrode and a coiled wire platinum auxiliary electrode (Bioanalytical Inc., West Lafayette, IN) (Aeschbacher et al., 2010).

Sorption edge measurements were carried out at trace Fe(II) concentrations (10^{-7} M) with 0.1 M NaCl as the background electrolyte (about 8×10^{-10} M Fe-55 in each tube). The solid to liquid ratio was about 1 g/L^{-}. In order to fix the pH at a specific value, several buffers were used at a concentration around 0.002 M. The following pH buffers were used: sodium acetate for pH 3.5-4.5, MES (2-(N-morpholino)ethanesulfonic acid) for pH 5.5-6.5, MOPS (3-(N-morpholino)propanesulfonic acid) for pH 7.0-7.5, TRIS (tris (hydroxymethyl)aminomethane) for pH 8.0-8.5 and CHES (N-cyclohexyl-2-aminoethanesulfonic acid) for pH 9.0-9.5. These buffers were observed not to affect the interaction between Fe(II) and the clay mineral surface (Soltermann et al., 2014b). Illite suspensions were contacted with ^{55}Fe tracered and electrochemically reduced Fe(II) solutions in 25 mL centrifuge tubes (polypropylene). After shaking the systems end-over-end for three days, the suspensions were centrifuged in the glove box at 35 000 rpm for 1 hour (Beckman-Coulter Ultra-centrifuge, Beckman Coulter, Krefeld, Germany). The ^{55}Fe activity in the supernatant was measured by liquid scintillation counting (Tri-Carb 2750 TR/LL liquid scintillation counter, Canberra Packard, Schwadorf, Austria) using Ultima Gold AB (PerkinElmer, America) as scintillation cocktail. The Fe(II) distribution ratio was obtained by applying the following equation (1).

$$R_d = \frac{c_{in} - c_{eq}}{c_{eq}} \cdot \frac{V}{m} (L \cdot kg^{-1}) \quad (1)$$

Where c_{in} and c_{eq} are the total initial and the equilibrium Fe(II) concentrations, respectively, V is the volume of the liquid phase and m is the mass of solid. The sorption edge was plotted as the logarithm of the distribution ratio R_d as function of pH (Baeyens and Bradbury, 1997; Bradbury and Baeyens, 1997). The sorption isotherm was measured following almost the same protocol, except that the pH was fixed at a specific value and the Fe(II) concentrations were varied from 10^{-7} M to 10^{-3} M (the tracer is the same as sorption edge). In this study, isotherms

were measured at three pH conditions, pH 5.0, pH 5.5 and pH 6.5. Two datasets were used for the sorption model development, the other was applied to test and verify the model. The calculation of the uncertainties of R_d and the uncertainties of sorbed Fe are shown in detail in the Supporting Information S1 and Table S1.

Samples were prepared separately for XRD measurement to make sure whether a Fe-precipitate was formed. These samples were prepared under the same condition as the sorption edge at pH 6.86 and pH 8.68, and as the sorption isotherm at 2×10^{-4} M Fe(II), except that more illite was added (7.5 g/L), i.e. about 0.3 g. Samples were sealed and stored under N_2 for transfer to the XRD facility (the PANalytical X'Pert Pro). XRD patterns were recorded with an Empyrean diffractometer using Cu Kα radiation (λ = 1.5406 Å) under a 45 kV working voltage and 40 mA current at room temperature. Step scanning was performed with an angular resolution of 0.01° at 25 s counting time.

2.2.3 Sorption model.

The two-site protolysis non-electrostatic surface complexation and cation exchange (2SPNE SC/CE) sorption model was developed by Baeyens and Bradbury (1997) to describe Ni and Zn sorption on Na-montmorillonite (Bradbury and Baeyens, 1997). Later on, it has been widely used to describe the uptake of various metals on clay minerals (Bradbury and Baeyens, 2002, 2009b; Bradbury et al., 2005; Bradbury and Baeyens, 1999; Bradbury and Baeyens, 2006; Bradbury and Baeyens, 2011; Poinssot et al., 1999). A mechanistic study of Fe(II) sorption on montmorillonite, whose structure is in many aspects similar to illite, was performed by Soltermann et al. (2014a; 2014b). In this model, a combination of surface complexation at the amphoteric surface hydroxyl groups (≡SOH sites) and cation exchange on the planar sites is used to explain the cations uptake. The protolysis behavior of clay minerals is described by two types of weak sites ($\equiv S^{w1}OH$ and $\equiv S^{w2}OH$), which have the same site capacity (4.0×10^{-4} mol kg^{-1}) but different protolysis constants, together with one type of strong site ($\equiv S^{S}OH$) with a higher affinity but a lower capacity, which shows the same protolysis constant as the $\equiv S^{w1}OH$ sites. The properties of purified Na-illite were fully characterized by Baeyens and Bradbury (2004). Values for the cation exchange capacity (CEC), the surface hydroxyl group capacity and protolysis constants, which were fixed parameters in the sorption model, are listed in Table 1. The model was implemented in the PHREEQC software (version 3.4.8 and database is the phreeqc.dat) that was used to perform the modelling. The input data is available in the support information Text S1.

Table 1: Cation exchange capacities, surface hydroxyl group capacities and protolysis constants of illite (Baeyens and Bradbury, 2004, Baeyens and Bradbury, 2009a) and hydrolysis reactions of Fe^{2+}.

Site types	Site capacities
$\equiv S^{S}OH$	2.0×10^{-3} mol/kg
$\equiv S^{W1}OH$	4.0×10^{-2} mol/kg
$\equiv S^{W2}OH$	4.0×10^{-2} mol/kg
CEC	2.25×10^{-1} eq/kg
Protolysis reactions	**Log $K_{protolysis}$**
$\equiv S^{S}OH + H^{+} \leftrightarrow \equiv S^{S}OH_2^{+}$	4.0
$\equiv S^{S}OH \leftrightarrow \equiv S^{S}O^{-} + H^{+}$	-6.2
$\equiv S^{W1}OH + H^{+} \leftrightarrow \equiv S^{W1}OH_2^{+}$	4.0
$\equiv S^{W1}OH \leftrightarrow \equiv S^{W1}O^{-} + H^{+}$	-6.2
$\equiv S^{W2}OH + H^{+} \leftrightarrow \equiv S^{W2}OH_2^{+}$	8.5
$\equiv S^{W2}OH \leftrightarrow \equiv S^{W2}O^{-} + H^{+}$	-10.5

Hydrolysis reactions	Log ^{OH}K
$Fe^{2+} + H_2O \leftrightarrow Fe(OH)^+ + H^+$	-9.1 ± 0.4
$Fe^{2+} + 2\ H_2O \leftrightarrow Fe(OH)_2^0 + 2\ H^+$	-20.6 ± 1.0
$Fe^{2+} + 3\ H_2O \leftrightarrow Fe(OH)_3^- + 3\ H^+$	-34.6 ± 0.4

2.3 Results and discussion

Fig. 1 shows Fe(II) sorption on illite as a function of pH, and comparison with sorption on montmorillonite (Soltermann et al., 2013; Soltermann et al., 2014), and the sorption isotherm at pH 5.0 ± 0.1, pH 5.5 ± 0.1 and pH 6.5 ± 0.1. As shown in Fig. 1a, the sorption edge data is similar to sorption on montmorillonite (or more precisely between the Wyoming montmorillonite and the Texas montmorillonite). R_d is constant at pH < 4, increases from pH 4 to pH 7 and reaches a plateau above pH 7. Interesting point is the sorption edge on IDP (Illite du Puy) is between the Texas montmorillonite (or the synthetic iron free montmorillnote) and the Wyoming montmorillonite. As observed in Soltermann et al., 2014a, sorbed Fe(II) was oxidized on Fe(III)-rich montmorillonite, whose structural Fe contents for STx and SWy are 0.5 wt%, 2.9 wt%, while that for illite is 5.18 wt% (Murad, E. and U. Wagner, 1994). This remind a similar oxidation is possible and will be discuss detially below. The three isotherms at different pH values are shown in Figure 1b. The isotherm sorption at pH 5.0 ± 0.1 and pH 6.5 ± 0.1 are used to achieve the best fit parameters, Isotherm sorption at pH 5.5 ± 0.1 is used to test and verify these parameters.

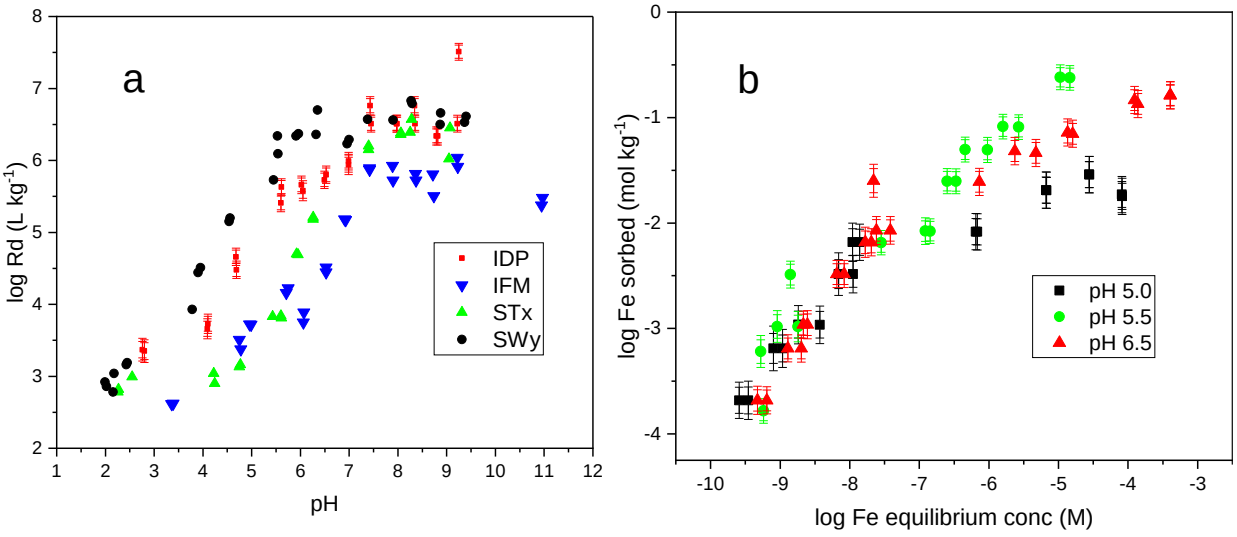

Figure 1: Experimentally measured sorption edge on IDP, IFM (synthetic iron free montmorillonite), STx (the Texas montmorillonite) and SWy (the Wyoming montmorillonite). (a), and sorption isotherm at pH 5.0 ± 0.1, pH 5.5 ± 0.1 and pH 6.5 ± 0.1 on IDP(b), for Fe(II) in 0.1 M NaCl. The total Fe concentration in the sorption edge experiment is 1×10^{-7} M. Illite concentration is 1.2 g/L in the sorption isotherm Data on montmorillonite is from Soltermann et al., 2013; Soltermann et al., 2014. (Color should be used in print)

In water under reducing conditions Fe^{2+} is expected to form $FeOH^+$, $Fe(OH)_2$, and $Fe(OH)_3^-$ aqua complexes. Under oxidizing conditions, Fe^{2+} oxidizes to Fe^{3+}, and further reacts with water to form $Fe(OH)_2^+$, $Fe(OH)_3$ and $Fe(OH)_4^-$. Similar hydrolysis reactions are expected for Fe^{2+} adsorbed on the illite surface. So, the Fe^{2+} behavior

in reducing conditions and in conditions having a redox potential according to equation 6 (which will be discussed in detail below) was calculated with PHREEQC and is given in Fig. 2. Fe speciation with the formation of a hematite precipitate is shown in Fig. S1 in the Supporting Information. Under the redox potential being considered, Fe^{2+} is the dominant species at pH < 6, and becomes gradually oxidized above pH 6. Oxidized Fe predominantly exists as $Fe(OH)_3$ at pH 7-9, with small amounts of $Fe(OH)_2^+$. $Fe(OH)_4^-$ gradually becomes predominant from pH 9. While Fe^{2+} and $FeOH^+$ is dominant from pH 2 to 9 and pH 9 to 10, respectively, if redox reactions are not taken into account. In this study, the sorption edge measurements of Fe(II) on illite were performed at a pH range from 2 to 10. So, the dominant Fe species are Fe^{2+}, $Fe(OH)_3$, and $Fe(OH)_4^-$, if oxidation was taken into account; or Fe^{2+} and $FeOH^+$ if oxidation was not taken into account.

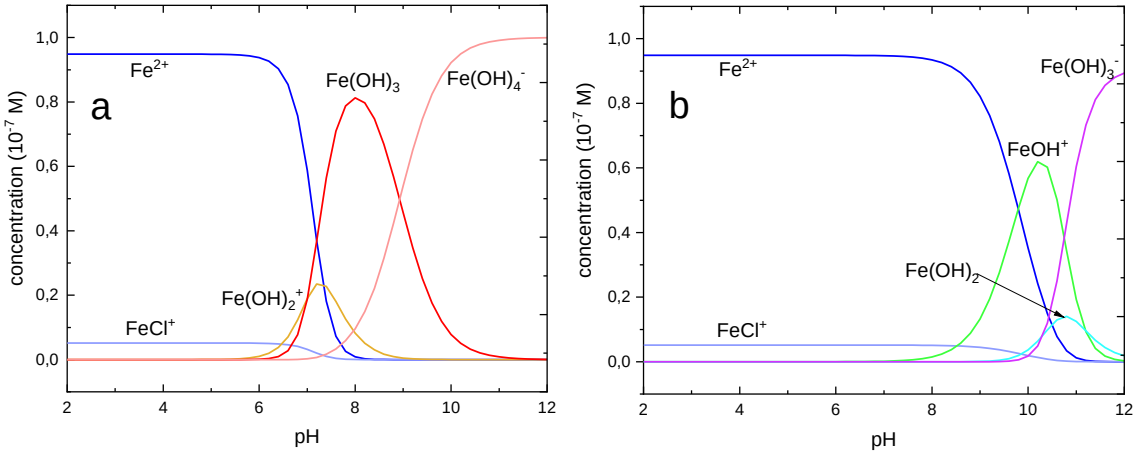

Figure 2: Fe speciation calculated as a function of pH a) with and b) without redox potential consideration following equation 6 at 0.1 M NaCl background electrolyte. The total Fe concentration is 1×10^{-7} M. (Color should be used in print).

2.3.1 Sorption model A: Fe(II) – illite interaction

The CEC, surface hydroxyl group sites density and protolysis constants of illite were fixed at values given by Baeyens and Bradbury (Baeyens and Bradbury, 2004, Baeyens and Bradbury, 2009a). The cation exchange reaction between Fe(II) and Na^+ was written as following (Gaines and Thomas, 1953):

$$Fe^{2+} + 2Na^+ - \text{Illite} \leftrightarrow Fe^{2+} - \text{Illite} + 2Na^+$$

The selectivity coefficient (K_c) was defined as:

$$^{Fe^{2+}}_{Na^+}K_c = \frac{N_{Fe^{2+}}}{(N_{Na^+})^2} \cdot \frac{\{Na^+\}^2}{\{Fe^{2+}\}} \quad (2)$$

Where $N_{Fe^{2+}}$ and N_{Na^+} are equivalent fractional occupancies, defined as the equivalents of Fe (or Na) sorbed per kilogram of illite divided by the CEC, and {} are the activities of cations in solution.

Two types of "weak surface sites" and one "strong site" are considered. The corresponding reactions are shown in equation 3.

$$\equiv S^{S,W1,W2}OH + Fe^{2+} \leftrightarrow \equiv S^{S,W1,W2}OFe^+ + H^+$$

The reaction equilibrium constant (K_M) for these reactions is defined as:

$$K_{Fe2+} = \frac{[\equiv S^{S,W1,W2}OFe^+]\cdot\{H^+\}}{[\equiv S^{S,W1,W2}OH]\cdot\{Fe^{2+}\}} \quad (3)$$

Where { } are the activities of the aqueous species and [ ] are the concentration of the surface complexes and hydroxyl groups at the strong and weak sites.

Reaction equilibrium constants without an electrostatic term were applied. Firstly, the equilibrium constants of cation exchange and complexation with the strong site were optimized by modelling of the sorption edge data. Then a best fit of the sorption isotherm data was obtained by adjusting the equilibrium constant for the complexation with the weak sites. The best-fit parameters are shown in Table 2. Model predictions are superimposed with experimental data in Fig. 3a, and show that the obtained constants of cation exchange and strong site complexation reproduce the experimental data. The obtained constant of cation exchange and surface complexation at the strong site were fixed in the modelling of sorption isotherm data, the constant of surface complexation at the weak site were changed manually. As shown in Fig. 3b and Fig. 3c, the model fit the experimental data considerably well. At low Fe(II) concentration ($<10^{-8}$ M), the surface complexation at the strong site is the dominant process. At high Fe(II) concentration ($>10^{-8}$ M), the surface complexation at the weak site become the dominant reaction. At higher Fe(II) concentration ($>10^{-4}$ M), cation exchange reaction control the Fe(II) sorption.

However, there are some deficiency. At low Fe(II) concentration ($<10^{-8}$ M), a model with complexation constant value of 4.1 ± 0.2 for the strong site would best describe the sorption isotherm data at pH 5.0 ± 0.1. It is 2.9 ± 0.1 for sorption isotherm at pH 6.5 ± 0.1. While the best fit complexation constant value for the strong site is 3.4 ± 0.2 at the sorption edge. Finally in this model, the value that best fitting the sorption edge was applied. At high Fe(II) concentration ($>10^{-8}$ M), the best fit complexation constant is 0.8 ± 0.3 for weak site at pH 5.0 ± 0.1, while 1.4 ± 0.2 is the best fit for complexation constant at weak site at pH 6.5 ± 0.1. the surface complexation at weak site make small difference at the sorption edge at low concentration (10^{-7} M in this experiment). Taken into account the isotherm sorption at pH 5.5 ± 0.1, whose best fit weak site complexation constant is 1.6 ± 0.2, the value 1.4 ± 0.1 was chosen.

Table 2: Fitted parameters of Fe(II) sorption on illite with sorption model, in which oxidation was not considered.

Cation exchange reaction	Log Kc
$2\ Na^{+}{-}illite + Fe^{2+} \leftrightarrow Fe^{2+}{-}illite + 2\ Na^{+}$	2.0 ± 0.1
Surface complexation reactions	**Log $^{S,W}K$**
$\equiv S^{S}OH + Fe^{2+} \leftrightarrow \equiv S^{S}OFe^{+} + H^{+}$	3.4 ± 0.2
$\equiv S^{W1}OH + Fe^{2+} \leftrightarrow \equiv S^{W1}OFe^{+} + H^{+}$	1.4 ± 0.1

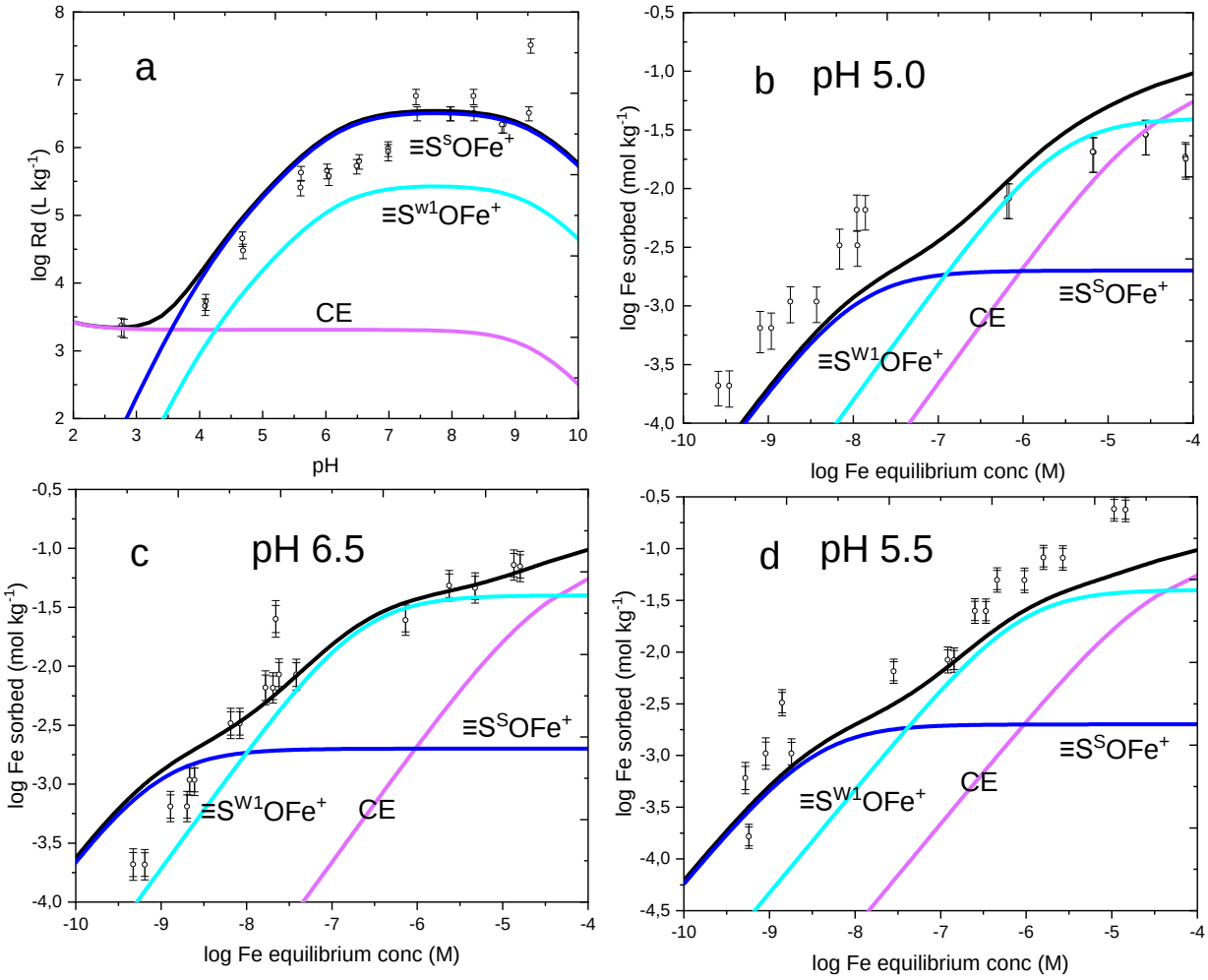

Figure 3: Fitting results of Fe(II) sorption on illite in sorption modle A, a) edge at Fe_{tot} 1×10^{-7} M; b) isotherm at pH 5.0 ± 0.1; c) isotherm at pH 6.5 ± 0.1; d) isotherm at pH 5.5 ± 0.1; 0.1 M NaCl was used as background electrolyte. Black line is the total sorption (that is total log Rd or total log adsorbed Fe). Purple line represents the cation exchange sorption. Blue and cyan blue represents strong and weak site complexation species, respectively. (Color should be used in print).

2.3.2 Sorption model B: Fe(II)/Fe(III) – illite interaction accounting for redox changes

As mentioned above, there are some flaw in sorption model A. Since the interfacial electron transfer was demonstrated to occur between aqueous Fe(II) and Fe-oxides, such as hematite, goethite, ferrihydrite and magnetite (Gorski and Scherer, 2009; Handler et al., 2009; Larese-Casanova and Scherer, 2007; Pedersen et al., 2005; Williams and Scherer, 2004; Yanina and Rosso, 2008). Furthermore, direct spectroscopic evidence was shown previously for the reduction of structural Fe(III) in a Fe-bearing smectite clay mineral (NAu-2, nontronite) by sorbed Fe(II) (Schaefer et al., 2011). Fe(II) sorption on Texas montmorillonite (STx), whose structural Fe-content was ≤ 0.5wt%, was proven to be consistent with the uptake behavior of other divalent transition metals. While much more sorbed Fe was observed on Wyoming montmorillonite, the sorption model was modified by taking a simple surface oxidation reaction of sorbed Fe(II) on edge sites into account, as shown in equation 4 (see details in Text S1). In this concept, the aqueous Fe(II) is first sorbed on the amphoteric edge sites (strong and weak site) and then undergoes an oxidation by structural Fe(III) (Soltermann et al., 2014a).

$$\equiv S^{S,W1,W2}OH + Fe^{2+} \leftrightarrow \equiv S^{S,W1,W2}OFe^{2+} + H^{+} + e^{-}$$

The reaction equilibrium constant is defined as:

$$K_{Fe3+} = \frac{[S^{S,W1,W2}{}_{OFe^{2+}}]\cdot\{H^{+}\}\cdot\{e^{-}\}}{[\equiv S^{S,W1,W2}{}_{OH}]\cdot\{Fe^{2+}\}} \quad (4)$$

The common convention of the electron activity, pe = -log{e} is used in PHREEQC to represent the redox state of the solution, which could be calculated from Eh with equation 5.

$$pe = 16.9Eh\ (V) \quad \text{at } 25°C \quad (5)$$

$$Eh\ (V) = -(0.031 \pm 0.002)\ pH + (0.483 \pm 0.009)$$

$$R^2 = 0.93 \quad (6)$$

The redox potential Eh is assumed to vary with pH. Because the concentration of Fe in the edge sorption experiments was too low, it was not possible to perform accurate Eh measurements with a Pt-ring redox electrode. The relationship of Eh and pH was found to be linear in a montmorillonite suspension as shown in equation 6 (Soltermann et al., 2014a). Because illite has a similar structure as montmorillonite and a significant amount of Fe(III) is present in purified Na-illite (Bradbury and Baeyens, 2009a; Murad, E. and U. Wagner, 1994), a similar behavior is expected in illite. Thus, the sorption model B modified with the oxidation of surface complexation. Since no reaction constants for iron free or low iron content illite are available, these constants for montmorillonite were used in this study on illite.

As shown in Fig. 2b, at a pH above 6, the oxidized Fe reacts with water and mainly forms $Fe(OH)_3$ and $Fe(OH)_4^-$. In this case, the model is extended with oxidized surface complexes further reacting with water. The equations 7 and 8 are the total reactions. It includes three reactions: Fe^{2+} complexation with a surface site, oxidation of surface complexed Fe^{2+} by an interfacial electron transfer to surface complexed Fe^{3+}, and a reaction of the surface complexed Fe^{3+} with water.

$$\equiv S^{S}OH + Fe^{2+} + 3H_2O \leftrightarrow \equiv S^{S}OFe(OH)_3^{-} + 4H^{+} + e^{-}$$

$$K_{Fe(OH)3} = \frac{[S^{S}OFe(OH)_3^{-}]\cdot\{H^{+}\}^{4}\cdot\{e^{-}\}}{[\equiv S^{S}OH]\cdot\{Fe^{2+}\}} \quad (7)$$

$$\equiv S^{S}OH + Fe^{2+} + 4H_2O \leftrightarrow \equiv S^{S}OFe(OH)_4^{2-} + 5H^{+} + e^{-}$$

$$K_{Fe(OH)4} = \frac{[S^{S}OFe(OH)_4^{2-}]\cdot\{H^{+}\}^{5}\cdot\{e^{-}\}}{[\equiv S^{S}OH]\cdot\{Fe^{2+}\}} \quad (8)$$

Table 3: Best fit parameters of the modified sorption model for illite with oxidative Fe(II) uptake

Cation exchange reaction	Log Kc
2 Na^+–illite + $Fe^{2+} \leftrightarrow Fe^{2+}$–illite + 2 Na^+	2.0 ± 0.1
Surface complexation reactions	**Log $^{S,W}K$**
$\equiv S^{S}OH + Fe^{2+} \leftrightarrow \equiv S^{S}OFe^{+} + H^{+}$	1.9 ± 0.3
$\equiv S^{W1}OH + Fe^{2+} \leftrightarrow \equiv S^{W1}OFe^{+} + H^{+}$	-1.7 ± 0.3
$\equiv S^{S}OH + Fe^{2+} \leftrightarrow \equiv S^{S}OFe^{2+} + H^{+} + e^{-}$	-2.2 ± 0.3
$\equiv S^{S}OH + Fe^{2+} + 3H_2O \leftrightarrow \equiv S^{S}OFe(OH)_3^{-} + 4H^{+} + e^{-}$	-22.0 ± 0.3
$\equiv S^{S}OH + Fe^{2+} + 4H_2O \leftrightarrow \equiv S^{S}OFe(OH)_4^{2-} + 5H^{+} + e^{-}$	-31.5 ± 0.2
$\equiv S^{W1}OH + Fe^{2+} \leftrightarrow \equiv S^{W1}OFe^{2+} + H^{+} + e^{-}$	-4.0 ± 0.3

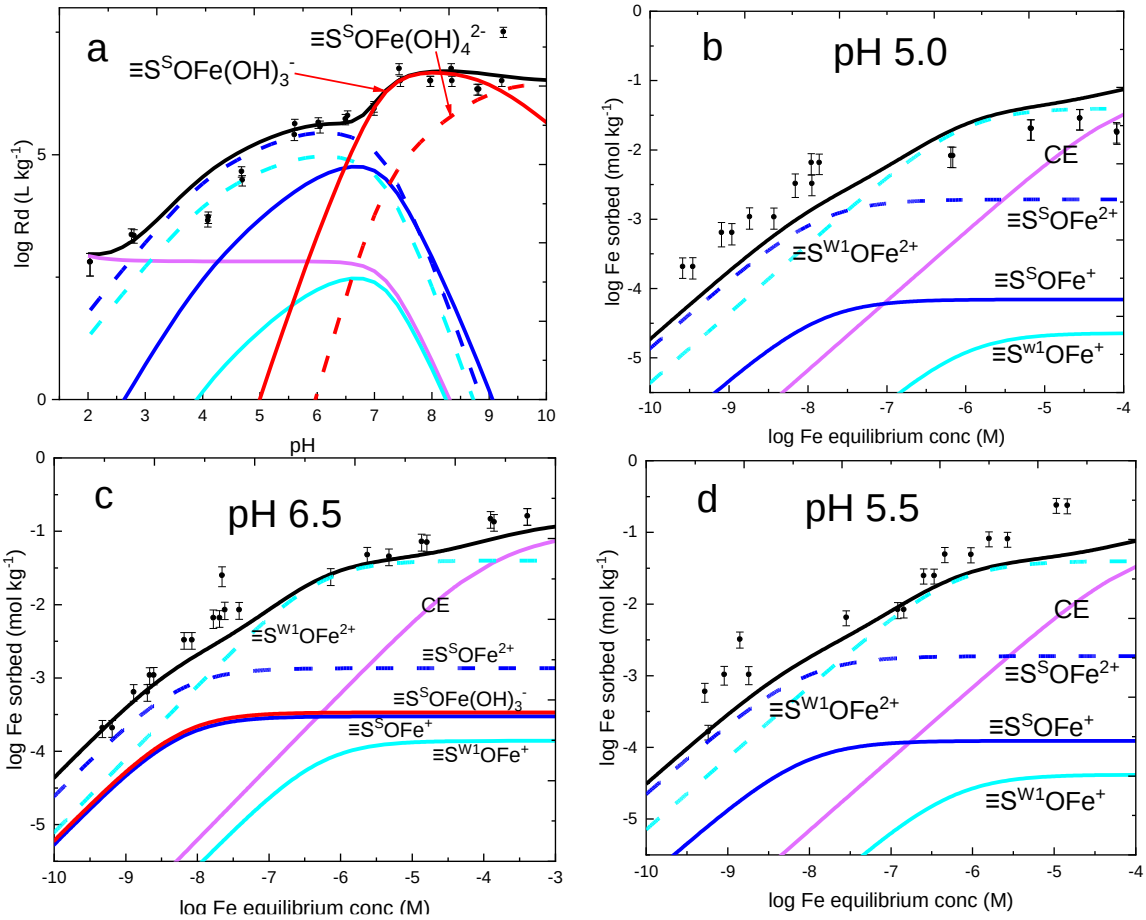

Figure 4: Fit result of Fe(II) sorption on illite in sorption model B, a) edge at Fe_{tot} 1×10^{-7} M; b) isotherm at pH 5.0 ± 0.1; c) isotherm at pH 6.5 ± 0.1 and d) isotherm at pH 5.5 ± 0.1; 0.1 M NaCl was used as background electrolyte. Black line is the total sorption (that is total log Rd or total log adsorbed Fe). (Color should be used in print).

The best fit results of the modelling are shown in Table 3 and Fig. 4. Parameters previously obtained for STx do not reproduce the experimental data accurately enough (compare the blue and cyan solid line with the black experimental data points in Fig. 4a). So, the sorption model was modified with a surface oxidation reaction. It should be noted that in the modified model, the $\equiv S^{S}OFe^{2+}$ species sharply decreased from about pH 6 as shown in Fig. 4a, which is consistent with Fe(II) being oxidized and forming hydroxide Fe(III) species from pH 6 (Fig. 2b). In combination with the speciation of Fe at the same redox potential, two more species, $\equiv S^{S}OFe(OH)_3^-$ and $\equiv S^{S}OFe(OH)_4^{2-}$ were introduced with log K value of -22.0 and -31.5, respectively. In this model, the oxidized surface complex on the strong site is dominant in all experimental pH conditions studied, while oxidation of surface complex at weak site occurs only at pH below 7. At pH < 6.5, the oxidation of the surface complex ($\equiv S^{S}OFe^{+}$ and $\equiv S^{W1}OFe^{+}$) is the predominant reaction. While at pH 6-9, the oxidation is controlled by equation 7 and produce $\equiv S^{S}OFe(OH)_3^-$, whereas $\equiv S^{S}OFe(OH)_4^{2-}$ becomes the main species at pH above 9. On the other hand, at a low Fe(II) equilibrium concentration ($<10^{-8}$ M) at all experimental pH, most of the sorbed Fe(II) species ($\equiv SOFe^{+}$) was oxidized. With increasing Fe concentration, the weak site complex oxidation and cation exchange reaction gradually become the dominant sorption mechanism. There is also drawback in modeling. The sorption

isotherm at low Fe(II) concentration especially at pH 5.0 ± 0.1 and pH 5.5 ± 0.1, a bigger values of the constant for the oxidation at strong site would fit the experimental better, which would result in an over estimation at low pH in the sorption edge. At high Fe(II) concentration, the underestimation of the data by the model can be explained by the formation of a Fe(III) precipitate (the saturation index is over 2.0 for hematite both at pH 5.5 ± 0.1 and 6.5 ± 0.1 at a Fe concentration above 10^{-5} M calculated from PHREEQC).

3.3 Sorption model C: extended model B including Fe precipitation

There could be another mechanism responsible for the seemingly high sorption of Fe at pH above 6 in the sorption edge. As shown in Fig. 2b, Fe(II) is gradually oxidized and forms Fe(III) species at pH 6.5 and more basic conditions. This may result in the formation of insoluble Fe(III) phases, for instance hematite, whose saturation index is higher than 2 at pH above 6.5. In this case, the measured Fe uptake from the solution could be explained by the precipitation of hematite. The modelling results considering hematite formation are shown in Fig. 5a (the red line represents sorption results from the contribution of a precipitate). The fitted parameters are the same as to sorption model B (Table 3), except reactions for forming $\equiv SOFe(OH)_3^-$, and $\equiv SOFe(OH)_4^{2-}$ are removed from this model. Similar as above, the fitted $\equiv SOFe^{2+}$ species sharply decrease from about pH 6 as shown in Fig. 5a (blue and cyan line). With the contribution of a hematite precipitate, the fitted log R_d values are perfectly consistent with experimental data. In the model, the oxidation of strong site and weak site surface complex is dominant at pH below 6 at low Fe(II) equilibrium concentration ($<10^{-7}$ M). Then the aqueous Fe(II) oxidizes from pH 6, and a precipitate is formed from then. However it is worth to notice that if a precipitate occurs above pH 6, such as 6.5, the equilibrium concentration of Fe in the solution should be constant once it reach the saturation concentration. However, a varying aqueous Fe(II) concentration was observed in the sorption isotherm at pH 6.5 ± 0.1, so the precipitate does not control the aqueous concentrations. Either the precipitate is induced by surface site, so the process is not controlled by saturation concentration.

Detailed solids characterization would be helpful to further verify whether oxidation, precipitation or both are occurred on the surface. In this work, no iron hydro-oxides or iron oxides precipitate was observed by XRD measurements on samples at pH 8.68, pH 6.86 with 10^{-7} M Fe and at pH 6.5 with 2×10^{-4} M Fe(II) (see Supporting Information Fig. S2). So, the presence of a Fe-precipitate is not confirmed by XRD measurements. Still, the formation of an amorphous precipitate could not be excluded. Therefore, more spectroscopic investigations would be necessary and are of great interest to validate the exact sorption mechanism.

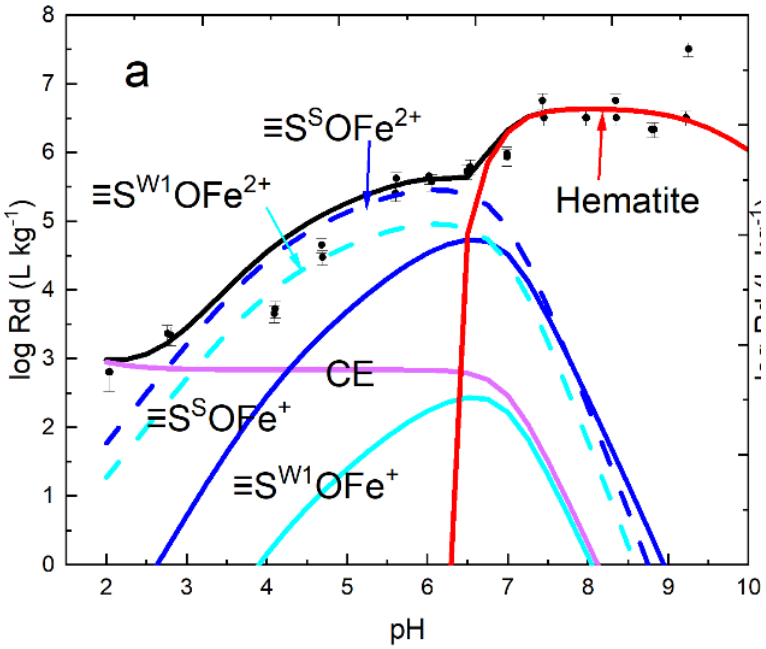

Figure 5: Fit result of Fe(II) sorption edge on illite in model modified with a) hematite and surface oxidation; 0.1 M NaCl was used as background electrolyte. Hematite allowed to precipitate if with saturation index exceeds 2.0. Black line is the total sorption (that is total log Rd or total log adsorbed Fe). (Color should be used in print).

2.4 Conclusion

Fe(II) sorption edge and sorption isotherm measurements on illite were carried out using the batch sorption technique. The uptake of Fe(II) by illite could be successfully, to a certain extent, reproduced using the 2 SPNE SC/CE (2 sites protolysis non-electrostatic surface complex/cation exchange) sorption model (Model A). According to the obtained results, surface complexation at strong site is dominant at low Fe(II) concentration, while complexation at weak site and cation exchange at planar site become dominant at high Fe(II) concentration. Further improvement of the model was made by including oxidation of Fe(II) surface complexes (Model B) and surface precipitation were also discussed (Model C). The modified model was validated against available experimental data to some extent since the parameters used in the modified model are taken from iron free montmorillonite. Sorption experimental data on low iron content illite is need to validate the models. Although both surface precipitation (Model C) and oxidation of surface complexes (Model B) could improve representation of the experimental data compared to the model A, neither of the models perfectly reproduce data at all the condition studied. Therefore, further spectroscopic characterization of the solid phases would be necessary to verify whether oxidation or precipitate or both are occurred on the surface.

In spite of the uncertain mechanism at high pH, the sorption of Fe(II) at pH below 6.5 is unequivocal with most surface complexes being oxidized to $\equiv S^{S}OFe^{2+}$ at low Fe concentration, and to $\equiv S^{W1}OFe^{2+}$ at high Fe concentration. Its reactions and correspond equilibrium constant could be used to couple with redox sensitive rediaonuclides in the safety assessment of repository.

Acknowledgements

This research is financially supported by the China Scholarship Council (CSC). The sorption experiments were carried out in Paul Scherrer Institut, Laboratory for Waste Management. The XRD measurement was performed in Institute of Geological science, University of Bern. we are grateful to all the colleagues and technicians, who helped us a lot in doing experiments and modelling.

References

Aeschbacher, M., Sander, M., Schwarzenbach, R.P., 2010. Novel Electrochemical Approach to Assess the Redox Properties of Humic Substances. Environmental Science & Technology 44, 87-93.

Altmann, S., 2008. 'Geochemical research: a key building block for nuclear waste disposal safety cases. Journal of Contaminant Hydrology 102, 174-179.

Andra, 2005. Dossier 2005 Argile: Safety evaluation of a geological repository.

Baeyens, B., Bradbury, M.H., 1997. A mechanistic description of Ni and Zn sorption on Na-montmorillonite Part I: Titration and sorption measurements. Journal of Contaminant Hydrology 27, 199-222.

Baeyens, B., Bradbury, M.H., 2004. Cation exchange capacity measurements on illite using the sodium and cesium isotope dilution technique: effects of the index cation, electrolyte concentration and competition: modeling. Clays and Clay Minerals 52, 421-431.

Baeyens B., Maes A., Cremers A., Henrion P.N. (1985) In situ physico-chemical characterisation of Boom clay. Radioactive Waste Management and the Nuclear Fuel Cycle 6, 391-408

Bradbury, M., Baeyens, B., 2002. Sorption of Eu on Na-and Ca-montmorillonites: experimental investigations and modelling with cation exchange and surface complexation. Geochimica et Cosmochimica Acta 66, 2325-2334.

Bradbury, M., Baeyens, B., 2009a. Sorption modelling on illite Part I: Titration measurements and the sorption of Ni, Co, Eu and Sn. Geochimica et Cosmochimica Acta 73, 990-1003.

Bradbury, M., Baeyens, B., 2009b. Sorption modelling on illite. Part II: Actinide sorption and linear free energy relationships. Geochimica et Cosmochimica Acta 73, 1004-1013.

Bradbury, M., Baeyens, B., Geckeis, H., Rabung, T., 2005. Sorption of Eu (III)/Cm (III) on Ca-montmorillonite and Na-illite. Part 2: Surface complexation modelling. Geochimica et Cosmochimica Acta 69, 5403-5412.

Bradbury, M.H., Baeyens, B., 1997. A mechanistic description of Ni and Zn sorption on Na-montmorillonite Part II: modelling. Journal of Contaminant Hydrology 27, 223-248.

Bradbury, M.H., Baeyens, B., 1999. Modelling the sorption of Zn and Ni on Ca-montmorillonite. Geochimica et cosmochimica acta 63, 325-336.

Bradbury, M.H., Baeyens, B., 2005. Modelling the sorption of Mn (II), Co (II), Ni (II), Zn (II), Cd (II), Eu (III), Am (III), Sn (IV), Th (IV), Np (V) and U (VI) on montmorillonite: Linear free energy relationships and estimates of surface binding constants for some selected heavy metals and actinides. Geochimica et Cosmochimica Acta 69, 875-892.

Bradbury, M.H., Baeyens, B., 2006. Modelling sorption data for the actinides Am (III), Np (V) and Pa (V) on montmorillonite. Radiochimica Acta 94, 619-625.

Bradbury, M.H., Baeyens, B., 2011. Predictive sorption modelling of Ni (II), Co (II), Eu (IIII), Th (IV) and U (VI) on MX-80 bentonite and Opalinus Clay: A "bottom-up" approach. Applied Clay Science 52, 27-33.

Brookshaw, D.R., Pattrick, R.A., Bots, P., Law, G.T., Lloyd, J.R., Mosselmans, J.F.W., Vaughan, D.J., Dardenne, K., Morris, K., 2015. Redox interactions of Tc (VII), U (VI), and Np (V) with microbially reduced biotite and chlorite. Environmental science & technology 49, 13139-13148.

De Cannière, P., Maes, A., Williams, S., Bruggeman, C., Beauwens, T., Maes, N., Cowper, M., 2010. Behaviour of selenium in Boom Clay. External Report, SCK• CEN-ER-120.

Gabis, V., 1958. Etude préliminaire des argiles oligocènes du Puy-en-Velay (Haute-Loire). Bulletin de Minéralogie 81, 183-185.

Gaines Jr, George L., and Henry C. Thomas. "Adsorption studies on clay minerals. II. A formulation of the thermodynamics of exchange adsorption." The Journal of Chemical Physics 21.4 (1953): 714-718.

Glaus, M.A., Frick, S., Rossé, R., Van Loon, L.R., 2010. Comparative study of tracer diffusion of HTO, 22Na+ and 36Cl− in compacted kaolinite, illite and montmorillonite. Geochimica et Cosmochimica Acta 74, 1999-2010.

Gorski, C.A., Klüpfel, L., Voegelin, A., Sander, M., Hofstetter, T.B., 2012. Redox properties of structural Fe in clay minerals. 2. Electrochemical and spectroscopic characterization of electron transfer irreversibility in ferruginous smectite, SWa-1. Environmental Science & Technology 46, 9369-9377.

Gorski, C.A., Klüpfel, L.E., Voegelin, A., Sander, M., Hofstetter, T.B., 2013. Redox properties of structural Fe in clay minerals: 3. Relationships between smectite redox and structural properties. Environmental Science & Technology 47, 13477-13485.

Gorski, C.A., Scherer, M.M., 2009. Influence of magnetite stoichiometry on FeII uptake and nitrobenzene reduction. Environmental Science & Technology 43, 3675-3680.

Handler, R.M., Beard, B.L., Johnson, C.M., Scherer, M.M., 2009. Atom exchange between aqueous Fe (II) and goethite: An Fe isotope tracer study. Environmental Science & Technology 43, 1102-1107.

Hofstetter, T.B., Neumann, A., Schwarzenbach, R.P., 2006. Reduction of nitroaromatic compounds by Fe (II) species associated with iron-rich smectites. Environmental Science & Technology 40, 235-242.

Jaisi, D.P., Dong, H., Morton, J.P., 2008. Partitioning of Fe (II) in reduced nontronite (NAu-2) to reactive sites: Reactivity in terms of Tc (VII) reduction. Clays and Clay Minerals 56, 175-189.

Jaisi, D.P., Dong, H., Plymale, A.E., Fredrickson, J.K., Zachara, J.M., Heald, S., Liu, C., 2009. Reduction and long-term immobilization of technetium by Fe (II) associated with clay mineral nontronite. Chemical Geology 264, 127-138. https://doi.org/10.1016/j.chemgeo.2009.02.018

Jaisi, D.P., Kukkadapu, R.K., Eberl, D.D., Dong, H., 2005. Control of Fe (III) site occupancy on the rate and extent of microbial reduction of Fe (III) in nontronite. Geochimica et Cosmochimica Acta 69, 5429-5440. https://doi.org/10.1016/j.gca.2005.07.008

Keeling, J.L., Raven, M.D., Gates, W.P., 2000. Geology and characterization of two hydrothermal nontronites from weathered metamorphic rocks at the Uley graphite mine, South Australia. Clays and Clay Minerals 48, 537-548.

Kefas, H.M., Patrick, D.O., Chiroma, T.M., 2007. Characterization of mayo-belwa clay. Leonardo Electronic Journal of Practices and Technologies 6, 123-130.

Larese-Casanova, P., Scherer, M.M., 2007. Fe (II) sorption on hematite: New insights based on spectroscopic measurements. Environmental Science & Technology 41, 471-477. https://doi.org/10.1021/es0617035

Latta, D.E., Neumann, A., Premaratne, W., Scherer, M.M., 2017. Fe (II)–Fe (III) electron transfer in a clay mineral with low Fe content. ACS Earth and Space Chemistry 1, 197-208.

Lázár, K., Máthé, Z., 2012. Claystone as a potential host rock for nuclear waste storage. Clay Minerals in Nature–Their Characterization, Modification and Application (InTech, 2012), 55-80.

Ma, B., Charlet, L., Fernandez-Martinez, A., Kang, M., Madé, B., 2019. A review of the retention mechanisms of redox-sensitive radionuclides in multi-barrier systems. Applied Geochemistry 100, 414-431.

Marques Fernandes, M. (2020). Personal communication.

McBeth, J., Lloyd, J., Law, G., Livens, F., Burke, I., Morris, K., 2011. Redox interactions of technetium with iron-bearing minerals. Mineralogical Magazine 75, 2419-2430.

Mogyorosi, K., Dekany, I., Fendler, J., 2003. Preparation and characterization of clay mineral intercalated titanium dioxide nanoparticles. Langmuir 19, 2938-2946.

Murad, E., and U. Wagner, 1994. The Mössbauer spectrum of illite. Clay Minerals 29.1, 1-10.

Nagra, 2002. Project Opalinus clay, demonstration of disposal feasibility forspent fuel, vitrified high-level waste and long-lived intermediate-levelwaste. Safety Report. Technical Report NTB 02-05 , Nagra, Wettingen, Switzerland.

Nayak, P.S., Singh, B., 2007. Instrumental characterization of clay by XRF, XRD and FTIR. Bulletin of Materials Science 30, 235-238.

Neumann, A., Olson, T.L., Scherer, M.M., 2013. Spectroscopic evidence for Fe (II)–Fe (III) electron transfer at clay mineral edge and basal sites. Environmental Science & Technology 47, 6969-6977.

Ondraf / Nirond, 2001. Safety assessment and feasibility Interim Report 2(Safir 2), Nirond 2001-05.

Pedersen, H.D., Postma, D., Jakobsen, R., Larsen, O., 2005. Fast transformation of iron oxyhydroxides by the catalytic action of aqueous Fe (II). Geochimica et Cosmochimica Acta 69, 3967-3977.

Peretyazhko, T., Zachara, J.M., Heald, S.M., Jeon, B.-H., Kukkadapu, R.K., Liu, C., Moore, D., Resch, C.T., 2008. Heterogeneous reduction of Tc (VII) by Fe (II) at the solid–water interface. Geochimica et Cosmochimica Acta 72, 1521-1539.

Poinssot, C., Baeyens, B., Bradbury, M.H., 1999. Experimental and modelling studies of caesium sorption on illite. Geochimica et Cosmochimica Acta 63, 3217-3227.

Schaefer, M.V., Gorski, C.A., Scherer, M.M., 2011. Spectroscopic evidence for interfacial Fe (II)− Fe (III) electron transfer in a clay mineral. Environmental Science & Technology 45, 540-545.

Soltermann, D., Baeyens, B., Bradbury, M.H., Marques Fernandes, M., 2014a. Fe (II) uptake on natural montmorillonites. II. Surface complexation modeling. Environmental Science & Technology 48, 8698-8705.

Soltermann, D., Marques Fernandes, M., Baeyens, B., Dähn, R., Miehé-Brendlé, J., Wehrli, B., Bradbury, M.H., 2013. Fe (II) sorption on a synthetic montmorillonite. A combined macroscopic and spectroscopic study. Environmental Science & Technology 47,

Soltermann, D., Marques Fernandes, M., Baeyens, B., Dähn, R., Joshi, P.A., Scheinost, A.C., Gorski, C.A., 2014b. Fe (II) uptake on natural montmorillonites. I. Macroscopic and spectroscopic characterization. Environmental Science & Technology 48, 8688-8697.

Tsarev, S., Waite, T.D., Collins, R.N., 2016. Uranium reduction by Fe (II) in the presence of montmorillonite and nontronite. Environmental Science & Technology 50, 8223-8230. https://doi.org/10.1021/acs.est.6b02000

Williams, A.G., Scherer, M.M., 2004. Spectroscopic evidence for Fe (II)− Fe (III) electron transfer at the iron oxide− water interface. Environmental Science & Technology 38, 4782-4790.

Yanina, S.V., Rosso, K.M., 2008. Linked reactivity at mineral-water interfaces through bulk crystal conduction. Science 320, 218-222.

Supporting materials

Sorption mechanism of Fe(II) on illite: sorption and modelling

Ping CHEN[a,*], Luc R. Van Loon[a], Maria do Sameiro Marques Fernandes[a], Sergey Churakov[a,b]

[a] Paul Scherrer Institut, Laboratory for Waste Management, 5232, Villigen PSI, Switzerland

[b] Institute of Geological science, University of Bern, Switzerland

Text S1 The uncertainty of R_d

$$R_d = \frac{c_{ini}-c_{eq}}{c_{eq}}\frac{V}{m}(L\cdot kg^{-1}) = \frac{c_{ini}}{c_{eq}}\frac{V}{m} - \frac{V}{m}$$

$$c_{ini} = \frac{c_s}{V}\cdot V_p$$

$$c_{eq} = \frac{c_c}{V_{sam}}\cdot V$$

Where c_s, c_c are the tracer stock concentration and the concentration of the tracer in the sample from the liquid scintillation counter. c_{ini} , c_{eq} are, the total initial and the equilibrium Fe(II) concentration, respectively. V_p and V_{sam} are the volume of liquid pipetted from the stock solution and the volume of the sample for liquid scintillation measurements. V is the total volume and m is the solid mass in the tubes. The relative uncertainty of c_{ini} and c_{eq} is defined as follows:

$$\mathrm{r.u}(c_{ini}) = \sqrt{r.u(c_s)^2 + r.u(V)^2 + r.u\left(V_p\right)^2}$$

$$\mathrm{r.u}\left(c_{eq}\right) = \sqrt{r.u(c_c)^2 + r.u(V_{sam})^2 + r.u(V)^2}$$

According to the law of error propagation, the uncertainty could be expressed as:

$$u\,(R_d) = \frac{c_{ini}}{c_{eq}}\frac{V}{m}\cdot\sqrt{r.u(c_{ini})^2 + r.u\left(c_{eq}\right)^2 + r.u(V)^2 + r.u(m)^2} + \frac{V}{m}\cdot\sqrt{r.u(V)^2 + r.u(m)^2}$$

$$u\,(R_d) = \frac{c_{ini}}{c_{eq}}\frac{V}{m}\cdot\sqrt{r.u(c_s)^2 + r.u(V)^2 + r.u\left(V_p\right)^2 + r.u(c_c)^2 + r.u(V_{sam})^2 + r.u(V)^2 + r.u(V)^2 + r.u(m)^2} + \frac{V}{m}\cdot\sqrt{r.u(V)^2 + r.u(m)^2}$$

The uncertainty of sorbed Fe

$$c_{sor} = \frac{c_{ini}\cdot V\cdot P}{m}$$

$$c_{ini} = (c_1\cdot V_1 + c_2\cdot V_2 + c_3\cdot V_3)/V$$

$$\mathrm{P} = 1 - \frac{c_{out}}{c_{in}}$$

Where c_{sor} and c_{ini} are the sorbed Fe and the initial concentration of Fe. V and m are the total volume of liquid and solid mass. P is the fraction of sorbed Fe. $c_{in}$and c_{out} are β counts before and after sorption. c_1, c_2 and c_3 are three stock solution, and V_1, V_2, and V_3 are the respective pipetted volumes for preparing the suspensions.

$$\mathrm{r.u}(c_{ini}) = \frac{c_1 \cdot V_1}{c_{ini} \cdot V} \cdot (r.u(c_1)^2 + r.u(V_1)^2 + r.u(V)^2)^{1/2} + \frac{c_2 \cdot V_2}{c_{ini} \cdot V} \cdot (r.u(c_2)^2 + r.u(V_2)^2 + r.u(V)^2)^{1/2} + \frac{c_3 \cdot V_3}{c_{ini} \cdot V} \cdot (r.u(c_3)^2 + r.u(V_3)^2 + r.u(V)^2)^{1/2}$$

relative uncertainty of c_1, c_2 and c_3 are assumed to be identical, because they are all prepared in same way. V_1, V_2, and $V_3$are also taken as identical.

$$\mathrm{r.u(P)} = (r.u(c_{in})^2 + r.u(c_{out})^2)^{1/2}$$

where c_{in} and c_{out} have the same meaning of c_{ini} and c_{eq} in R_d calculation. So, the same equation can be used to calculate the uncertainty.

$$\mathrm{r.u}(c_{sor}) = (r.u(c_{ini})^2 + r.u(P)^2 + r.u(V)^2 + r.u(m)^2)^{1/2}$$

Table S1 relative uncertainty (r.u) on the parameters

parameter	r.u
V	0.1
V_p	0.01
V_{sam}	0.05
m	0.1
V_1, V_2, and V_3	0.01

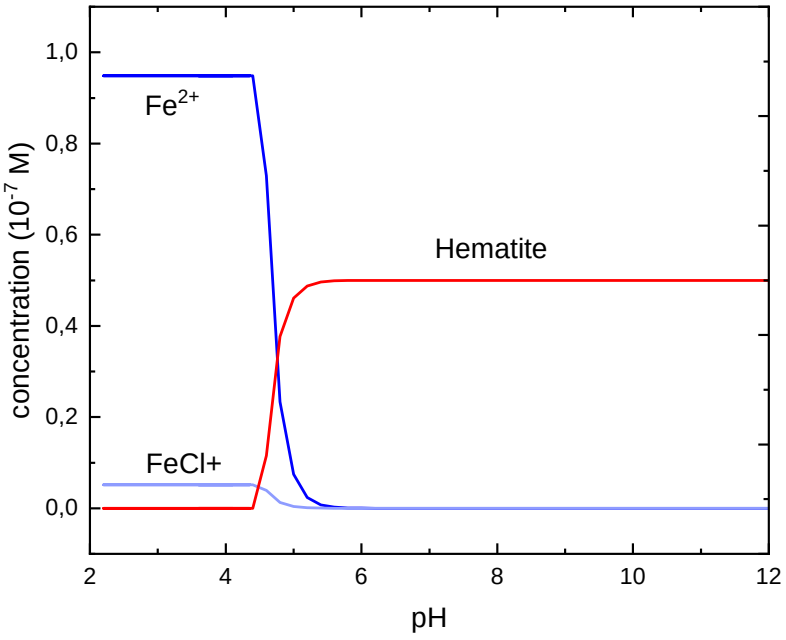

Figure. S1 Fe speciation at changing experimental potential with formation of hematite (Fe_2O_3). 0.1 M NaCl was used as electrolyte, total Fe is 10^{-7} M. hematite was assumed to precipitate at saturation index over 2. (Color should be used in print).

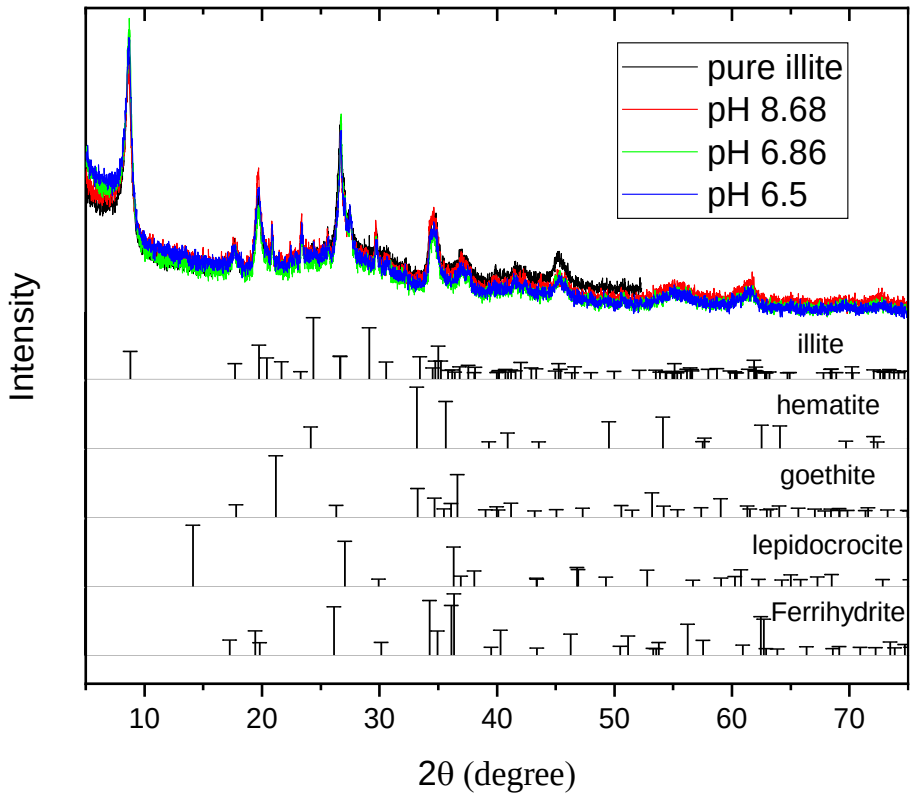

Figure. S2.XRD measurement result of samples after Fe(II) sorption. No difference was observed compared with pure illite. (Color should be used in print).

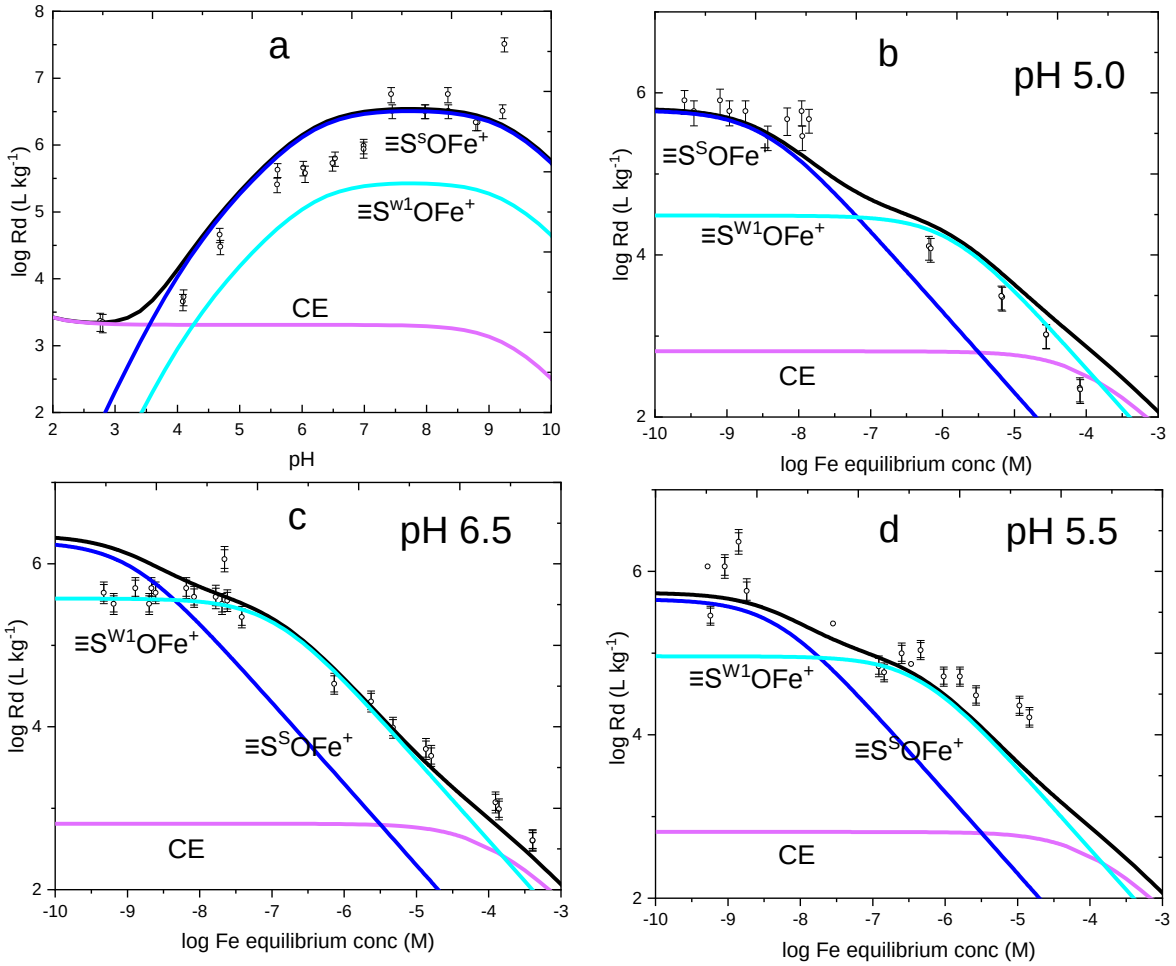

Figure. S3 Fitting results of Fe(II) sorption on illite, a) edge at Fe_{tot} 1×10^{-7} M; b) isotherm at pH 5.0; c) isotherm at pH 6.5; d) isotherm at pH 5.5; 0.1 M NaCl was used as background electrolyte. Black line is the total sorption (that is total log Rd or total log adsorbed Fe). Purple line represents the cation exchange sorption. Blue and cyan blue represents strong and weak site complexation species, respectively. (Color should be used in print).

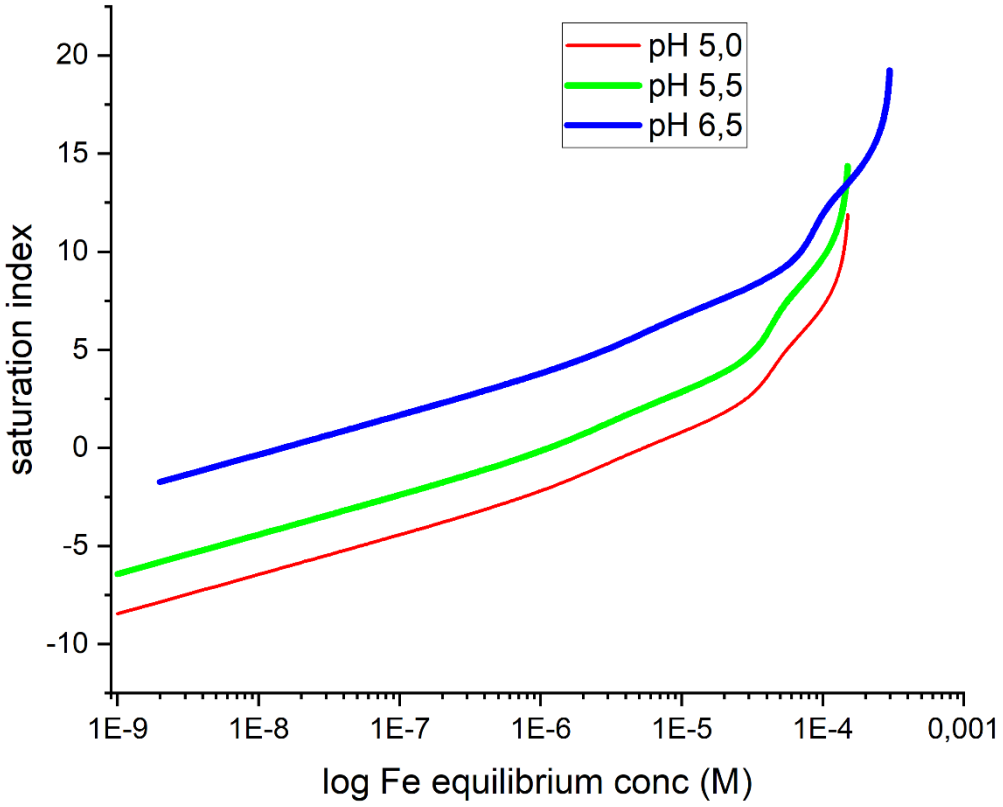

Figure. S4 the saturation index of hematite at different pH conditions over Fe concentration. Calculation is done by PHREEQC.

Text S1. Code for modelling

Words or sentences following string # means explanation.

1 Sorption edge

```
# Fe Edge on Na-Mont, 2SPNE-SC/CE model
# Source data: Fe uptake on natural montmorillonite, EST, 2014
# Activity coefficients: Davies equation
DATABASE c:\phreeqc\database\phreeqc.dat
SOLUTION_MASTER_SPECIES
# element   species   alk gfw_formula element_gfw
 Fe       Fe+2     0.0    Fe     55.845

SURFACE_MASTER_SPECIES
 S_s S_sOH     # strong sites on illite, S_sOH for SsOH

 # two type of weak sites, S_waOH for Sw1OH, S_wbOH for Sw2OH
 S_wa S_waOH
 S_wb S_wbOH

SURFACE_SPECIES
 # surface species hydrolysis
 S_sOH = S_sOH
 S_sOH + H+ = S_sOH2Cl; log_k 4.0; -no_check; -mole_balance S_sOH2Cl
 S_sOH = S_sONa + H+; log_k -6.2; -no_check; -mole_balance S_sONa

 S_waOH = S_waOH
 S_waOH + H+ = S_waOH2Cl; -log_k 4.0; -no_check; -mole_balance S_waOH2Cl
 S_waOH = S_waONa + H+; -log_k -6.2;  -no_check; -mole_balance S_waONa

 S_wbOH = S_wbOH
 S_wbOH + H+ = S_wbOH2Cl; -log_k 8.5; -no_check; -mole_balance S_wbOH2Cl
 S_wbOH = S_wbONa + H+; -log_k -10.5; -no_check; -mole_balance S_wbONa

SOLUTION_SPECIES
 # Fe hydrolysis
  Fe+2 = Fe+2              #;     -gamma 5.26 0.121; -dw 6.9e-10
  Fe+2 + H2O = Fe(OH)+ + H+; log_k -9.1       #; -gamma 5.26 0.121; -dw 6.9e-10
  Fe+2 + 2H2O = Fe(OH)2 +2H+; log_k -20.6  #; -gamma 5.26 0.121; -dw 6.9e-10
  Fe+2 + 3H2O = Fe(OH)3- + 3H+; log_k -34.6                #; -gamma 5.26 0.121; -dw 6.9e-10
  Fe+2 + Cl-  = FeCl+;   log_k -0.1605

EXCHANGE_SPECIES
# cation exchange sites...
  Fe+2 + 2X- = FeX2; -log_k          22.0; #        logK for Fe(II) exchange was from Fe uptake on natural montmorillonite, EST, 2014
  Na+ + X- = NaX; -log_k 10

SURFACE_SPECIES
 # strong sites
  S_sOH + Fe+2 = S_sOFeCl + H+; log_k 1.9; -no_check; -mole_balance S_sOFeCl  # logK for Fe(II) exchange was from Fe uptake on natural
montmorillonite, EST, 2014
  S_sOH + Fe+2 = S_sOFeCl2 + H+ + e-; log_k -2.2; -no_check; -mole_balance S_sOFeCl2 # logK for Fe(II) being oxidized was fitted manually
  S_sOH + Fe+2 + 3H2O = S_sOFe(OH)3Na + 4H+ + e-; log_k -22.0; -no_check; -mole_balance S_sOFe(OH)3Na # logK for Fe(II) being oxidized
and hydrolized was fitted manually
  S_sOH + Fe+2 + 4H2O = S_sOFe(OH)4Na2 + 5H+ + e-; log_k -31.5; -no_check; -mole_balance S_sOFe(OH)4Na2 # logK for Fe(II) being
oxidized and hydrolized was fitted manually

 # weak a sites
  S_waOH + Fe+2 = S_waOFeCl + H+; log_k -1.7; -no_check; -mole_balance S_waOFeCl    # logK for Fe(II) exchange was from Fe uptake on
natural montmorillonite, EST, 2014
  S_waOH + Fe+2 = S_waOFeCl2 + H+ + e-; log_k -4.0; -no_check; -mole_balance S_waOFeCl2 # logK for Fe(II) being oxidized was fitted
manually

SOLUTION 1
 Na 100;
 Cl 100 charge; # solution component
 #S:L = 1g/L
SURFACE 1; -equil 1; -no_edl
# surface sites capacity
```

```
 S_waOH 4.0e-5
 S_sOH 2e-6
Exchange 1; -equil 1;
# cation exchange capacity
 X 2.25e-4
PHASES 1
 Fix_pH; H+ = H+
PHASES 2
 Fix_pe; e- = e-
EQUILIBRIUM_PHASES
 Fix_pH -11 NaOH
 Fix_pe -2.3998 O2(g)
REACTION 1
 FeCl2 1e-7
```

2 Sorption isotherm

```
DATABASE c:\phreeqc\database\phreeqc.dat
SOLUTION_MASTER_SPECIES
# element   species   alk gfw_formula element_gfw
 Fe       Fe+2     0.0    Fe     55.845

SURFACE_MASTER_SPECIES
 S_s S_sOH      # strong sites on illite, S_sOH for SsOH

 # two type of weak sites, S_waOH for Sw1OH, S_wbOH for Sw2OH
 S_wa S_waOH
 S_wb S_wbOH

SURFACE_SPECIES
# surface species hydrolysis
 S_sOH = S_sOH
 S_sOH + H+ = S_sOH2Cl; log_k 4.0; -no_check; -mole_balance S_sOH2Cl
 S_sOH = S_sONa + H+; log_k -6.2; -no_check; -mole_balance S_sONa

 S_waOH = S_waOH
 S_waOH + H+ = S_waOH2Cl; -log_k 4.0; -no_check; -mole_balance S_waOH2Cl
 S_waOH = S_waONa + H+; -log_k -6.2;  -no_check; -mole_balance S_waONa

 S_wbOH = S_wbOH
 S_wbOH + H+ = S_wbOH2Cl; -log_k 8.5; -no_check; -mole_balance S_wbOH2Cl
 S_wbOH = S_wbONa + H+; -log_k -10.5; -no_check; -mole_balance S_wbONa

SOLUTION_SPECIES
# Fe hydrolysis
  Fe+2 = Fe+2              #;      -gamma 5.26 0.121; -dw 6.9e-10
  Fe+2 + H2O = Fe(OH)+ + H+; log_k -9.1       #; -gamma 5.26 0.121; -dw 6.9e-10
  Fe+2 + 2H2O = Fe(OH)2 +2H+; log_k -20.6  #; -gamma 5.26 0.121; -dw 6.9e-10
  Fe+2 + 3H2O = Fe(OH)3- + 3H+; log_k -34.6                #; -gamma 5.26 0.121; -dw 6.9e-10
  Fe+2 + Cl-  = FeCl+;   log_k -0.1605

EXCHANGE_SPECIES
# cation exchange sites...
  Fe+2 + 2X- = FeX2; -log_k          22.0;       #  logK for Fe(II) exchange was from Fe uptake on natural montmorillonite, EST, 2014
  Na+ + X- = NaX; -log_k 10

SURFACE_SPECIES
 # strong sites
  S_sOH + Fe+2 = S_sOFeCl + H+; log_k 1.9; -no_check; -mole_balance S_sOFeCl  # logK for Fe(II) exchange was from Fe uptake on natural
montmorillonite, EST, 2014
  S_sOH + Fe+2 = S_sOFeCl2 + H+ + e-; log_k -2.2; -no_check; -mole_balance S_sOFeCl2 # logK for Fe(II) being oxidized was fitted manually
  S_sOH + Fe+2 + 3H2O = S_sOFe(OH)3Na + 4H+ + e-; log_k -22.0; -no_check; -mole_balance S_sOFe(OH)3Na # logK for Fe(II) being oxidized
and hydrolized was fitted manually
```

```
  S_sOH + Fe+2 + 4H2O = S_sOFe(OH)4Na2 + 5H+ + e-; log_k -31.5; -no_check; -mole_balance S_sOFe(OH)4Na2 # logK for Fe(II) being oxidized and hydrolized was fitted manually

 # weak a sites
  S_waOH + Fe+2 = S_waOFeCl + H+; log_k -1.7; -no_check; -mole_balance S_waOFeCl    # logK for Fe(II) exchange was from Fe uptake on natural montmorillonite, EST, 2014
  S_waOH + Fe+2 = S_waOFeCl2 + H+ + e-; log_k -4.0; -no_check; -mole_balance S_waOFeCl2 # logK for Fe(II) being oxidized was fitted manually

SOLUTION 1
 Na 100;
 Cl 100 charge; #  solution component
PHASES 1
 Fix_pH; H+ = H+
PHASES 2
 Fix_pe; e- = e-
USE SOLUTION 1
EQUILIBRIUM_PHASES 1
 Fix_pH -5 NaOH # pH was fixted at 5
 Fix_pe -5.5432 O2(g) 1 #calculate from pe = 16.9*Eh =16.9*(-0.031pH +0.483),
 SURFACE 1; -equil 1; -no_edl
 # surface sites capacity
 S_waOH 4.0e-5
 S_sOH 2e-6
 Exchange 1; -equil 1;
 # cation exchange capacity
 X 2.25e-4  #
 REACTION
 FeCl2  1
 100*1e-9 100*1e-8 100*1e-7 100*1e-6 100*1e-4 100*1e-3
INCREMENTAL_REACTIONS true
```

3 Impact of Fe(II) on ^{99}Tc diffusion behavior in illite

Ping CHEN[a,b], Sergey V. Churakov[a,b], Martin Glaus[a], Luc Robert Van Loon[a, *]

[a] Paul Scherrer Institut, Laboratory for Waste Management, 5232, Villigen PSI, Switzerland

[b] Institute of Geological science, University of Bern, Switzerland

* corresponding author

Abstract

A comprehensive understanding of the geochemical behavior of ^{99}Tc is of great importance for safe disposal of radioactive waste and remediation of contaminated environmental sites. Illite is one of the most common constituents of clay rocks, and thus used in this work as a model system for studying the retention and transport of ^{99}Tc in clay-rich systems. In this study, a through-diffusion technique was applied to investigate the diffusion behavior of Tc in compacted illite clay under oxic and anoxic conditions. Particular focus of this investigation was on the role of Fe(II) on the redox state and mobility of Tc in clay. As the diffusion cells contained stainless steel filters for confining the clay plug, ^{99}Tc-diffusion in the filters was assessed first, followed by ^{99}Tc diffusion in the illite column with or without Fe-loading. Two types of Fe(II) loadings in illite were considered, surface complexed Fe(II) on illite edge sites and Fe(II) added as pyrite grains. COMSOL Multiphysics was used to analyze the diffusion data. The measured filter porosity was about 0.2 and the effective diffusion coefficient, D_e, for Tc (as TcO_4^-) in the filter was 0.59×10^{-10} m^2/s. Tc diffusion in illite under ambient conditions showed a typical anion diffusion behavior with D_e in the range $0.38\text{-}0.44\times10^{-10}$ m^2/s and the anion accessible porosity ε of approximately 0.2. In the presence of Fe(II), D_e for Tc migration in illite was one order of magnitude lower, showing that Fe(II) has a significant effect on the migration of ^{99}Tc. Analysis of the Tc distribution in the system suggests that most Tc was retarded at the filters, especially the ones connected to the high concentration reservoir. The remaining Tc quantities were immobilized at sample boundaries next to the filters with higher concentrations observed in the domains close to the reservoirs. Almost no Tc was immobilized in the middle part of the sample, where the Fe(II) was preloaded. This observation contradicts the anticipation, because Tc was expected to be immobilized in the middle of the sample preloaded with Fe(II). A possible explanation is that a delocalized redox reaction may occur, which means that electrons from the oxidation of the preloaded Fe(II) in the central part of the cell are transferred to the filter via the walls of the steel diffusion cell. Tc reacts with the electrons in the filter at a relative slow rate, which results in most of the Tc retarded in the filter, while some small amounts of it may diffuse through the clay.
Key words: Tc diffusion; Fe(II) impact; delocalized redox reaction; Tc retarded.

3.1 Introduction

The safe disposal of nuclear waste is a prerequisite for the further use of nuclear power for energy production. The multi-barrier deep geological waste disposal is an internationally accepted concept in nuclear waste management, especially for the vitrified high-level radioactive waste and spent nuclear fuel (WNA, 2021). Multi-barrier disposal systems comprise engineered barriers, such as the glass solidification matrix, disposal casks and backfill materials, and a natural barrier, which is the host rock. These barriers play an essential role in the long-term safety of a repository. Radionuclides released from the waste matrix will react with barrier materials, diffuse

through the porous barriers around the repository, and may finally reach the biosphere. Depending on the half-life of the radioisotopes, a significant part of the radionuclides will decay to stable nuclei during their migration through the near and far field (Churakov et al., 2020). To assess the repository safety, all involved barriers must be evaluated for their ability and contribution to prevent or retard radionuclides from reaching the biosphere. A lot of attention has been given to the behavior of radionuclides in host rocks (Huber et al., 2017; Li et al., 2012; Neil et al., 2020; Shih et al., 2017; Yang et al., 2018). Clay rocks could be a beneficial host rock for a radioactive waste repository due to a very low hydraulic conductivity, the ability to self-sealing of open cracks and fissures, and the excellent retention of radionuclides (Grambow, 2016; Jlassi et al., 2017). Examples of such clay rocks are the Callovo-Oxfordian Argillite in France (ANDRA, 2001; Bonin, 1998), the Boom Clay in Belgium (ONDRAF/NIRAS., 2001), the Opalinus Clay in Switzerland (Nagra, 2002), and the Horonobe sediments in Japan (Aoki, 2002). These clay rocks are composed of several clay minerals such as illite, smectite, illite/smectite, kaolinite and chlorite, silicates and carbonates.

^{99}Tc is one of the key nuclides in spent nuclear fuel due to its long half-life and its high fission yield in reactors (Lieser, 2008). ^{99}Tc also plays an essential role in the remediation of areas contaminated by the leakage of radioactive waste in short-term storage sites (Zachara et al., 2007b). The mobility of Tc in the environment strongly depends on its redox state. Its most stable species in an oxic environment is pertechnetate, $Tc(VII)O_4^-$, which hardly reacts with or sorbs on natural and engineered materials, resulting in its high mobility in the environment (Um and Serne, 2005; Zachara et al., 2007a). Under reducing conditions, Tc will be reduced to Tc(IV), which can be retarded by forming TcO_2-like clusters (Fredrickson et al., 2009; Morris et al., 2008; Peretyazhko et al., 2008) or co-precipitating with Fe oxides (Peretyazhko et al., 2008; Plymale et al., 2011; Zachara et al., 2007a) and/or sulfides (Lukens et al., 2005; Wharton et al., 2000) depending on the reductant. A comprehensive understanding of the behavior of ^{99}Tc in clays is of great importance for evaluating the long-term safety of a repository and the remediation of contaminated environments.

Fe is a ubiquitous reducing agent in nature. Fe(II) was shown to be an active reductant in the environment for redox-sensitive nuclides (Huang et al., 2021). Fe content in Opalinus Clay (expressed as Fe_2O_3) was measured to be about 6.5 wt.% (Wu et al., 2009). The corrosion of engineered materials is another important iron source in a deep geological repository. Thus, it is necessary to investigate the impact of Fe(II) on ^{99}Tc behavior in clay. The behavior of ^{99}Tc in crushed clay minerals such as nontronite (Jaisi et al., 2009; Shi et al., 2016; Yang et al., 2012), montmorillonite (Bishop et al., 2011; Huber et al., 2015; Norrfors et al., 2016) and smectite (Qafoku et al., 2017), and the influence of Fe have been widely investigated in batch experiments. To the best of our knowledge, the behavior of Tc in illite - a major clay mineral in many clay rocks - and the influence of Fe on its diffusion behavior in compacted illite have not been studied so far. In this study, the diffusive mobility of Tc in natural compacted illite and the impact of Fe on the diffusion process was investigated. Two types of Fe(II)-loaded illite were used: Fe(II) sorbed on the surface of illite and Fe(II) added as pyrite grains. To assess the transport relevant parameters of the diffusion cell, the diffusion of tritiated water (HTO) and Tc through stainless steel filters were measured prior to the diffusion experiments through illite samples. Further, through- and out-diffusion with HTO, which is a non-sorbing species, were performed prior to the diffusion studies of Tc in compacted illite.

3.2 Methods and materials

3.2.1 Illite preparation

The illite used in this study was from Le Puy-en-Velay, France (Gabis, 1958). Samples of illite were treated following a purification protocol as described in Baeyens and Bradbury (2004). The protocol described in Glaus et al. (2010) was applied to remove Ca-phases as much as possible. Details are described in a previous work (Chen et al., 2022). Aliquots of the purified illite were modified with Fe(II) by applying the sorption method. To this end, a MES (2-(N-morpholino)ethanesulfonic acid)-buffer (pH 5)) was prepared in a 0.1 M NaCl solution and transferred into the glove box after purging with N_2. Then, 0.1676 g of $FeCl_2$ solid and 10 g of illite were added to the buffer in the glove box. The mixture was left to equilibrate for more than 3 days on a shaker. After settling down overnight, the supernatant was removed and the modified illite was left to dry in the box. About 30 mmol/kg Fe(II) was loaded on illite by this sorption procedure. According to our previous study (Chen et al., 2022), under these conditions, 100 % of the strong surface complexation sites (S^sOH = 2 mmol/kg) and about 35 % of the weak surface complexation sites (S^wOH = 80 mmol/kg) were loaded with Fe(II). Another aliqout of the illite was mixed with pyrite to reach a content of 8 wt.%. The pyrite was purchased from Huanyala, Peru. The crushed pyrite was leached with 1 M HCl and stirred for more than 24 hours to remove the surface oxidation layer. Subsequently, it was cleaned and dried with acetone. The natural pyrite content of Opalinus Clay is about 1.1 wt% on average, while the total Fe content is about 6-7 wt% (calculated as Fe_2O_3) (Wu et al., 2009). All chemicals used were of suprapur grade quality.

3.2.2 Diffusion experiments with stainless steel filters

Stainless steel filters were used in the experiments (stainless steel: 316 L, pore diameter: 10 µm, diameter: 25.4 mm, thickness: 1.62 mm). Some basic properties of the filters were measured and listed in Table S1 and Table S2 for HTO and Tc diffusion, respectively. The porosity of the filters were measured by the weight difference before and after saturating the filters with Milli-Q water.

A special cell developed by Glaus et al. (2008), as shown in Figure S1 (supporting information), was used to carry out diffusion of tracers through the filters and to evaluate their diffusion parameter values. The porous filter was placed between two reservoirs. Advective tracer transport was prevented by the use of FKM (fluoroelastomer) flat seals (Angst + Pfister, Switzerland) that encased the filters. About 100 mL of 0.1 M NaCl were added as electrolyte solution to both reservoirs. The solution was left to saturate the filters for more than 12 hours to remove any air trapped in the pores of the filters. Tracers were added to the source reservoir. Magnetic stirrers were used to maintain instantaneous mixing in both reservoirs. Samples from both reservoirs were taken for activity measurements of HTO and ^{99}Tc at given time intervals. Activities were measured by a Packard Tri-carb 3170TR/SL liquid scintillation counter (PerkinElmer, U.S), using Ultima Gold XR (PerkinElmer, U.S) as scintillation cocktail. The breakthrough curve for each tracer was obtained by plotting the accumulated activity or mass in the target reservoir as a function of time. Five parallel experiments for both HTO and $^{99}TcO_4^-$ were performed to improve the accuracy of the measurements and to estimate the uncertainties.

As stated in Aldaba et al. (2014) and Glaus et al. (2008), the initial phase (up to 6 hours) of the breakthrough curve of a tracer can be treated as being pseudo-linear because the concentration in the source reservoir did not change significantly during this time span. *De*, effective diffusion coefficients of a tracer diffusing through the filter were calculated by equation 1:

$$D_e = \frac{\alpha d}{S C_0} \quad (1)$$

Where α (mol/s) is the slope of the linear part of the breakthrough curve (linear regression was used to obtain the slope), d (m) is the thickness of the filter, S (m^2) is the cross-sectional area of the filter, C_0 (mol/m^3) is the initial concentration in the source reservoir.

3.2.3 Diffusion experiments with compacted illite

The through-diffusion of ^{99}Tc (pertechnetate, TcO_4^-) was performed both under oxic and anoxic conditions. The diffusion setup and experimental procedures were the same as those used for through-diffusion experiments by Van Loon et al. (2003). A schematic drawing of the diffusion setup is shown in Figure S2 in the supporting information. The illite sample was compacted in a sample holder and sandwiched by two stainless steel filter plates (stainless steel: 316 L, pore diameter: 10 µm, diameter: 25.4 mm, thickness: 1.62 mm). After closing the cells with two end plates, the cells were connected to two reservoirs containing 0.1 M NaCl. In order to avoid the loaded Fe diffusing out from the column and reacting with Tc in the reservoirs, Fe-loaded illite was sandwiched between pretreated illite. The thickness of the Fe-loaded illite was 2 mm and that of the pretreated illite two times 4 mm. The compacted illite was initially saturated with 0.1 M NaCl for one month. Then, through-diffusion of HTO was performed. To this end, about 300 Bq/ml of HTO were added to the high-concentration reservoir. As soon as a steady-state was reached, out-diffusion of HTO was started by changing the HTO solution with HTO-free 0.1 M NaCl solution at both sides of the diffusion cell. After all HTO had diffused out of the illite, diffusion of ^{99}Tc was conducted. To this end, about 300 Bq/ml TcO_4^- were added to a 0.1 M NaCl solution and connected to the high-concentration reservoir. The solutions in the downstream reservoir were changed regularly to keep the tracer concentration at a low level resulting in a maximum concentration gradient. The tracer concentration of HTO and ^{99}Tc in both reservoirs were measured by liquid scintillation counting (LSC) using a Packard Tri-carb 3170TR/SL liquid scintillation counter (PerkinElmer, U.S), with Ultima Gold XR (PerkinElmer, U.S) as scintillation cocktail. A summary of the diffusion systems and conditions is given in Table 1.

Table 1: Effective diffusion coefficient, D_e and ε of filter for HTO and Tc diffusion.

Filter propertys	HTO	Tc
C_0 (10^{-7} mol/m^3)	1.528 ± 0.079	2.331 ± 0.008
d (cm)	0.1633 ± 0.0007	0.1606 ± 0.0023
S (cm^2)	5.061 ± 0.008	5.054 ± 0.016
ε	0.205 ± 0.003	0.212 ± 0.005
[a] D_e (10^{-10} m^2/s)	0.966 ± 0.107	0.589 ± 0.095
[b] D_e (10^{-10} m^2/s)	1.06 ± 0.11	0.585 ± 0.060

[a] values calculated according to equation 1

[b] values obtained from COMSOL modelling

After Tc-diffusion, the illite column was removed from the diffusion cell and the Tc diffusion profile determined. The columns were sliced into 60 slices, 200 µm thick slices in the pretreated Fe-free illite and 100 µm thick slices in the Fe-loaded illite. The sliced illite and the filters were extracted by 1 M HNO_3 for 2 days.

Then, the extracted solutions were analyzed for ^{99}Tc by LSC.

3.2.4 Diffusion modelling with COMSOL Multiphysics

COMSOL Multiphysics was used to fit the flux and the amount of accumulated tracer in the downstream reservoir. COMSOL Multiphysics is a cross-platform finite element analysis, solver and multiphysics simulation software. It is a convenient tool for solving coupled partial differential equations. A general equation for tracer diffusion in porous media can be written as follows:

$$\frac{\partial(\theta c_i)}{\partial t} + \frac{\partial(\rho c_{P,i})}{\partial t} + \frac{\partial(a_V c_{G,i})}{\partial t} + u \cdot \nabla c_i = \nabla \cdot \left[\left(D_{D,i} + D_{e,i}\right)\nabla c_i\right] + R_i + S_i \qquad (2)$$

where c_i (mol/m^3) is the molar concentration of species i in the pore solution, $c_{P,i}$ (mol/kg) the amount adsorbed onto solid particles, $c_{G,i}$ (mol/m^3) is the concentration of species i in the gas phase, ε_p represents the porosity, θ and a_V are the liquid volume fraction and the gas volume fraction, respectively, and they are unitless. ρ (kg/m^3) is the matrix density defined as $\rho = (1 - \varepsilon_p)/\rho_p$, with ρ_p (kg/m^3) being the solid density. u (m/s) is the mass averaged velocity vector. D_D (m^2/s) is the dispersion tensor, R_i (mol/m^3/s) is the reaction rate and S_i (mol/m^3/s) source term.

In this study, there is no other tracer source, no advection, and dispersion. The porous media, illite, is saturated, which leads to $\theta = \varepsilon_p$, $u = 0$, and $D_D = 0$. Therefore, equation 2 can be simplified to:

$$\frac{\partial(\varepsilon_p c_i)}{\partial t} + \frac{\partial(\rho c_{P,i})\big)}{\partial t} = \nabla \cdot \left[\left(D_{e,i}\right)\nabla c_i\right] + R_i \qquad (3)$$

Since the filters have a disc shape, diffusion of HTO and Tc through the filter in the cell (Figure S1) can be treated as a 1D model. A mean value of porosity, density, cross section area, and thickness for filters was used in the model (values listed in Table 1). Reservoirs at the up and downstream were represented by a 1D interval with length L (m) equal to V/S, where V (m^3) is the volume of the reservoir solution and S (m^2) is the cross section of the filter. A high value (1×10^{-3} m^2/s) was assigned to the diffusion coefficient of the tracers in the reservoirs to mimic fast mixing in the solution. The D_e was optimized manually to give a best fit of the experimental data.

The setup of the COMSOL model for tracer diffusion through clay is shown in Figure 1.

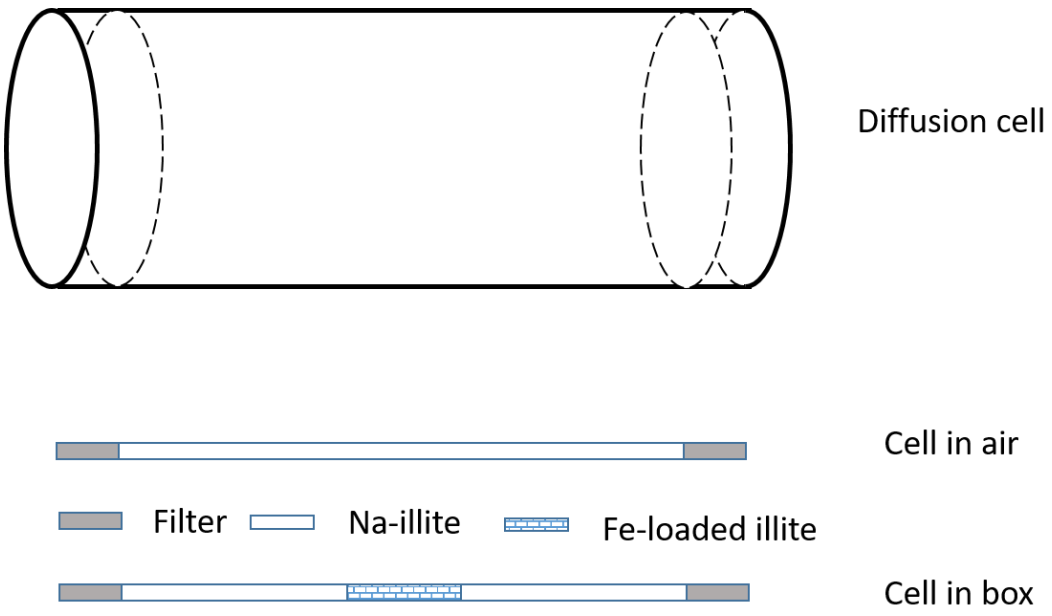

Figure 1: 1D COMSOL model configuration.

The initial condition in the experiment corresponds to a zero-tracer concentration inside the filter and clay column. The boundary condition is the monitored tracer concentration at the high concentration reservoir, and a zero concentration at the downstream reservoir. The flux and the accumulated mass at the downstream reservoir, were fitted keeping all parameters constant except D_e and the rock capacity factor, ($\alpha = \varepsilon + \rho K_d$, where ρ is the bulk dry density and K_d is the distribution coefficient for tracer). A code developed with COMSOL and Matlab was used to optimize these two parameters.

For modeling of Tc diffusion through Fe(II)-loaded illite, the D_e and α for Na-illite obtained above were used as fixed parameters. The D_e and α for Fe(II)-loaded illite were the only fitting parameters.

3.3 Results and discussion

3.3.1 Diffusion of HTO and Tc through filters

To have a good statistical estimate for HTO and Tc diffusion in the filters, five independent experiments were conducted for each tracer using different filter samples from the same delivery batch. Figure 2 shows the accumulated amount of tracer in the target reservoir and the concentration in the source reservoir for one of the filters (the other results are shown in the supporting information in Figure S3 and Figure S4). As shown in Figure 2, the concentration in the source reservoir decreased slightly (less than 3% for HTO diffusion and less than 2% for TcO_4^- diffusion). The breakthrough curve in the downstream reservoir increased linearly in the initial phase (6 h in HTO diffusion, 7 h for Tc diffusion) with R^2 (the coefficient of determination, which indicates the goodness of regression analysis) around 0.99 for HTO diffusion and 0.97 for Tc diffusion. The effective diffusion coefficient of HTO and Tc diffusion in the filter were calculated according to equation 1, the porosity was measured by the weight method described in previous section. The averaged transport parameters for the filters obtained in 5 independent samples are listed Table 1. The individual parameters derived for each filter sample are listed in the

supporting information in Table S1 and Table S2.

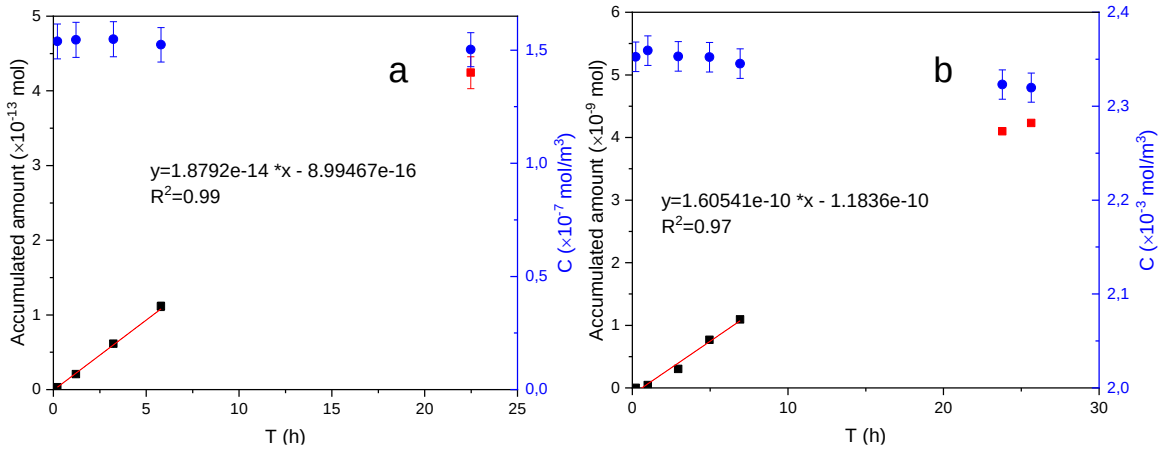

Figure 2: Accumulated amount of tracer (rectangles) in the target reservoir and its concentration (bullets) in the source reservoir for a) HTO and b) Tc diffusion experiments with filters alone. Red points are experimental data that were not used in the regression analysis. The error bars represent the uncertainties caused by all measurements involved in the experiment.

The mean value for the D_e(HTO) in the filter is $(0.966 \pm 0.107)\times10^{-10}$ m^2/s, which is close to the value 1.1×10^{-10} m^2/s reported by Aldaba et al. (2014) for the same filter type while using the same diffusion technique. The small differences are within the measurement uncertainties. This could be confirmed by analyzing the differences in filter porosity obtained from diffusion experiments with Tc and HTO using the same filter type. The D_e(Tc) in filters has been measured for the first time. These data are essential for the further investigations of Tc migration in clay rock, where stainless steel filters are usually used for confining the clay.

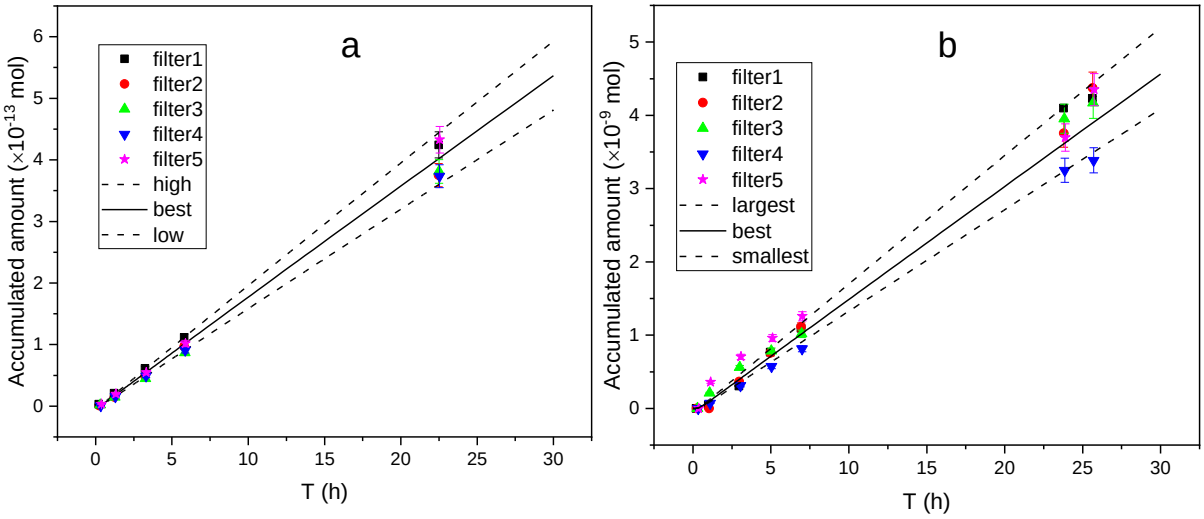

Figure 3: Accumulated mass of a) HTO and b) Tc in the downstream reservoir. Symbols represent experimental data and the curves are the COMSOL modeling result. The error bars represent the uncertainties caused by all measurements involved in the experiment.

As mentioned in section 2.2, at the initial phase, the accumulated mass in the downstream reservoir increased linearly. As shown in Figure 3, the modelling results agree well with the experimental data. The effective diffusion efficient of HTO and Tc obtained for different filters were in the range (0.95-1.17)×10^{-10} m^2/s and (0.525-0.645)×10^{-10} m^2/s, respectively. The best-fit value for HTO diffusion coefficient in the filter is 1.06×10^{-10} m^2/s, which is almost identical to the value obtained by Aldaba et al. (2014). This value is slightly larger than the one calculated with equation 1. These differences might result from the parameter values used. Respective values for porosity, cross section area, thickness and initial concentration were used to calculate the effective diffusion coefficient with equation 1. In the COMSOL model, mean values of porosity, density, cross section area and thickness were used as fixed parameters. However, within the uncertainty, the effective diffusion coefficient of HTO in stainless steel filters is consistent with literature values. Therefore, the value of D_e = 0.585×10^{-10} m^2/s for Tc diffusion in stainless steel filters was used in the modelling of Tc migration in compacted system in the filter-clay-filter sandwich setup.

3.3.2 HTO diffusion through compacted illite

Due to the symmetry of the diffusion cell, the diffusion experiment can be interpreted using a one-dimensional mathematical model. The theoretical background for the diffusion modelling in one-dimensional through- and out-diffusion setup is described in detail in Van Loon et al. (2003). The tracer concentration profile across the clay column is assumed to be linear at steady state. So, the accumulated activity in the downstream reservoir is:

$$A_{dif}^{t} = S \cdot L \cdot C_0 \cdot \left(\frac{D_e \cdot t}{L^2} - \frac{\alpha}{6} - \frac{2 \cdot \alpha}{\pi^2} \sum_{n=1}^{\infty} \frac{(-1)^n}{n^2} \cdot \exp\left(-\frac{D_e \cdot n^2 \cdot \pi^2 \cdot t}{L^2 \cdot \alpha}\right)\right) \quad (4)$$

As time increases, it becomes:

$$A_{dif}^{t} = S \cdot L \cdot C_0 \cdot \left(\frac{D_e \cdot t}{L^2} - \frac{\alpha}{6}\right) \quad (5)$$

Where S is the cross-section area of the clay column (m^2), L is the length of the column (m), C_0 is the concentration of tracer at the upstream boundary, (mol/m^3), D_e is the effective diffusion coefficient, (m^2/s), and α is the rock capacity factor. It is obvious from equation 5 that the accumulated activity at the downstream boundary linearly increases at steady state.

The obtained D_e and α from through-diffusion were used to predict the flux at both boundaries during out-diffusion. The diffusive fluxes at both boundaries (Van Loon et al., 2003) are:

At x=0, $$J(0,t) = 2 \cdot C_0 \cdot \frac{D_e}{L} \cdot \sum_{n=1}^{\infty} exp^{-\left(\frac{n \cdot \pi}{L}\right)^2 \cdot \frac{D_e}{\alpha} \cdot t} = 2 \cdot J_L \cdot \sum_{n=1}^{\infty} exp^{-\left(\frac{n \cdot \pi}{L}\right)^2 \cdot \frac{D_e}{\alpha} \cdot t} \quad (6)$$

and

At x=L, $$J(L,t) = 2 \cdot C_0 \cdot \frac{D_e}{L} \cdot \sum_{n=1}^{\infty} (-1)^n \cdot exp^{-\left(\frac{n \cdot \pi}{L}\right)^2 \cdot \frac{D_e}{\alpha} \cdot t} = 2 \cdot J_L \cdot \sum_{n=1}^{\infty} (-1)^n \cdot exp^{-\left(\frac{n \cdot \pi}{L}\right)^2 \cdot \frac{D_e}{\alpha} \cdot t} \quad (7)$$

The experimental data and the model fit well and the derived diffusion parameters from through- and out-diffusion

of HTO under atmospheric conditions are in good agreement as shown in Figure 4 and Table 2, respectively. Using the same values of D_e and α, we were able to reproduce the observed fluxes at both boundaries in the out-diffusion experiments, which increases the credibility in the model and the experimental setup. The effective diffusion coefficient of HTO is consistent with the literature value (range from $(1.06 \pm 0.12)\times10^{-10}$ m^2/s to $(1.65 \pm 0.07)\times10^{-10}$ m^2/s in this study; $(1.30 \pm 0.30)\times10^{-10}$ m^2/s in Glaus et al., 2010). It has to be noted that a discrepancy is observed in Figure 4c between the modelled and experimental data for HTO out-diffusion in a 1 cm illite cell. The reason for this discrepancy may be the longer time span for taking the first sample.

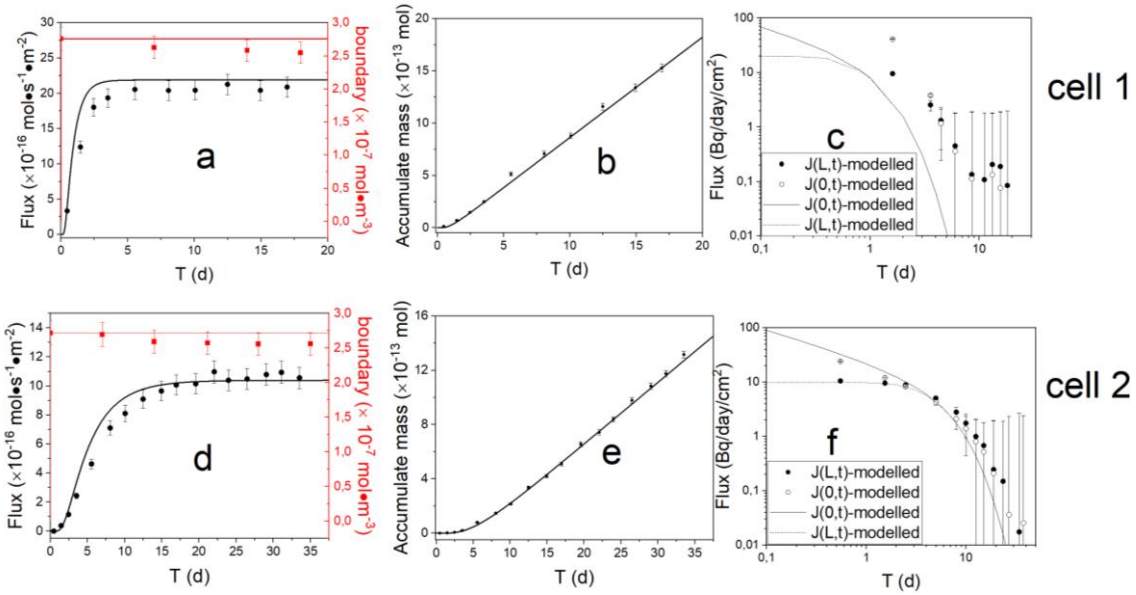

Figure 4: Experimental data (symbols with error bar) and fitted data (curves) of HTO in through- and out-diffusion experiments. Through-diffusion data are fitted with COMSOL Multiphysics. Out-diffusion is modelled with equations 6 and 7 using parameters (D_e and α) from through-diffusion. a) and d) are the tracer concentrations (red) in the source reservoir and flux (black) in the downstream reservoir. b) and e) are the accumulated tracer masses in the downstream reservoir. c) and f) are the flux at both boundaries in out-diffusion. a, b and c are data for cell with 1 cm length, while d, e and f are those for the 3 cm cell. The error bars represent the uncertainties caused by all measurements involved in the experiment.

The data for HTO diffusion conducted in the glove box under N_2 atmosphere is shown in the supporting information in Figure S5. The α has a significant influence on the flux in the out-diffusion. A larger α value could better reproduce the flux at times beyond 2 days (or at a later stage). Nevertheless, a α value of approximately 0.3 could basically fit the through- and out-diffusion data for HTO in cell 1 and cell 2.

Table 2: Overview of the diffusion fitting results.

	Cell 1	Cell 2	Cell 3	Cell 4	Cell 5	Cell 6
Bulk dry density (g/cm^3)	1.72 ± 0.01	1.71 ± 0.01	1.72 ± 0.01	1.71 ± 0.01	1.71 ± 0.01	1.71 ± 0.01
Column length (cm)	1	3	1	1	1	1
Experimental conditions	In Air	In Air	N_2-atm.	N_2-atm.	N_2-atm.	N_2-atm.
Fe-loaded	No	No	Yes (sorbed)	Yes (sorbed)	Yes (pyrite)	Yes (pyrite)

HTO	D_e ($\times 10^{-10}$ $m^2 s^{-1}$)	1.06 ± 0.12	1.29 ± 0.07	1.50 ± 0.08	1.65 ± 0.07	1.57 ± 0.08	1.11 ± 0.05
diffusion	α	0.31 ± 0.08	0.33 ± 0.03	0.12 ± 0.12	0.19 ± 0.15	0.19 ± 0.19	0.15 ± 0.15
Tc	D_e ($\times 10^{-12}$ $m^2 s^{-1}$)	38.1 ± 2.60	44.5 ± 1.20	1.12 ± 0.05	0.50 ± 0.03	0.46 ± 0.04	0.75 ± 0.05
diffusion	α	0.16 ± 0.02	0.18 ± 0.02	0.05 ± 0.03	0.40 ± 0.02	0.45 ± 0.03	0.05 ± 0.02

3.3.3 Tc diffusion through compacted illite

The diffusion of Tc was performed after out-diffusion of HTO, using the same illite samples. Similar to HTO, the effective diffusion coefficient, D_e, and the rock capacity, α (listed in Table 2), were obtained by modelling with COMSOL Multiphysics. The experimental data and modelling results under oxic conditions are shown in Figure 5.

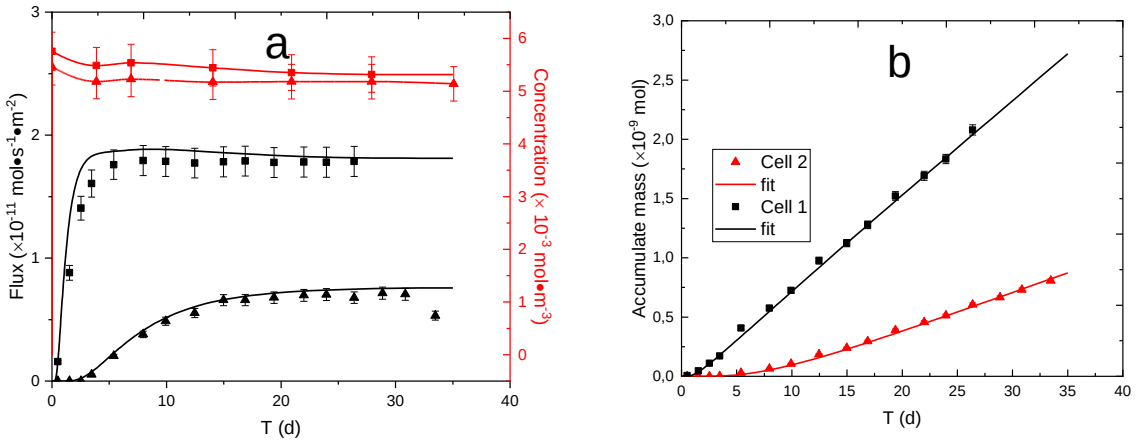

Figure 5: The measured and modelled flux, the evolution of concentration in the high concentration reservoir (a) and accumulated mass in the downstream reservoir (b) under oxic conditions. The error bars represent the uncertainties caused by all measurements involved in the experiment.

In the case of ^{99}Tc diffusion in illite under oxic conditions, the flux and total accumulated mass curves show a typical through-diffusion behavior, i.e. both the flux and total accumulated mass go through two stages, a transient stage at the beginning of the experiment and a steady-state stage later on. The tracer concentration profile is linear in a homogeneous and isotropic porous medium at steady state, and the flux is proportional to the concentration gradient (Van Loon and Soler, 2003). This means that the longer the column, the smaller the flux at the lower boundary, which is shown in Figure 5a. It is reasonable that more time is needed for diffusion through a longer column. Compared to HTO diffusion, the D_e(Tc) under air atmosphere is one order of magnitude smaller and the α is also smaller by a factor of approximately 2 (shown in Table 2), independent on the length of the clay plug. Because pertechnetate (TcO_4^-) is known as weakly or not reacting with clays under oxidizing conditions, the smaller D_e and α values are most probably because of the negative charge of illite and pertechnetate, leading to anion exclusion effects. As a result, the diffusion accessible porosity for TcO_4^- in illite is lower compared to the one of HTO. Also, the effective diffusion coefficient is lower because of anion exclusion. A similar reduction of effective diffusion coefficients of anions compared to HTO was observed for diffusion of $^{36}Cl^-$ and $^{125}I^-$ through Opalinus clay (Van Loon et al., 2003). The bigger diameter of pertechnetate results in a lower water diffusion coefficient, $D_{0,\,TcO4}$ = 1.95 x 10^{-9} m^2 s^{-1} 25 °C (Sato et al., 1996) compared to $D_{0,HTO}$ = 2.20 x 10^{-9} m^2 s^{-1} 25 °C (Li

and Gregory, 1974) which may further contribute to a slower diffusion in illite compared to HTO. The length of the clay column has only a small influence on the value of D_e and α for both HTO and Tc. Therefore, Tc diffusion experiments under anoxic conditions were carried out only on 1 cm clay columns.

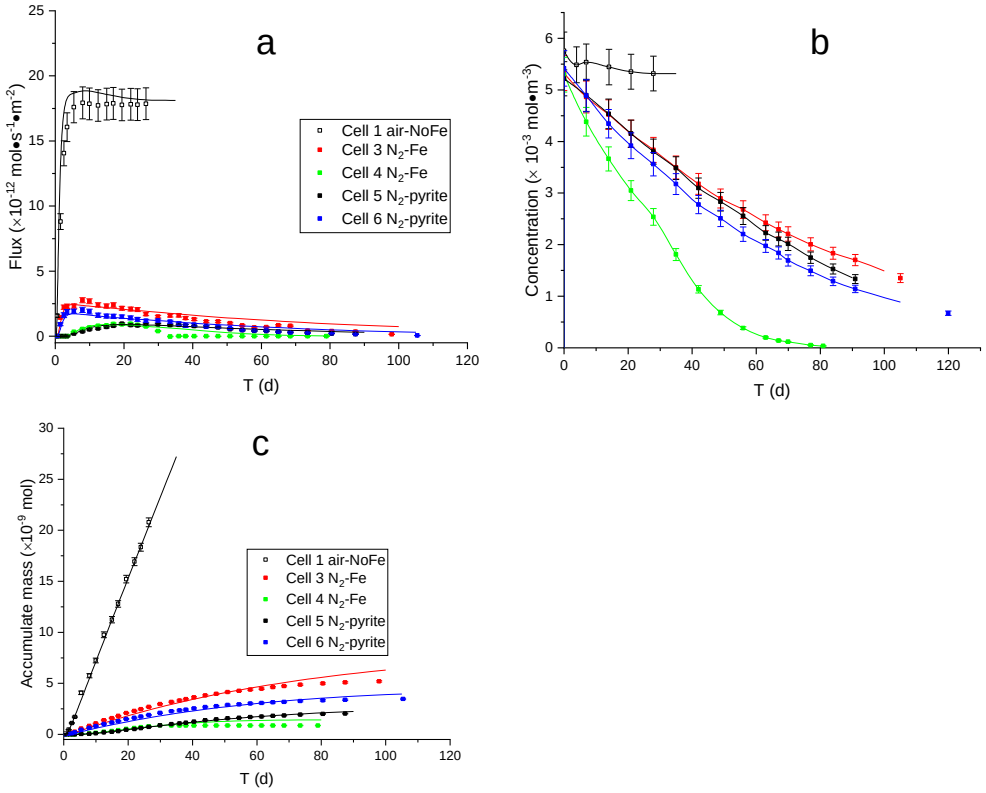

Figure 6: The measured and modelled flux (a), the evolution of concentration in the high concentration reservoir (b) and accumulated mass in the downstream reservoir (c). The error bars represent the uncertainties caused by all measurements involved in the experiment.

As shown in Figure 6, a significant difference was observed for Tc diffusion under oxic and anoxic conditions. The flux is about one order of magnitude smaller for diffusion under anoxic conditions compared to that under oxic condition. The flux pattern is also different showing no typical steady-state stage (Figure 6a for cell 3, 4, 5 and 6) compared to diffusion under oxic conditions. The flux increases initially non-linearly, reaching a maximum and then decreases towards zero. This can be explained by the evolution of Tc concentration in the high concentration reservoir that was decreasing continuously almost to zero. At oxic conditions and in the absence of Fe(II), there is only a slight decrease in the concentration of ^{99}Tc in the high concentration reservoir (Figure 6b, cell 1). The accumulated mass increases non-linearly at a lower rate and finally stops increasing and stays at a constant level, indicating that there is no further mass transfer (Figure 6c, cell 3, 4, 5, 6). As shown in Table 2, D_e for Tc diffusing in presence of Fe(II), are about one or two orders of magnitude smaller than in absence of Fe(II). Theoretically, D_e is related to porosity (in which the tracer diffuses), tortuosity (accounts for path lengthening), and constrictivity (accounts for a variation of the pore diameter along the diffusion pathway) according to:

$$D_e = D_w \cdot \varepsilon \frac{\delta}{\tau^2} \quad (8)$$

Where D_w represents the diffusion coefficient in bulk water, ε is the porosity, δ the constrictivity, and τ the tortuosity. Preloading of illite with Fe(II) should not have a significant effect on these 3 factors. This means that D_e and ε for diffusion of Tc in the Fe-loaded illite is expected to be similar to those in natural illite. According to Fick's first law, the diffusive flux is proportional to the concentration gradient, D_e representing the proportionality factor. In the COMSOL model, the filter is assumed to have no influence on Tc migration. So, the concentration gradient of Tc in clay is calculated from the concentration of Tc in the source reservoir. Thus, the observed low flux in the experiment can only be fitted when a low diffusion coefficient and porosity value is assumed. Based on the observation that a large amount of Tc was measured in the filter in contact with the source reservoir, it has to be assumed that the concentration of TcO_4^- in the filter is much lower than in the source reservoir, leading to a much lower concentration gradient in the clay. With such an assumption, the effective diffusion coefficient would be much higher. A detailed description of this process is given in the following section. Note that the values for the rock capacity factor α also show a significant difference for diffusion experiments conducted under air and under anoxic conditions. The diffusion parameters for the diffusion of HTO, which is a non-sorbing tracer, shows slightly different parameter values for diffusion of Tc in oxic and anoxic conditions. However, in view of the uncertainties on these parameters, the differences are not significant.

3.3.4 Tc distribution in the illite samples

Modeling of the Tc distribution in the illite column might help to understand the diffusion process of Tc in the Fe-loaded illite. Therefore, the Tc concentration profile in the illite column was measured immediately after finishing the diffusion experiments. As shown in Table 3, it was observed that approximately 96% of Tc was located in the filter at the source reservoir, while only 2% of Tc was found in the filter close to the target reservoir. The total mass loss of Tc in the source reservoir is slightly lower than the mass of Tc found in the filters, the clay plug and the target reservoir. This is probably due to the uncertainty of the measurements and analytical procedures. The tracer distribution in the illite column as shown in Figure 7 indicated only trace amounts of Tc in the clay column. A closer inspection of the profile reveals that Tc is more likely to be immobilized at both boundaries of the clay column, with higher concentrations observed at the high concentration reservoir. This observation is more pronounced in samples with Fe(II) loaded by the sorption method. Adsorbed Fe(II) seems to be more readily available for Tc reduction than Fe(II) present as pyrite. In the middle part of the clay column (at 4-6 mm), where Fe(II) was introduced before starting the diffusion, almost no Tc is observed. This is somewhat surprising, because the presence of Fe(II) should enhance Tc immobilization, resulting in significant higher Tc concentrations in the Fe-loaded clay phase.

Table 3: Mass balance of Tc calculated for diffusion cell 5.

	Loss or increase in mass (mol)	Total (mol)	Percentage (%)
Loss of Tc in the source reservoir	3.90×10^{-7}	3.90×10^{-7}	

Tc in filter at upstream	4.03 x 10^{-7}		95.87
Tc in clay	7.11 x 10^{-10}		0.17
Tc in filter at downstream	9.18 x 10^{-9}	4.20 x 10^{-7}	2.19
Mass of Tc accumulated in target reservoir	2.05 x 10^{-9}		0.49
Loss of Tc by sampling in source reservoir	5.40 x 10^{-9}		1.29

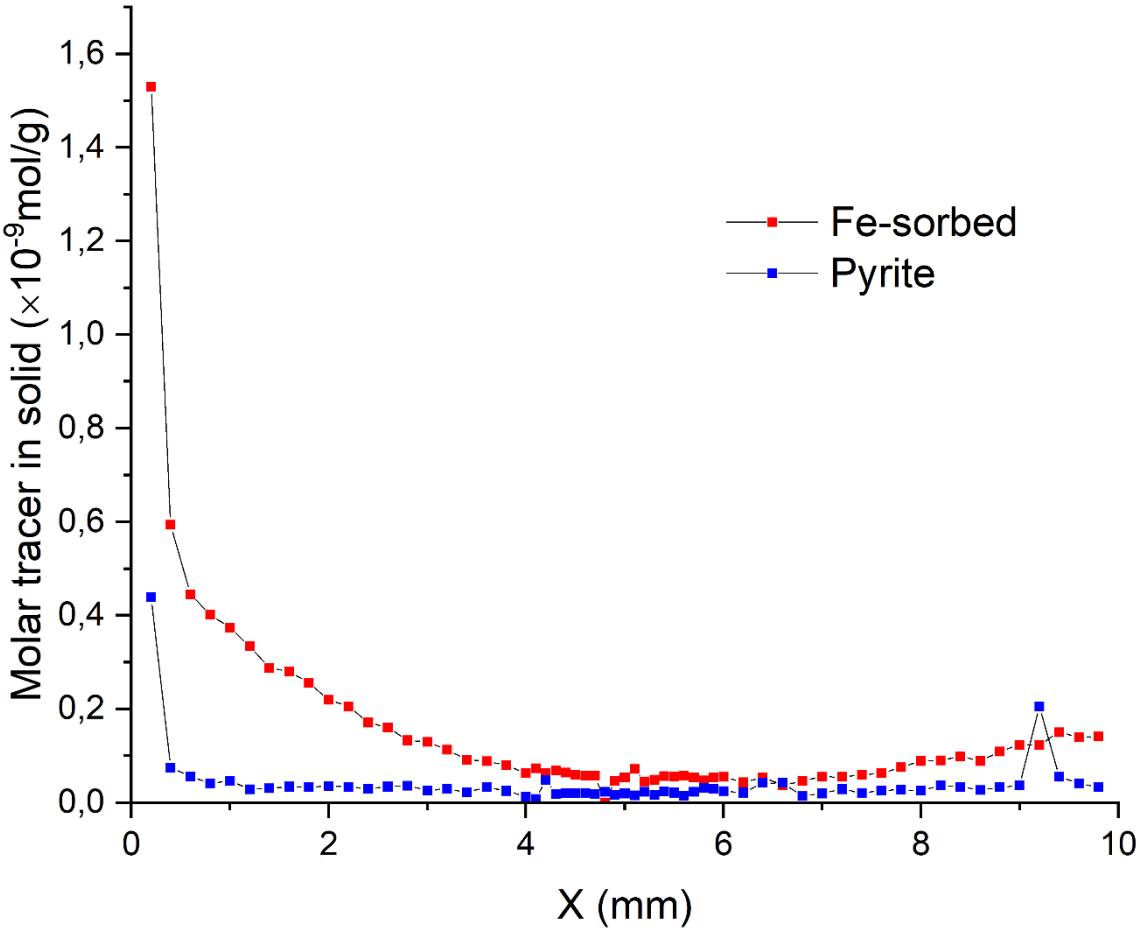

Figure 7: The Tc distribution in Fe(II)-loaded illite after diffusion in the glove box. Two types of Fe(II) was loaded, Fe-sorbed and pyrite (red and blue).

One possibility is that the Fe(II) present in the middle part of the cell diffused towards the filters and reservoirs and reduced Tc(VII) to Tc(IV). However, this is unlikely to occur because we showed in a recent publication (Chen et al., 2002) that Fe(II) strongly sorbs on the illite surface. Scoping calculations using this sorption model indicated that Fe(II) did not sifgnificantly desorb and diffuse towards the filters during the resaturation phase. Another possibility is that a delocalized redox reaction might occur in the diffusion cell. This means that the reduction and oxidation occurs at different places similar to what happens in steel corrosion. In this study, electrons produced from the oxidation of preloaded Fe(II) might be transferred via the walls of the steel diffusion

cell to the filters. Then TcO_4^- reacts with the electrons and precipites as TcO_2 in the filter. Because the reaction between Tc and Fe(II) is relatively slow, a small amount of Tc was not reduced and was able to migrate as TcO_4^- through the illite.

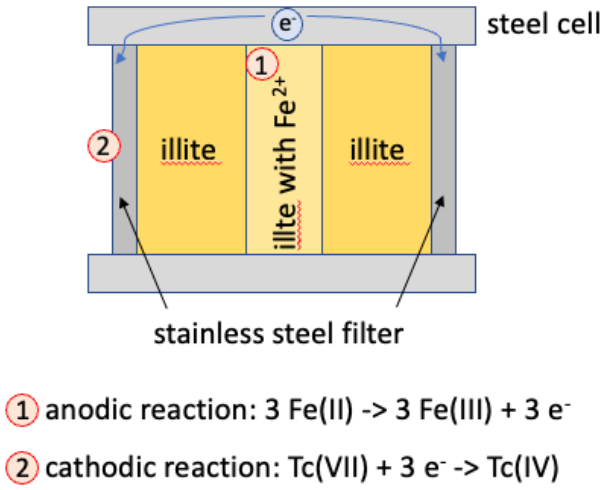

Figure 8: Sketch of the diffusion cell showing the locations where oxidation and reduction reactions take place. Due to the use of steel cells, electrons from the oxidation reaction of Fe^{2+} in the central part of the illite clay plug can be transferred via the walls of the steel cell to the steel filters where reduction of TcO_4^- can occur.

3.4 Conclusions

The properties of Tc diffusion in stainless filters were measured for the first time. The results show that the filter has an anion accessible porosity of about 0.2 and the D_e for Tc in the filter is 0.59×10^{-10} m^2/s. The influence of Fe(II) on Tc-diffusion in illite was investigated by a through-diffusion technique. HTO diffusion was used to check the correct performance of the diffusion cells. The measured porosity and D_e values were in agreement with values reported in an earlier study. Tc-diffusion in natural illite without Fe(II) was performed under oxic conditions at two different lengths of the illite column and diffusion in Fe(II)-loaded illite was performed under anoxic conditions in a N_2 glove box. Two types of Fe(II)-loading were studied, i.e. Fe(II) sorbed on weak and strong sites by surface complexation and Fe(II) added as pyrite. The first type of Fe(II) corresponds to Fe(II) from the corrosion of mainly canister materials and pyrite represents the main Fe(II) source in clay rocks. Compared to HTO, the effective diffusion coefficient of Tc is smaller, which suggests that Tc diffuses as an anion (TcO_4^-) in illite. The length of the illite column has no or only a minimal impact on Tc diffusion, resulting in similar D_e and α values. The effective diffusion coefficient of Tc in Fe(II)-loaded illite is about an order of magnitude smaller than in illite without Fe(II). The concentration profile of Tc in illite that was preloaded with Fe(II) as sorbed Fe or present in pyrite showed an anomalous behavior. No significant effect of Fe(II) on the concentration of Tc in the illite could be observed. Moreover, 96% of the Tc was immobilized in the confining filter at the source reservoir boundary. This suggests that delocalized redox reactions might occur in diffusion cell so that electrons

from the oxidation of the preloaded Fe(II) was transferred to the filter via the walls of the steel diffusion cell and Tc was probably reduced and immobilized before reaching the clay column. For further diffusion studies, diffusion cells made of non-conductive materials should be used.

Declaration of competing interest

Acknowledgements

This research is financially supported by the China Scholarship Council (CSC). The experiments were carried out at the Paul Scherrer Institut in the Laboratory for Waste Management. We acknowledge Petar Bunic and Sabrina Frick for their assistance with the diffusion experiments.

References

Aldaba, D., Glaus, M., Leupin, O., Van Loon, L., Vidal, M., Rigol, A., 2014. Suitability of various materials for porous filters in diffusion experiments. Radiochimica Acta 102, 723-730.

ANDRA, 2001. Référentiel géologique du site de Meuse/Haute Marne. Rapp. A RP ADS 99-005. Agence nationale pour la gestion des déchets radioactifs (Andra), Châtenay-Malabry, France.

Aoki, K., 2002. Recent activities at underground research laboratories in Japan. Proceedings of the International Symposium NUCEF 2001, Tokai, Ibaraki, Japan. JAERI-Conf 2002-004.

Baeyens, B., Bradbury, M.H., 2004. Cation exchange capacity measurements on illite using the sodium and cesium isotope dilution technique: effects of the index cation, electrolyte concentration and competition: modeling. Clays and Clay Minerals 52, 421-431.

Bishop, M.E., Dong, H., Kukkadapu, R.K., Liu, C., Edelmann, R.E., 2011. Bioreduction of Fe-bearing clay minerals and their reactivity toward pertechnetate (Tc-99). Geochimica et Cosmochimica Acta 75, 5229-5246.

Bonin, B., 1998. Deep geological disposal in argillaceous formations: studies at the Tournemire test site. Journal of Contaminant Hydrology 35, 315-330.

Chen, P., Van Loon, L.R., Fernandes, M.M., Churakov, S., 2022. Sorption mechanism of Fe (II) on illite: Sorption and modelling. Applied Geochemistry 143, 105389.

Churakov, S.V., Hummel, W. and Fernandes, M.M., 2020. Fundamental research on radiochemistry of geological nuclear waste disposal. Chimia, 74(12), pp.1000-1000.

Fredrickson, J.K., Zachara, J.M., Plymale, A.E., Heald, S.M., McKinley, J.P., Kennedy, D.W., Liu, C., Nachimuthu, P., 2009. Oxidative dissolution potential of biogenic and abiogenic TcO2 in subsurface sediments. Geochimica et Cosmochimica Acta 73, 2299-2313.

Gabis, V., 1958. Etude préliminaire des argiles oligocènes du Puy-en-Velay (Haute-Loire). Bulletin de Minéralogie 81, 183-185.

Glaus, M.A., Frick, S., Rossé, R., Van Loon, L.R., 2010. Comparative study of tracer diffusion of HTO, 22Na+ and 36Cl− in compacted kaolinite, illite and montmorillonite. Geochimica et Cosmochimica Acta 74, 1999-2010.

Glaus, M.A., Rossé, R., Van Loon, L.R., Yaroshchuk, A.E., 2008. Tracer diffusion in sintered stainless steel filters: measurement of effective diffusion coefficients and implications for diffusion studies with compacted clays. Clays and Clay Minerals 56, 677-685.

Grambow, B., 2016. Geological disposal of radioactive waste in clay. Elements 12, 239-245.

Huang, J., Jones, A., Waite, T.D., Chen, Y., Huang, X., Rosso, K.M., Kappler, A., Mansor, M., Tratnyek, P.G., Zhang, H., 2021. Fe (II) redox chemistry in the environment. Chemical reviews 121, 8161-8233.

Huber, F., Heck, S., Truche, L., Bouby, M., Brendlé, J., Hoess, P., Schäfer, T., 2015. Radionuclide desorption kinetics on synthetic Zn/Ni-labeled montmorillonite nanoparticles. Geochimica et Cosmochimica Acta 148, 426-441.

Huber, F.M., Totskiy, Y., Marsac, R., Schild, D., Pidchenko, I., Vitova, T., Kalmykov, S., Geckeis, H., Schäfer, T., 2017. Tc interaction with crystalline rock from Äspö (Sweden): Effect of in-situ rock redox capacity. Applied geochemistry 80, 90-101.

Jaisi, D.P., Dong, H., Plymale, A.E., Fredrickson, J.K., Zachara, J.M., Heald, S., Liu, C., 2009. Reduction and long-term immobilization of technetium by Fe (II) associated with clay mineral nontronite. Chemical Geology 264, 127-138.

Jlassi, K., Krupa, I., Chehimi, M.M., 2017. Chapter 1: Overview: clay preparation, properties, modification. In Clay-Polymer Nanocomposites, Jlassi, K., Chehimi, M.M., Thomas S. (Eds.). Elsevier.

Li, C., Wang, C., Liu, X., Zheng, Z., Wang, L., Zhu, Q., Kang, M., Chen, T., Liu, C., 2012. Effects of ionic strength and humic acid on 99TcO4− sorption and diffusion in Beishan granite. Journal of Radioanalytical and Nuclear Chemistry 293, 751-756.

Lieser, K.H., 2008. Nuclear and radiochemistry: fundamentals and applications. John Wiley & Sons.

Lukens, W.W., Bucher, J.J., Shuh, D.K., Edelstein, N.M., 2005. Evolution of technetium speciation in reducing grout. Environmental Science & Technology 39, 8064-8070.

Morris, K., Livens, F., Charnock, J., Burke, I., McBeth, J., Begg, J., Boothman, C., Lloyd, J., 2008. An X-ray absorption study of the fate of technetium in reduced and reoxidised sediments and mineral phases. Applied Geochemistry 23, 603-617.

Neil, C.W., Telfeyan, K., Sauer, K.B., Ware, S.D., Reimus, P., Boukhalfa, H., Roback, R., Brug, W.P., 2020. Iodine effective diffusion coefficients through volcanic rock: Influence of iodine speciation and rock geochemistry. Journal of Contaminant Hydrology 235, 103714.

Nagra, 2002. Project Opalinus Clay: safety report: demonstration of disposal feasibility for spent fuel, vitrified high-level waste and long-lived intermediate-level waste (Entsorgungsnachweis). Nagra Technical Report NTB 02-05, Nagra, Wettingen, Switzerland.

Norrfors, K.K., Marsac, R., Bouby, M., Heck, S., Wold, S., Lützenkirchen, J., Schäfer, T., 2016. Montmorillonite colloids: II. Colloidal size dependency on radionuclide adsorption. Applied Clay Science 123, 292-303.

ONDRAF/NIRAS 2001. *SAFIR-2 Second Safety Assessment and Interim Report*. Belgian Agency for Radioactive Waste for Enriched Fissile Materials. Report NIROND 2001-06 E.

Peretyazhko, T., Zachara, J.M., Heald, S.M., Jeon, B.-H., Kukkadapu, R.K., Liu, C., Moore, D., Resch, C.T., 2008. Heterogeneous reduction of Tc (VII) by Fe (II) at the solid–water interface. Geochimica et Cosmochimica Acta 72, 1521-1539.

Plymale, A.E., Fredrickson, J.K., Zachara, J.M., Dohnalkova, A.C., Heald, S.M., Moore, D.A., Kennedy, D.W., Marshall, M.J., Wang, C., Resch, C.T., 2011. Competitive reduction of pertechnetate (99TcO4−) by dissimilatory metal reducing bacteria and biogenic Fe (II). Environmental Science & Technology 45, 951-957.

Qafoku, O., Pearce, C.I., Neumann, A., Kovarik, L., Zhu, M., Ilton, E.S., Bowden, M.E., Resch, C.T., Arey, B.W., Arenholz, E., 2017. Tc (VII) and Cr (VI) interaction with naturally reduced ferruginous smectite from a redox transition zone. Environmental Science & Technology 51, 9042-9052.

Sato, H., Yui, M., Yoshikawa, H., 1996. Ionic diffusion coefficients of Cs^{+}, Pb^{2+}, Sm^{3+}, Ni^{2+}, SeO_4^{2-} and TcO_4^{-} in free water determined from conductivity measurements. Journal of Nuclear Science and Technology 33, 950-955.

Shi, B., Liu, K., Wu, L., Li, W., Smeaton, C.M., Beard, B.L., Johnson, C.M., Roden, E.E., Van Cappellen, P., 2016. Iron isotope fractionations reveal a finite bioavailable Fe pool for structural Fe (III) reduction in nontronite. Environmental Science & Technology 50, 8661-8669.

Shih, Y.-H., Tsai, T.-L., Chen, L.-C., Su, T.-Y., Lee, C.-P., Tsai, S.-C., 2017. Determination of sorption and diffusion parameters of ^{99}Tc in crushed granite using through-diffusion experiments. Journal of Radioanalytical and Nuclear Chemistry 311, 1111-1116.

Um, W., Serne, R.J., 2005. Sorption and transport behavior of radionuclides in the proposed low-level radioactive waste disposal facility at the Hanford site, Washington. Radiochimica Acta 93, 57-63.

Van Loon, L., Soler, J., Bradbury, M., 2003. Diffusion of HTO, $^{36}Cl^{-}$ and $^{125}I^{-}$ in Opalinus Clay samples from Mont Terri: Effect of confining pressure. Journal of Contaminant Hydrology 61, 73-83.

Van Loon, L.R., Soler, J.M., 2003. Diffusion of HTO, $^{36}Cl^{-}$, $^{125}I^{-}$ and $^{22}Na^{+}$ in Opalinus Clay: Effect of confining pressure, sample orientation, sample depth and temperature. Technical Report NTB 03-07, Nagra, Wettingen, Switzerland.

Wharton, M., Atkins, B., Charnockab, J., Livens, F., Pattrick, R., Collison, D., 2000. An X-ray absorption spectroscopy study of the coprecipitation of Tc and Re with mackinawite (FeS). Applied Geochemistry 15, 347-354.

World Nuclear Association, 2023. Storage and Disposal of Radioactive Waste. Available at: Storage and Disposal Options for Radioactive Waste - World Nuclear Association (world-nuclear.org). Storage and Disposal Options for Radioactive Waste - World Nuclear Association (world-nuclear.org)

Wu, T., Amayri, S., Drebert, J., Loon, L.R.V., Reich, T., 2009. Neptunium (V) sorption and diffusion in Opalinus Clay. Environmental Science & Technology 43, 6567-6571.

Yang, J., Kukkadapu, R.K., Dong, H., Shelobolina, E.S., Zhang, J., Kim, J., 2012. Effects of redox cycling of iron in nontronite on reduction of technetium. Chemical Geology 291, 206-216.

Yang, X., Ge, X., He, J., Wang, C., Qi, L., Wang, X., Liu, C., 2018. Effects of mineral compositions on matrix diffusion and sorption of 75Se (IV) in granite. Environmental Science & Technology 52, 1320-1329.

Yuan-Hui, L., Gregory, S., 1974. Diffusion of ions in sea water and in deep-sea sediments. Geochimica et Cosmochimica acta 38, 703-714.

Zachara, J.M., Heald, S.M., Jeon, B.-H., Kukkadapu, R.K., Liu, C., McKinley, J.P., Dohnalkova, A.C., Moore, D.A., 2007a. Reduction of pertechnetate [Tc (VII)] by aqueous Fe (II) and the nature of solid phase redox products. Geochimica et Cosmochimica Acta 71, 2137-2157.

Zachara, J.M., Serne, J., Freshley, M., Mann, F., Anderson, F., Wood, M., Jones, T., Myers, D., 2007b. Geochemical processes controlling migration of tank wastes in Hanford's vadose zone. Vadose Zone Journal 6, 985-1003.

Supporting information

Impact of Fe(II) on ^{99}Tc diffusion behavior on illite

Ping CHEN[a,b], Sergey V. Churakov[a,b], Martin Glaus[a], Luc Robert Van Loon[a, *]

[a] Paul Scherrer Institut, Laboratory for Waste Management, 5232, Villigen PSI, Swizterland

[b] Institute of Geological science, University of Bern, Switzerland

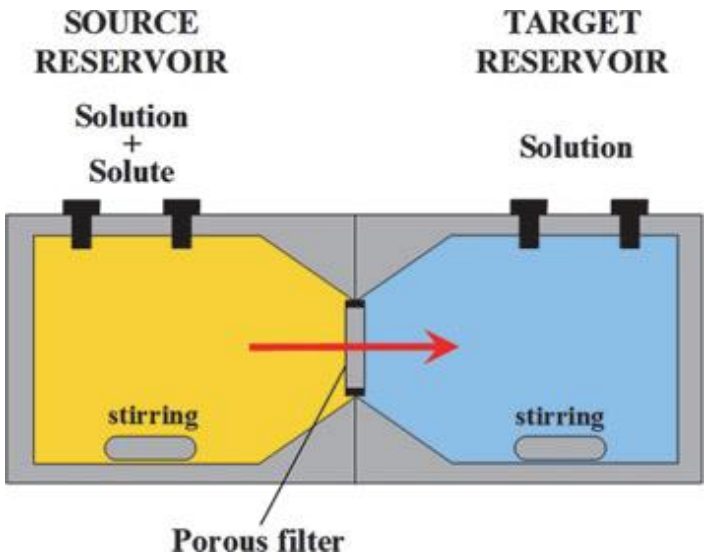

Figure S1: Sketch of cell for diffusion parameter measurement in filter. (Figure taken from Aldaba et al. , 2014)

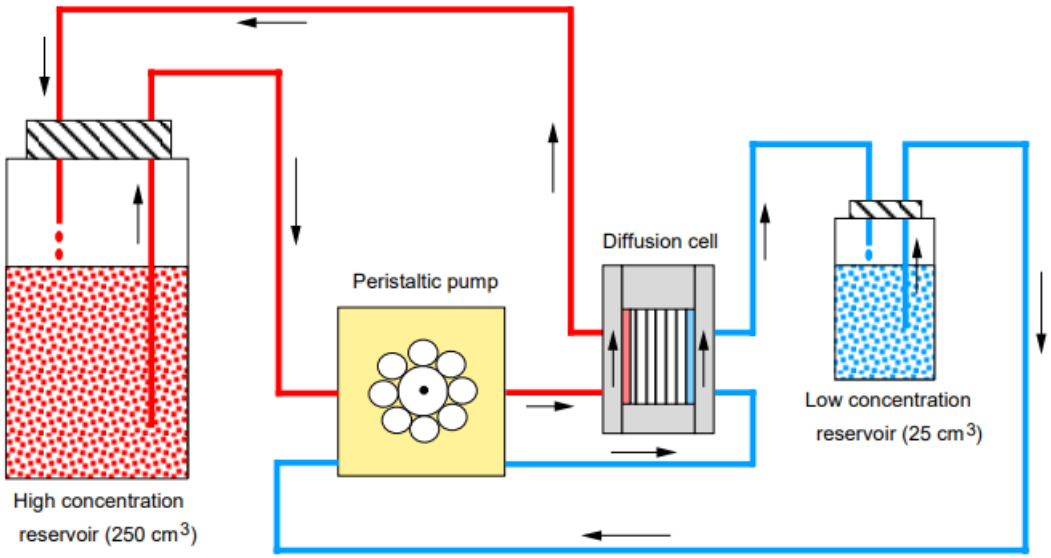

Figure S2: Experimental setup of the diffusion experiments. (Figure taken from Van Loon,L,R et al., 2003)

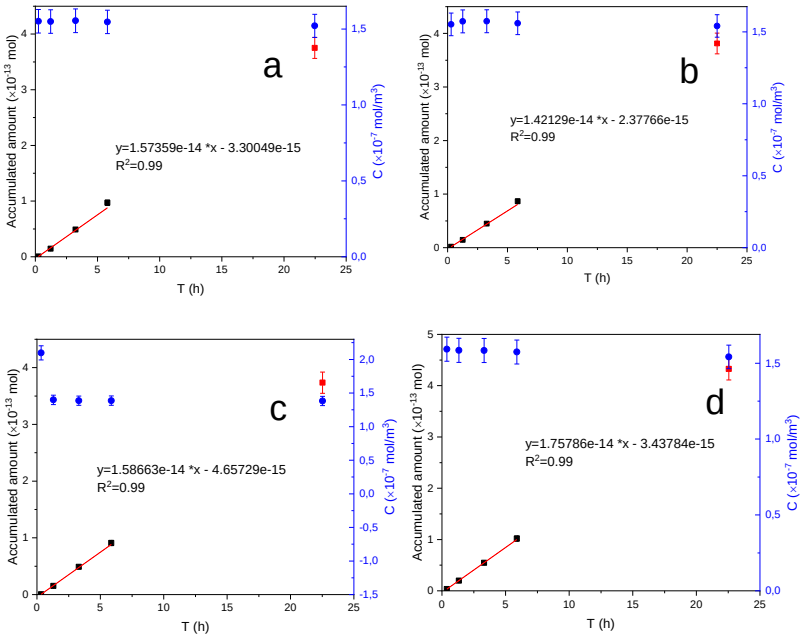

Figure S3: Breakthrough curve and the concentration at the source reservoir of HTO in rest 4 filters.

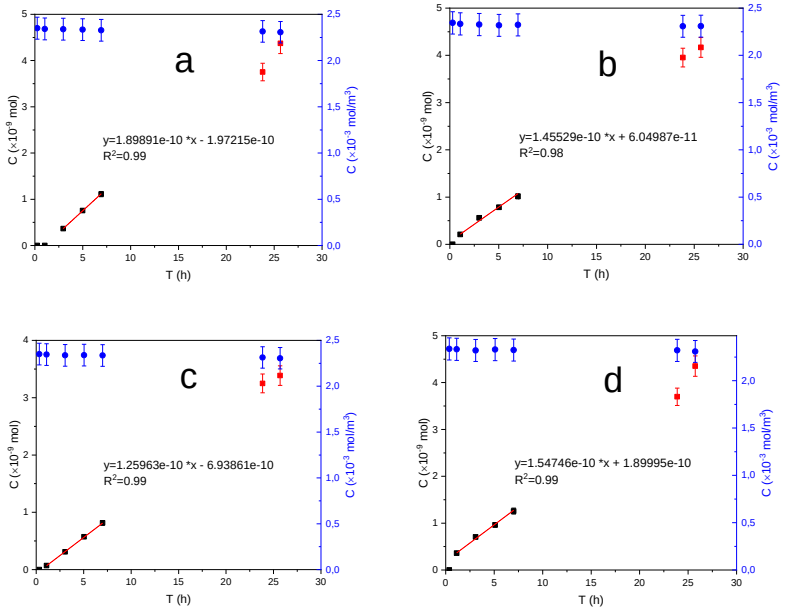

Figure S4: Breakthrough curve and the concentration at the source reservoir of Tc in rest 4 filters.

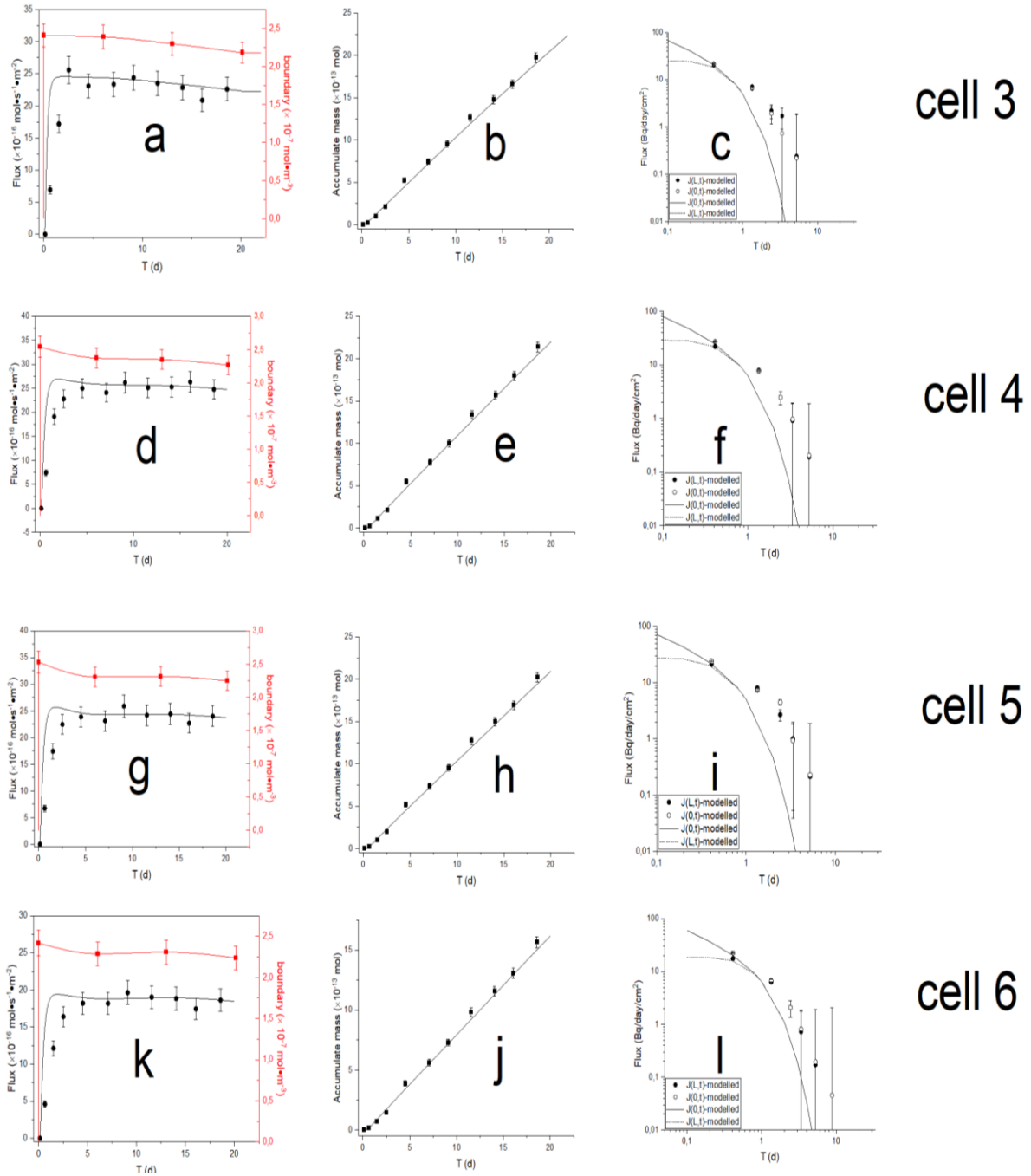

Figure S5: Experimental (symbols with error bar) and fitted (curves) diffusion data of HTO in the under anoxic conditions. Through-diffusion data are fitted with COMSOL Multiphysics. Out-diffusion is modelled with parameters from through-diffusion. a, d, g, and k are the tracer concentration (red) in high reservoir and flux (black) in the low reservoir for cell 2 to cell 6. b, e, h, and j are accumulated tracer in low concentration reservoir. c, f, i and l are out-diffusion flux at both boundaries.

Table S1: Filter parameters used in the HTO diffusion

Filters	1	2	3	4	5
d (cm)	0.1639	0.1639	0.1631	0.1622	0.1632
r (cm)	1.2700	1.2675	1.2685	1.2700	1.2690
S (cm^2)	5.067	5.047	5.063	5.067	5.059
α (10^{-14} mol/h)	1.8792	1.5736	1.4213	1.5866	1.7579
ε	0.2071	0.2020	0.2001	0.2052	0.2079
C_0 (10^{-7} mol/m3)	1.5441	1.5516	1.566	1.3901	1.5872
D_e (10^{-10} m^2/s)	10.935	9.1486	8.1215	10.149	9.9244

Table S2 Filter parameters used in the Tc diffusion

Filters	1	2	3	4	5
d (cm)	0.1610	0.1642	0.1594	0.1602	0.1582
r (cm)	1.2695	1.2700	1.2680	1.2685	1.2650
S (cm^2)	5.063	5.067	5.051	5.063	5.027
α (10^{-10} mol/h)	1.8792	1.5736	1.4213	1.5866	1.7579
ε	0.2152	0.2054	0.2083	0.2123	0.2165
C_0 (10^{-3} mol/m3)	2.3435	2.3307	2.3227	2.3322	2.3241
D_e (10^{-11} m^2/s)	6.05113	7.3339	5.4924	4.7471	5.8205

4 Reactive transport modelling of diffusive mobility and retention of TcO_4^- in Opalinus Clay with PFLOTRAN

Ping Chen[1)], Luc R. Van Loon[2)], Steffen Koch[3)], Peter Alt-Epping[1)], Tobias Reich[3)], Sergey Churakov[1,2)],

[1] *Institute for Geological Sciences, University of Bern, CH-3012 Bern, Switzerland*
[2] *Laboratory for Waste Management, Paul Scherrer Institut, CH-5232 Villigen PSI, Switzerland*
[3] *Department of Chemistry, Johannes Gutenberg-Universität Mainz, DE-55099 Mainz, Germany*

Graphic Summary

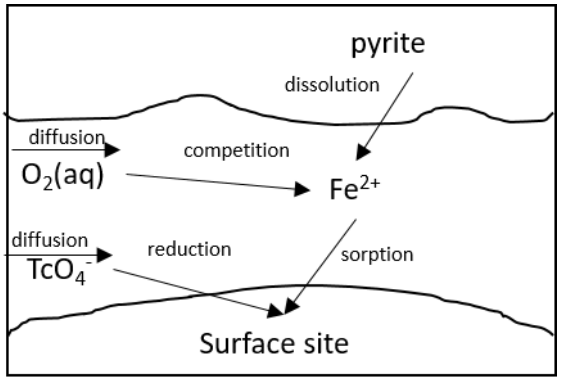

Abstract

Tc-99 has drawn widespread concern because of its long half-life, high fission yield and high mobility in research of radioactive waste disposal and environmental remediation. TcO_4^- through-diffusion experiments in Opalinus clay (OPA) were performed under air and under argon atmosphere with a diffusion technique developed by Van Loon et al. (2003). No noticeable Tc-breakthrough was observed for over one year while the total Tc concentration in the source reservoir was steadily decreasing under both air and argon atmosphere. The total Tc activity distribution in the clay sample along the diffusion direction was obtained by slicing the OPA clay samples retrieved from the diffusion cells, using the abrasive peeling technique (Van Loon et al., 2005). In the case of diffusion under air atmosphere, almost no Tc was measured in that part of the sample close to source reservoir, while much more Tc was measured under argon atmosphere. A reasonable explanation for this observation is that the reductive retention of Tc plays a significant role during the transport. A reactive transport model was constructed to simulate the diffusion process whereby the diffusion of Tc was coupled with redox reactions. Even though reduction of TcO_4^- by aqueous Fe^{2+} is thermodynamically feasible, it is not observed in the experiment. Furthermore, Fe^{2+} associated with solid phase was demonstrated to be more active than aqueous Fe^{2+}. Instead, surface complexation redox reaction is proposed. Dissolution rate of pyrite, equilibrium constant and diffusion coefficient of TcO_4^- were considered as possible factors controlling the redox reaction. Modeling results show that TcO_4^- diffuses into the clay and is partially reduced into surface complexed Tc(IV) by pyrite. When TcO_4^- transport under air atmosphere, O_2 competitively consumes Fe^{2+} and pyrite, result in no Tc immobilized in the related zone.

Keywords: reactive transport model, Tc, Opalinus clay, diffusion, redox reaction, PFLOTRAN

4.1 Introduction

Because of high mobility in the environment, long half-life ($T_{1/2}$ = 2.1 x 10^5 years) and high fission yield in nuclear reactors(Lieser, 2008), ^{99}Tc is one of the important radionuclides in the field of safety assessment of a repository for radioactive waste and for the remediation of subsurface contamination at reprocessing sites(Burgeson et al., 2005; Chatterjee et al., 2020). These properties have stimulated numerous studies on ^{99}Tc geochemical and transport behavior. Tc is a redox sensitive element. Its most stable form in the oxidizing environment is pertechnetate, Tc(VII)O_4^-, which is highly soluble(Poineau et al., 2009; Shi et al., 2012; Tagami, 2003). While exposed to reducing conditions, Tc(VII) is reduced to Tc(IV) and precipitates as TcO_2 (Fredrickson et al., 2009; Morris et al., 2008; Peretyazhko et al., 2008), TcS_2-like solids(Lukens et al., 2005; Wharton et al., 2000) and/or is incorporated into iron oxides or sulfides(Peretyazhko et al., 2008; Plymale et al., 2011; Zachara et al., 2007). Thus, reducing conditions significantly limit ^{99}Tc mobility. Consequently, great interest was evoked to the influence of reducing sources in the subsurface, especially in the role of Fe(II)(Huang et al., 2021). Clay minerals play an important role - as host rock and/or as backfill materials - in many repository concepts(ANDRA, 2001; Aoki, 2002; Bonin, 1998; Grambow, 2016; ONDRAF/NIRAS., 2001; radioactifs and Johnson, 2002), and molecular diffusion was identified as the principal mechanism of nuclide transport in such dense clay materials. Numerous diffusion experiments with radio nuclides were carried out in clay(Glaus et al., 2015; Joseph et al., 2017; Joseph et al., 2013; Kasar et al., 2016; Tachi and Yotsuji, 2014; Van Loon et al., 2003; Wang et al., 2017), including ^{99}Tc(Bruggeman et al., 2010; Li et al., 2012; Tsai et al., 2017; Wu et al., 2014). Though most of these studies improved our knowledge on the Tc behavior in clays in a qualitative way, a quantitative description of the reaction and transport processes is largely missing. Ochs et al. (2001) developed an integrated sorption-diffusion model based on the electric double layer (EDL) theory to predict the apparent diffusivity of TcO_4^- and other nuclides(Ochs et al., 2001; Tachi et al., 2014a; Tachi et al., 2014b) in clays. The drawback of this model is that sorption is characterized with a distribution coefficient (K_d) but no detailed information on the reaction mechanism is included.

In this study, the reactive transport code PFLOTRAN (www.pflotran.org) is used to develop a model that simulates diffusion of ^{99}Tc coupled to chemical (redox) reactions. Important parameters, such as rate constants for mineral reactions and the effective diffusion coefficient for Tc, are calibrated against experimental results. Constraining these parameters based on experimental data is indispensable for predicting the long-term behavior of Tc in the subsurface. Hence, the quantitative model presented here is of great importance for the safety assessment of geological repositories for radioactive waste.

4.2 Materials and Methods

4.2.1 Opalinus Clay

The Opalinus Clay (OPA) used in this study was taken from the Mont Terri (MT) Underground Research Laboratory (URL) in Switzerland (internal charge designation; BLT14). The mineral composition was not determined for this specific sample but an average composition is given in Table 1.

Table1: Average mineral composition of OPA (NAGRA (2002)(Nagra, 2002)

Mineral	**Amount (wt)%**

calcite	13 ± 8
quartz	14 ± 4
albite	1 ± 1
potassium feldspar (K-spar)	1 ± 1.6
siderite	3 ± 1.8
pyrite	1.1 ± 0.5
organic carbon	0.8 ± 0.5
illite	23 ± 2
illite/smectite-alternating layer	11 ± 2
chlorite	10 ± 2
kaolinite	22 ± 2

4.2.2 Diffusion experiments with HTO and $^{99}TcO_4^-$

The design of the through-diffusion experiments on which this study is based, is described in detail in Van Loon et al. (2003)(Van Loon and Soler, 2003). A schematic presentation is shown in Figure. 1. The intact OPA sample is sandwiched between two porous steel filters and mounted in a diffusion cell, which is connected with two reservoirs via tubes. Both reservoirs were filled with an artificial OPA pore water.

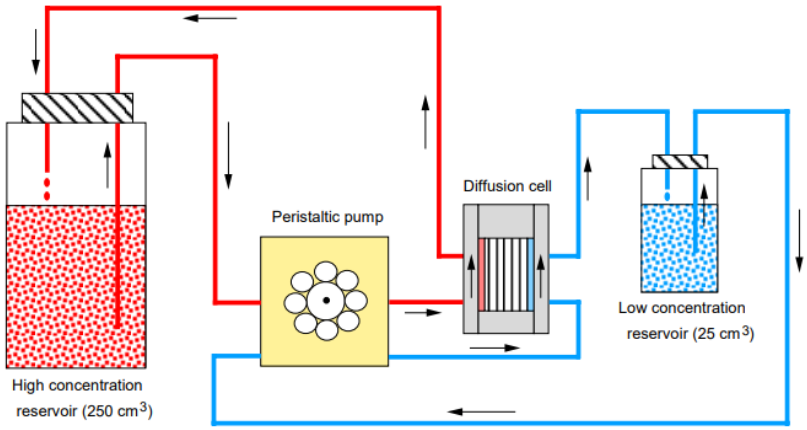

Figure. 1: Scheme of the through-diffusion experimental setup (Van Loon et al. 2003)(Van Loon and Soler, 2003).

The composition of the pore water is given in Table 2. The OPA pore water was synthesized following the method described in Pearson(Pearson, 1998). The pH and alkalinity of the pore water corresponds to the one in equilibrium with the atmospheric pCO_2. In one of the reservoirs, a $^{99}TcO_4^-$ tracer was added to the pore water. This reservoir is further denoted as the source reservoir, while only OPA pore water was placed in the other reservoir which is further denoted as the downstream reservoir. Solutions in both reservoirs were circulated in closed circuits by a peristaltic pump. The experiment under argon atmosphere was performed in a glove box filled with argon at 25 ºC, whereas the experiment under air atmosphere was performed in a heating chamber at 60 ºC. The pH in the reservoir was 7.6 and 8.4 for diffusion under air and argon atmosphere, respectively. The slightly higher pH of the pore water under argon atmosphere was caused by degassing of the water used for artificial pore water creation, and in the glove box the pCO_2 is close to zero.

Table 2: Composition of the artificial OPA pore water used in the diffusion experiments.

Element	Concentration (mM)
Na	2.40×10^{-1}
K	1.61×10^{-3}
Mg	1.69×10^{-2}
Ca	2.58×10^{-2}
Sr	0.505×10^{-3}
Cl	3.00×10^{-1}
SO_4	1.41×10^{-2}
Alkalinity	0.476×10^{-3}
I (mM)	3.90×10^{-1}
pH	7.6

Before starting the diffusion experiments, the samples were preconditioned for 4-5 weeks by circulation of the OPA pore water on each side of the samples in order to allow full saturation and chemical equilibrium. After 5 weeks, diffusion of tritiated water (HTO) was initiated, with the diffusion direction being perpendicular to the bedding orientation in both cases. Diffusion of HTO prior to ^{99}Tc was conducted 1) to yield the diffusion parameters (effective diffusion coefficient, D_e, and porosity, φ) of HTO for the clay samples and 2) to check the proper set-up of the diffusion experiment. The source reservoir (210 ml) was spiked with a HTO tracer (apporx. 1500 Bq/dm^3). The evolution of HTO in the downstream reservoir (20 ml) was monitored over time by changing the reservoir at regular time intervals and measuring the accumulated activity with Liquid Scintillation Counting (LSC) using a Hidex 300 SL liquid szintillation counter (Hidex) and Ultima Gold™ XR (Perkin Elmer) as scintillation cocktail. When the system reached steady state (constant flux), out-diffusion of HTO was initiated by replacing the solution in both reservoirs with artificial OPA porewater without HTO and repeating the reservoir change process on each side until no more HTO activity could be detected. When HTO had diffused out, the ^{99}Tc tracer (apporx. 500 Bq/dm³) was added to the source reservoir. The evolution of the ^{99}Tc activity in both source and downstream reservoirs was monitored. Small volumes of solutions were sampled and activities were measured by Liquid Scintillation Counting (LSC), using Ultima Gold™ LLT (Perkin Elmer) as scintillation cocktail. It is worth noting that no Tc breakthrough was detected for over one year while the total Tc concentration in the source reservoir was steadily decreasing under both air and argon atmosphere. After about one year, the diffusion experiment with $^{99}TcO_4^-$ was stopped and the OPA samples were retrieved from the diffusion cells, air dried and sliced using the abrasive peeling technique described in Van Loon et al.(Van Loon and Eikenberg, 2005). This process worked well using a waterproof silicon-carbide P220 sandpaper (type: CP918A; company: VSM). Mass determination for each slice was done by comparing the weight of the individual sample cups (fully prepared with sandpaper) before and after slicing using a precision scale. The theoretical thickness of the individual slices $l_{i,theo}$ was calculated from the slice weight and sample density, using the following formula:

$$l_{i,theo} = \frac{m_i}{\rho \cdot \pi \cdot (r_s^2 - r_c^2)}$$

with m_i being the slice mass, ρ the sample density (taken from data sheet), r_s the sample radius, r_c the radius of central borehole . The real thickness of the slice was calculated by:

$$l_i = l_{i,theo} \cdot k,$$

where k is an empirically determined correction factor, calculated as

$$k = \frac{\Delta l_{total}}{\Sigma l_{i,theo}},$$

with Δl_{total} being the measured difference in sample length before and after complete slicing and $\Sigma l_{i,theo}$ being the sum of the initially calculated theoretical values $l_{i,theo}$ of each slice. This was done in order to check and account for potential accumulated errors, since the results from mass determination in a number of cases showed fluctuations greater than the smallest significant value given by the scale, maybe due to the small mass differences compared to the much larger total sample mass and volume. In comparison, Δl_{total} could be determined with much greater precision, providing a good reference. The values for k obtained were 1.040 (argon atmosphere experiment) and 1.067 (air atmosphere experiment).

The slices were then extracted overnight with 1 M HNO_3 and analyzed with LSC. Finally the total Tc activity distribution in the clay sample along the diffusion direction was calculated.

4.3 Reactive transport model including surface complexation redox reactions

4.3.1 Mathematical framework

PFLOTRAN 4.0 was used to model diffusion coupled to reactions involving Tc under aerobic and anaerobic conditions. PFLOTRAN is an open source, state-of-the-art reactive transport code (Lichtner et al.(Lichtner et al., 2015)). The governing mass conservation equations for the geochemical transport mode for a multiphase system is written in terms of a set of independent aqueous primary or basis species with the form

$$\frac{\partial}{\partial t}\left(\varphi \sum_\alpha s_\alpha \psi_j^\alpha\right) + \nabla \cdot \sum_\alpha \Omega_j^\alpha = Q_j - \sum_m \nu_{jm} I_m - \frac{\partial s_j}{\partial t} \quad (1)$$

and

$$\frac{\partial \varphi_m}{\partial t} = V_m I_m \quad (2)$$

for minerals with molar volume V_m, reaction rate I_m and volume fraction φ_m. The term involving S_j describes sorption processes. The quantity ψ_j^α denotes the total concentration of the j^{th} primary species A_j^{pri}. Sums over α in Eqn. (1) are over all fluid phases in the system Ω_j^α is the total flux for species-independent diffusion. The quantity Q_j denotes a source/sink term and φ represents the porosity. In this study, only diffusion and reactions are taken into account, thus, equation 1 could be simplified as:

$$\frac{\partial}{\partial t}\left(\varphi \sum S \psi_j\right) - \nabla \cdot \sum(\varphi s D_j^0 \cdot \nabla \psi_j) = - \frac{\partial s_j}{\partial t} \quad (3)$$

$$D_e = \varphi D_p = \varphi \tau D_j^0 \quad (4)$$

The effective diffusion coefficient D_e, the pore diffusion coefficient D_p, and the diffusion coefficient of species j in water D_j^0 are related via the porosity φ and the tortuosity τ via equation 4.

4.3.2 Transport part in the model

Consistent with the design of the diffusion cell, the geometry of model is a 1D cylindrical model (Figure. 2). The clay column is sandwiched between two filters. The cylinder is discretized into 140 cells in the axial direction,

using 10 nodes for each filter, 100 nodes for the clay and 10 nodes for each reservoir with a length calculated by dividing the reservoir solution volume by the cross section of the diffusion cell. In the radial direction, only one node is assigned with a length calculated from the cross section of the diffusion cell.

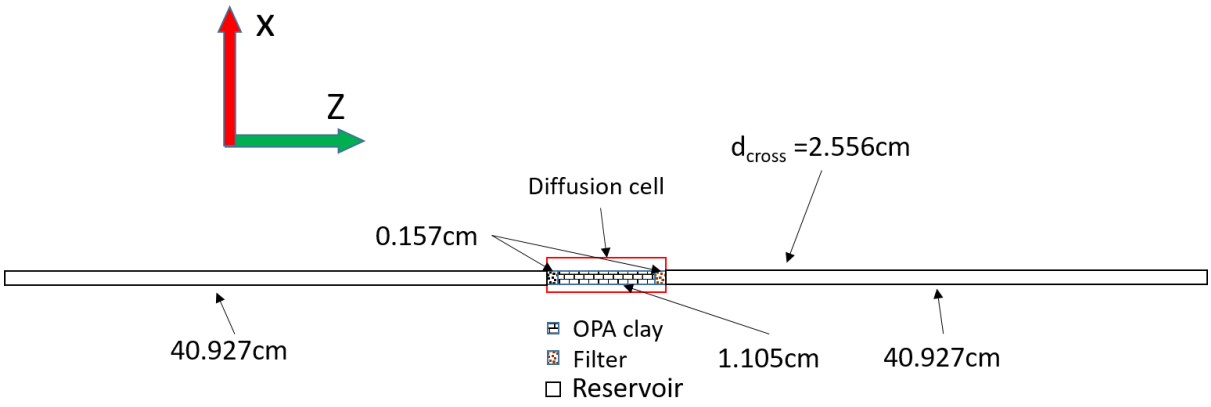

Figure. 2: Schematic view of the reactive transport model.

Geometrical properties of the different components in the model are summarized in Table 3. The tortuosity τ in clay is calculated according to Eq. 4 by fitting the model with HTO diffusion results as discussed later. The tortuosity τ in filter is calculated from the D_e of HTO diffusion in filter and the filter porosity (D_e =1.06×10^{-10} m^2/s, filter porosity φ = 0.20; Chen et al., under review).

Table 3: Geometrical parameters of the different model components

Parameters	**air**	**argon**
Clay porosity φ	0.16	0.20
Filter porosity φ	0.20	0.20
Reservoir porosity φ	1	1
Clay length L (cm)	1.110	1.105
Diameter d (cm)	2.545	2.556
Tortuosity in clay τ	/	/
Tortuosity in filter τ	0.247	0.247

4.3.3 Chemical reactions in the model

The retardation of ^{99}Tc in Opalinus Clay is strongly related to the redox reactions that might occur between Fe(II) and TcO_4^- that diffuses from the solution into the rock. Fe(II) in OPA is present in different forms. Mazurek et al.(Mazurek et al., 2023) recently showed that the majority of Fe in un-weathered OPA is present as Fe(II) in clay minerals, followed by Fe(II) in siderite, Fe(III) in clay minerals and nano-goethite, and Fe(II) in pyrite (Figure. 3).

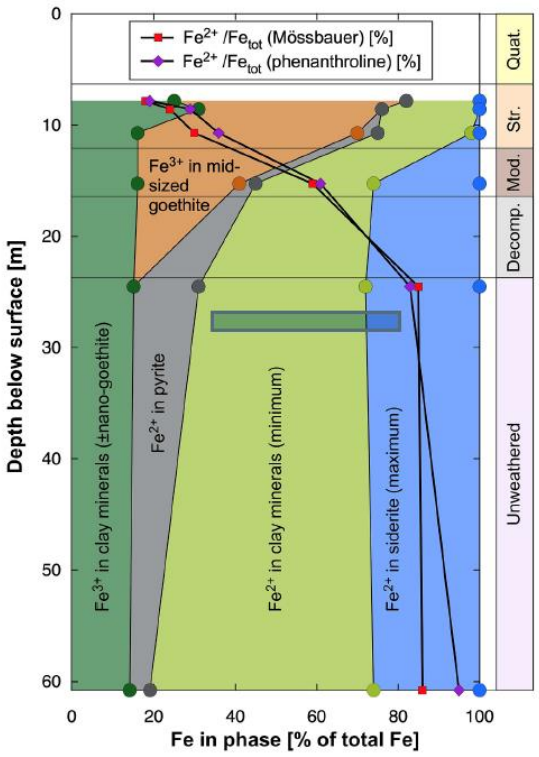

Figure. 3: Distribution of Fe in OPA between different solid phases (Figure taken from Mazurek et al.(Mazurek et al., 2023)).

Fe(II) present in the porewater is therefore in equilibrium with different solid phases (pyrite, siderite and clay minerals) as schematically shown in Figure 4. The equilibrium with pyrite and siderite is defined by the solubility products (K_s) and the equilibrium with clay minerals by sorption-desorption reactions involving ion exchange and surface complexation reactions with strong (-SO) and weak (-WO) sites on the edges of clay minerals(Chen et al., 2022).

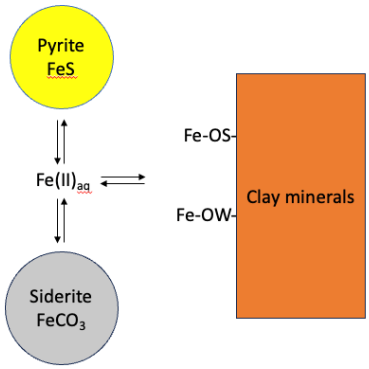

Figure. 4: Speciation equilibria of Fe(II) in OPA

The redox reactivity of Fe(II) species depends strongly on the speciation. It is known that dissolved Fe(II) has the lowest redox reactivity whereas Fe(II) in solid phases shows the highest reactivity(Peretyazhko et al., 2008). The study of Hoving et al.(Hoving et al., 2017) on the redox properties of clay-rich sediments by mediated electrochemical analysis showed that Fe associated with clay minerals showed the highest redox reactivity. Combined with the information given in Mazurek et al.(Mazurek et al., 2023), it can be assumed that the Fe(II) associated with clay minerals such as illite might be the most important reaction partner for the reduction/immobilisation of TcO_4^- in OPA.

The clay and pore water composition in Table 1 and Table 2 are used in the chemical model. The default database for PFLOTRAN "hanford.dat" is used to define stabilities and solubilities of secondary species and minerals, respectively. Although it is thermodynamically feasible that TcO_4^- reacts with aqueous Fe^{2+} to form a Tc(IV) precipitate, this reaction was not considered in the model because it is known from the literature that sorbed Fe(II) or Fe(II) in a solid phase is more reactive. Therefore, a redox reaction between surface complexed Fe(II) and Tc(VII) is proposed (Eq 5 and Eq 6 in Table 4). The two-site protolysis non-electrostatic surface complexation and cation exchange (2SPNE SC/CE) sorption model was used. Illite was assumed to be the only mineral with active surface sites. The properties of illite were fully characterized by Baeyens and Bradbury(Baeyens and Bradbury, 2004) and the related properties have been taken from Chen et al.(Chen et al., 2022), such as cation exchange capacity (CEC), the surface hydroxyl group capacity, protolysis constants and equilibrium constant for Fe sorbed on surface. The redox reactions involved in the model are summarized in Table 4.

Table 4: Properties of illite, redox and solubility reactions used in the reactive transport model describing the transport and Fe(II)-mediated immobilization of ^{99}Tc in OPA.

Site types	Site capacities	
$\equiv S^SOH$	2.0×10^{-3} mol/kg	
$\equiv S^{W1}OH$	4.0×10^{-2} mol/kg	
$\equiv S^{W2}OH$	4.0×10^{-2} mol/kg	
CEC	2.25×10^{-1} eq/kg	
Protolysis reactions	Log $K_{protolysis}$	
$\equiv S^SOH + H^+ \leftrightarrow \equiv S^SOH_2^+$	4.0	
$\equiv S^SOH \leftrightarrow \equiv S^SO^- + H^+$	-6.2	
$\equiv S^{W1}OH + H^+ \leftrightarrow \equiv S^{W1}OH_2^+$	4.0	
$\equiv S^{W1}OH \leftrightarrow \equiv S^{W1}O^- + H^+$	-6.2	
$\equiv S^{W2}OH + H^+ \leftrightarrow \equiv S^{W2}OH_2^+$	8.5	
$\equiv S^{W2}OH \leftrightarrow \equiv S^{W2}O^- + H^+$	-10.5	
Reactions	Log K	Eq.
$\equiv SSO(TcO_2)_{0.3333}Fe^{2+} + 0.6665H_2O = 0.3333TcO_4^- + 0.3333H^+ + 1Fe^{2+} + \equiv SSOH$	/	(5)
$\equiv SWaO(TcO_2)_{0.3333}Fe^{2+} + 0.6665H_2O = 0.3333TcO_4^- + 0.3333H^+ + 1Fe^{2+} + \equiv SWaOH$	/	(6)
$Fe^{3+} + 0.5H_2O = 0.25O_2(g) + Fe^{2+} + H^+$	-7.7654	(7)
$FeS_2 + H_2O = Fe^{2+} + 0.25H^+ + 0.25SO_4^{2-} + 1.75HS^-$	-24.6534	(8)
$FeCO_3 + H^+ = Fe^{2+} + HCO_3^-$	-0.192	(9)
$HS^- + 2O_2(g) = H^+ + SO_4^{2-}$	132.5203	(10)

Dissolution reactions of the mineral components in OPA as shown in Table 1 are kinetically controlled. The dissolution rate constants of the minerals in OPA are taken from Palandri et al.(Palandri and Kharaka, 2004), except for pyrite, whose value caused numerical problems in the simulations. As observed in Mazurek et al.(Mazurek et al., 2023), goethite is the main product of Fe(III) phases after weathering. Therefore, goethite is assumed as a possible Fe(III) precipitate. The dissolution reaction of chlorite is not available in database. Instead, the data for Clinochlore-7A was used as a proxy. Possible illite/smectite layer are treated in this model as illite.

The reactive surface area of 1 m^2/m^3 was assumed for all solids. The final reaction product of Tc(VII) reduced by surface complexed Fe(II) is not exactly clear. In the model it is assumed to be $\equiv SSO(TcO_2)_{0.3333}Fe^{2+}$ and $\equiv SWaO(TcO_2)_{0.3333}Fe^{2+}$, even though it may also be reduced to form TcO_2, TcS_2 and/or it may be incorporated into other minerals. Note that in simulations involving aerobic conditions an artificial mineral "O_2(s)" is introduced in the source reservoir to act as a buffer for O_2(aq) at equilibrium with atmospheric O_2(g). But because of a convergence problem, the "O_2(s)" was only added to the source reservoir.

The species diffusion coefficient of $^{99}TcO_4^-$, the reaction rate of pyrite and the equilibrium constants of surface complexation redox reactions of Tc are the fitting parameters and will be assessed to achieve optimal agreement with the experimental results. All simulation setup and thermodynamic data were selected assuming room temperature conditions.

4.4 Results and discussion

4.4.1 HTO diffusion in Opalinus Clay

The comparison of fitted and measured fluxes of HTO is shown in Figure. 5. As can be seen, there is a good agreement between the model predictions and the experimental results for both air and argon atmosphere conditions. The values of D_e for HTO diffusion in OPA are 3.20×10^{-11} m²/s and 1.92×10^{-11} m²/s for air and argon atmosphere, respectively. The D_e values are a little bit larger than the value given in Van Loon et al.(Van Loon et al., 2003). This good match between fitted and experimental data indicates that the model works well for diffusion of non-sorbing tracers. The porosity φ of HTO in OPA are 0.16 and 0.20 for air and argon atmosphere, respectively, which are consistent with values in Wu et al.(Wu et al., 2009) and Joseph et al.(Joseph et al., 2013), whose value range from 0.15 to 0.18. The D_0 of HTO in water is about 2.15×10^{-9} m^2 s^{-1} at 25 °C(Yuan-Hui and Gregory, 1974). According to Eq 4, the tortuosity τ in filter are calculated and listed in Table 3. The tortuosity τ in clay were calculated as 0.093 and 0.045 for air and argon conditions, respectively.

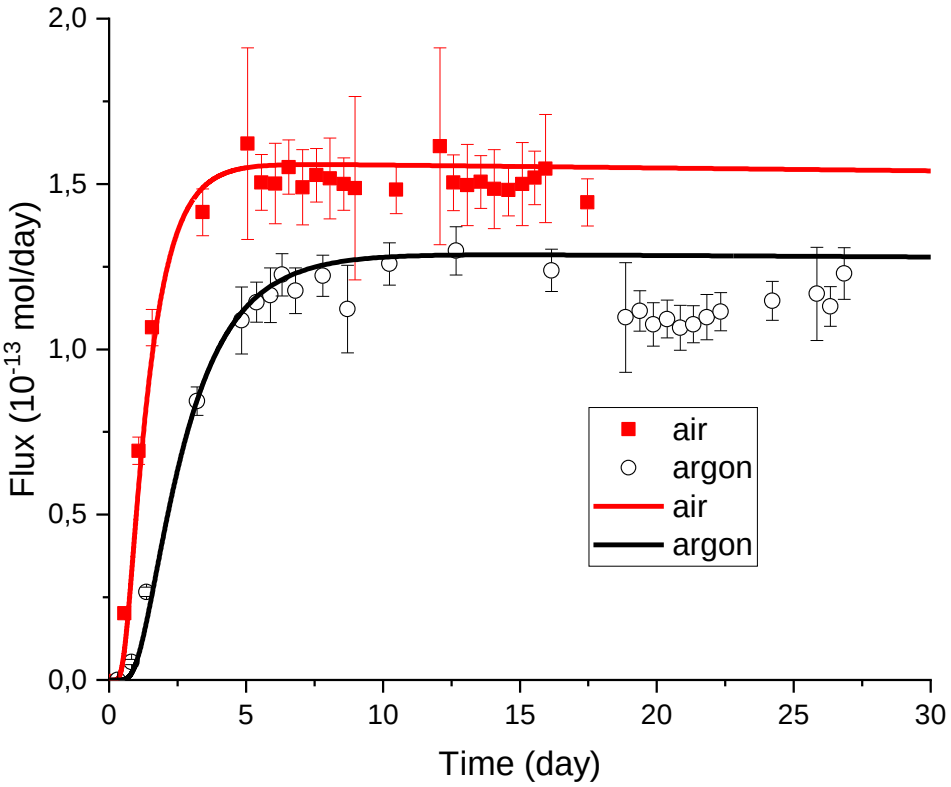

Figure. 5 Comparison of fitted and experimental flux data of HTO in OPA.

4.4.2 Diffusion of ^{99}Tc in Opalinus Clay

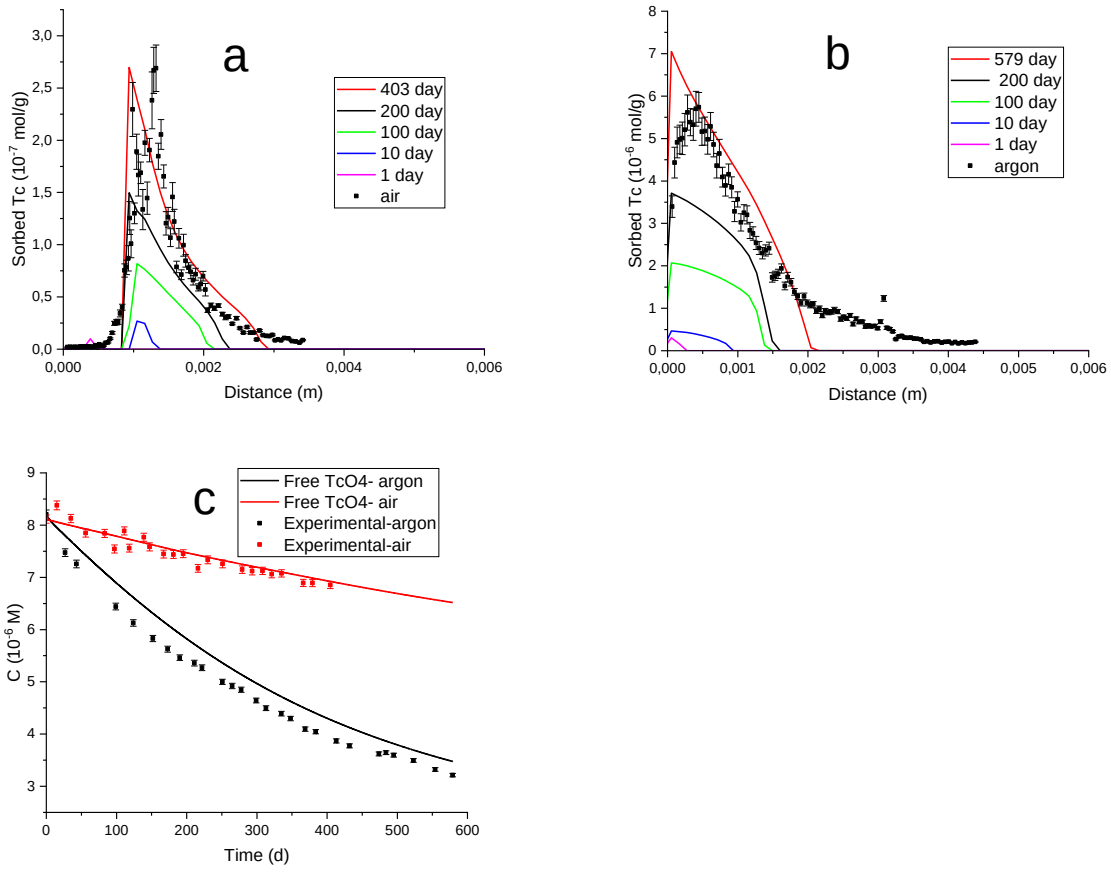

Figure. 6 Comparison of experimental data and modeling results for the model considering the reduction of Tc(VII) by surface complexed Fe(II). Simulation time correspond to 579 and 403 days of the experiments for under argon air atmosphere, respectively. The trend of Tc distribution for a) under air conditions; b) under argon conditions; c) concentration of TcO_4^- in the source reservoir.

As shown in Figure. 6, both the final Tc distribution in OPA and the Tc concentration in the source reservoir as predicted with model A fit reasonably well with the experimental data for diffusion under air and under argon atmosphere. In model A, the possible illite/smectite-alternating layer is also treated as illite. The position of the Tc peak can be reproduced quite good, but not the observed tailing. Especially for the experiments under argon atmosphere, the model tail is too sharp. The best fit parameters for this model are summarized in Table 5. Note that the obtained best fit parameters in this model are not the same for diffusion under argon and air atmosphere.

Table 5: Parameters for best fit.

Parameter	Model A		Model B	
	air	argon	air	argon
Reaction rate pyrite ($\times 10^{-6}$ mol/m^2/s)	0.5	1.5	0.06	0.2
Species diffusion coefficient $D_{0(TcO_4^-)}$ ($\times 10^{-9}$ m^2/s)	0.35	0.8	0.6	0.6
Equilibrium constant log K	-15.8	-18.6	-17.0	-17.0

Species diffusion coefficient of aqueous O_2 is 0.11×10^{-9} m^2/s for model A and 0.10×10^{-9} m^2/s for model B. The equilibrium constant is for reactions 5 and 6 in table 4.

It is not optimal that model requires different transport parameters and equilibrium constants for the same species. One possible factor that might improve the model is the amount of surface sites, or the amount of active/available surface sites. As can be seen from the clay minerals reported in Table 2, besides illite there is also a substantial amount of kaolinite and chlorite, which can also sorb Fe(II) and thus can contribute to the reduction of Tc(VII). But only illite and illite/smectite mixed layer clay minerals were under considered in model A. Thus, the amount of illite should be adjusted according to the amount of kaolinite and chlorite. The resaturation of the OPA with pore water for 5 weeks was conducted before the tracer diffusion experiments. While saturation of OPA under an argon atmosphere will prevent the oxidation of Fe(II)-species, resaturation of OPA under oxic atmosphere will result in partial oxidation of dissolved and sorbed Fe(II). This lead to a decrease of Fe(II)-loaded sorption sites on the clay minerals. In the model, the oxidation reaction of sorbed Fe(II) species was not implemented, only the oxidation of aqueous Fe(II) species was included. A decrease of the illite amount for under air atmosphere might somehow mimic the oxidation of sorbed Fe(II). Therefore, the amount of illite was modified in the model B. For diffusion under argon atmosphere, the amount of kaolinite was included in the amount of illite, which increases the amount of active surface sites. For diffusion under air atmosphere, the amount of illite was decreased to mimic the oxidized sorbed Fe(II). Model B gives slightly better results as shown in Figure 7. Even though there are still significant deviations between the experimental data and the model results for both the evolution of the Tc concentration in the reservoir source reservoirs and the final Tc distribution in the OPA, the obtained parameters are much better and make sense: the same species diffusion coefficient for under air and argon atmosphere could be used, as well as the same equilibrium constant for reaction 5 and 6 as shown in Table 5. The different reaction rates for pyrite may caused by the different driving forces for pyrite dissolution. For under argon condition, the driving force is TcO_4^-, while it may become O_2 for under air atmosphere.

The different temperatures for diffusion experiments under air and argon atmosphere might also improve model B. The temperature affects the diffusion coefficient, but because the activation energy is unknown for Tc species, it was difficult to assign a value to the species diffusion coefficient at 60 ºC. Temperature also affects the equilibrium constant, but no information is available that indicates whether the reactions 5 and 6 are exothermic or endothermic, Considering the temperature effects will definitely make the model more realistic and have to be included in future modeling work.

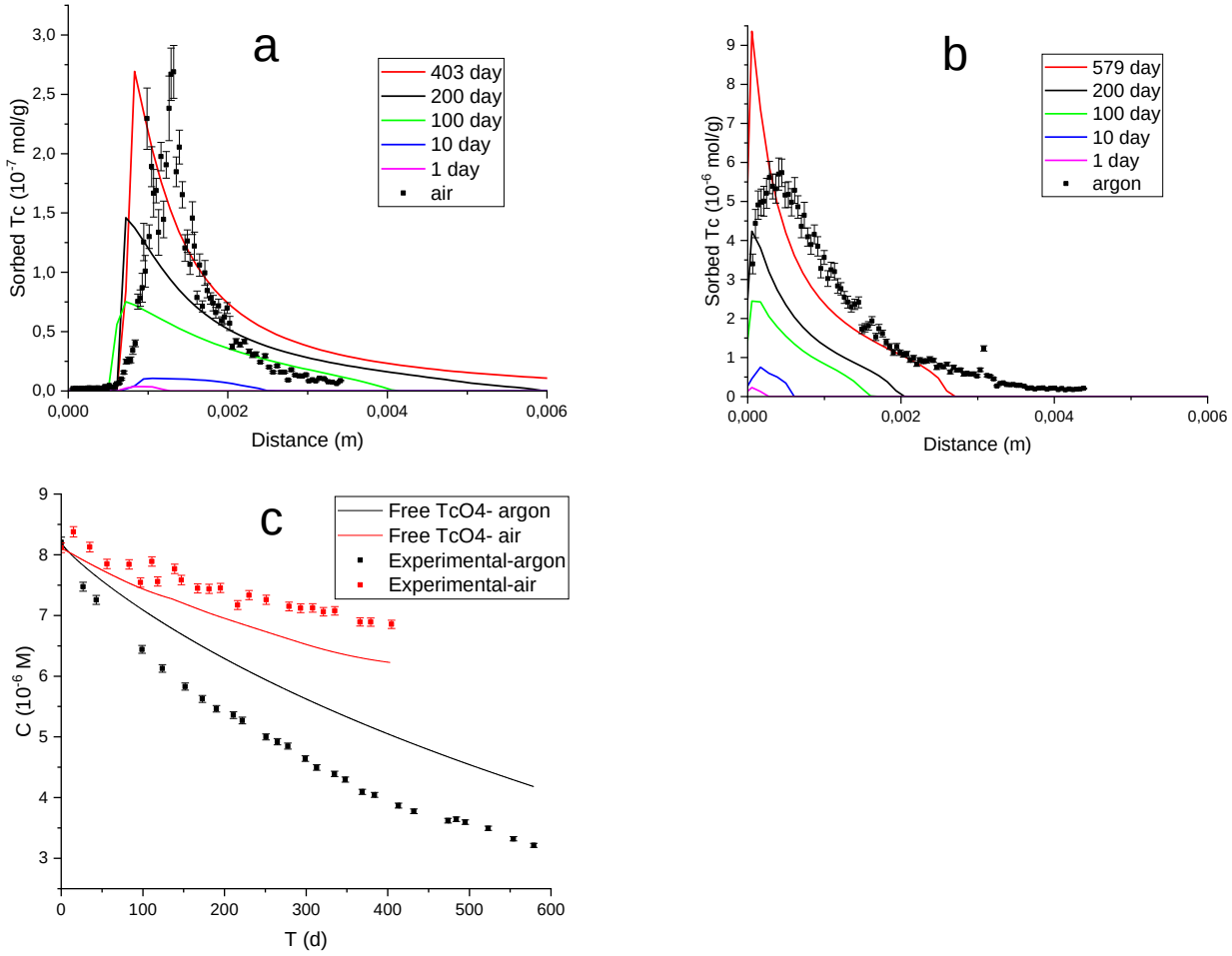

Figure. 7: Comparison of experimental data and modeling results obtained with model B (model with modified surface site capacity). Simulation runs 579 days for under argon and 403 days for under air atmosphere. The trend of Tc distribution for a) under air atmosphere; b) under argon atmosphere; c) concentration of TcO_4^- in high concentration reservoir.

4.5 Conclusions

A simple reactive transport model coupling diffusion and chemical reactions was developed in this study to reproduce experimental data of Tc diffusion through the Opalinus Clay. Some important parameters were obtained for future research, such as species diffusion coefficient of TcO_4^-, the dissolution rate of pyrite and the equilibrium constant of TcO_4^- reacting with clay surface site. Modeling results show that the final Tc distribution is a result of a complex process, in which diffusion of TcO_4^- and dissolved O_2, redox reactions, and pyrite oxidation are

coupled. Under argon atmosphere, diffused TcO_4^- reacts with surface sites and sorbed Fe(II). The depletion of Fe^{2+} drives the dissolution of pyrite. This process only occurs in the clay near the source reservoir, because the diffusive flux of TcO_4^- into the core is very low and limits the rate of pyrite oxidation dissolution, whereas for diffusion experiments conducted under air atmosphere , O_2 could oxidize Fe^{2+}, which results in no Tc being retarded in the zone where O_2 is available.

Since this model is simplified, especially for the surface site capacity, more efforts could be devoted to aspects that confirm the surface site capacity or the exact clay mineral component, or confirmation of Tc speciation in clay, introducing a more representative OPA mineralogy, the effect of the clay surface charge in transport and the change of porosity.

Reference

ANDRA, 2001. Référentiel géologique du site de Meuse/Haute Marne. Rapp. A RP ADS 99-005

de l'Agence nationale pour la gestion des déchets radioactifs, Châtenay-Malabry, France.

Aoki, K., 2002. Recent activities at underground research laboratories in Japan.

Baeyens, B., Bradbury, M.H., 2004. Cation exchange capacity measurements on illite using the sodium and cesium isotope dilution technique: effects of the index cation, electrolyte concentration and competition: modeling. Clays and Clay Minerals 52, 421-431.

Bonin, B., 1998. Deep geological disposal in argillaceous formations: studies at the Tournemire test site. Journal of Contaminant Hydrology 35, 315-330.

Bruggeman, C., Maes, N., Aertsens, M., Govaerts, J., Martens, E., Jacops, E., Van Gompel, M., Van Ravestyn, L., 2010. Technetium retention and migration behaviour in Boom Clay. External Report. Mol, Belgium, SCK• CEN. SCK• CEN-ER-101.

Burgeson, I.E., Deschane, J.R., Blanchard Jr, D., 2005. Removal of technetium from Hanford tank waste supernates. Separation science and technology 40, 201-223.

Chatterjee, S., Holfeltz, V.E., Hall, G.B., Johnson, I.E., Walter, E.D., Lee, S., Reinhart, B., Lukens, W.W., Machara, N.P., Levitskaia, T.G., 2020. Identification and Quantification of Technetium Species in Hanford Waste Tank AN-102. Analytical Chemistry 92, 13961-13970.

Chen, P., Van Loon, L.R., Fernandes, M.M., Churakov, S., 2022. Sorption mechanism of Fe (II) on illite: Sorption and modelling. Applied Geochemistry 143, 105389.

Fredrickson, J.K., Zachara, J.M., Plymale, A.E., Heald, S.M., McKinley, J.P., Kennedy, D.W., Liu, C., Nachimuthu, P., 2009. Oxidative dissolution potential of biogenic and abiogenic TcO2 in subsurface sediments. Geochimica et Cosmochimica Acta 73, 2299-2313.

Glaus, M., Aertsens, M., Appelo, C., Kupcik, T., Maes, N., Van Laer, L., Van Loon, L., 2015. Cation diffusion in the electrical double layer enhances the mass transfer rates for Sr2+, Co2+ and Zn2+ in compacted illite. Geochimica et Cosmochimica Acta 165, 376-388.

Grambow, B., 2016. Geological disposal of radioactive waste in clay. Elements 12, 239-245.

Hoving, A.L., Sander, M., Bruggeman, C., Behrends, T., 2017. Redox properties of clay-rich sediments as assessed by mediated electrochemical analysis: separating pyrite, siderite and structural Fe in clay minerals. Chemical Geology 457, 149-161.

Huang, J., Jones, A., Waite, T.D., Chen, Y., Huang, X., Rosso, K.M., Kappler, A., Mansor, M., Tratnyek, P.G., Zhang, H., 2021. Fe (II) redox chemistry in the environment. Chemical reviews 121, 8161-8233.

Joseph, C., Mibus, J., Trepte, P., Müller, C., Brendler, V., Park, D.M., Jiao, Y., Kersting, A.B., Zavarin, M., 2017. Long-term diffusion of U (VI) in bentonite: Dependence on density. Science of the Total Environment 575, 207-218.

Joseph, C., Van Loon, L., Jakob, A., Steudtner, R., Schmeide, K., Sachs, S., Bernhard, G., 2013. Diffusion of U (VI) in Opalinus Clay: Influence of temperature and humic acid. Geochimica et Cosmochimica Acta 109, 74-89.

Kasar, S., Kumar, S., Bajpai, R., Tomar, B., 2016. Diffusion of Na (I), Cs (I), Sr (II) and Eu (III) in smectite rich natural clay. Journal of environmental radioactivity 151, 218-223.

Li, J., Dai, W., Xiao, G., Wang, H., Zhang, Z., Wu, T., 2012. Pertechnetate diffusion in GMZ bentonite. Journal of Radioanalytical and Nuclear Chemistry 293, 763-767.

Lichtner, P.C., Hammond, G.E., Lu, C., Karra, S., Bisht, G., Andre, B., Mills, R., Kumar, J., 2015. PFLOTRAN user manual: A massively parallel reactive flow and transport model for describing surface and subsurface processes. Los Alamos National Lab.(LANL), Los Alamos, NM (United States); Sandia ….

Lieser, K.H., 2008. Nuclear and radiochemistry: fundamentals and applications. John Wiley & Sons.

Lukens, W.W., Bucher, J.J., Shuh, D.K., Edelstein, N.M., 2005. Evolution of technetium speciation in reducing grout. Environmental science & technology 39, 8064-8070.

Mazurek, M., Wersin, P., Hadi, J., Grenèche, J.-M., Prinpreecha, N., Traber, D., 2023. Geochemistry and palaeo-hydrogeology of the weathered zone in the Opalinus Clay. Applied Clay Science 232, 106793.

Morris, K., Livens, F., Charnock, J., Burke, I., McBeth, J., Begg, J., Boothman, C., Lloyd, J., 2008. An X-ray absorption study of the fate of technetium in reduced and reoxidised sediments and mineral phases. Applied Geochemistry 23, 603-617.

Nagra, 2002. Projekt Opalinuston–Synthese der geowissenschaftlichen Untersuchungs-ergebnisse. Entsorgungsnachweis für abgebrannte Brennelemente, verglaste hochaktive sowie langlebige mittelaktive Abfälle. Nagra Wettingen.

Ochs, M., Lothenbach, B., Wanner, H., Sato, H., Yui, M., 2001. An integrated sorption–diffusion model for the calculation of consistent distribution and diffusion coefficients in compacted bentonite. Journal of Contaminant Hydrology 47, 283-296.

ONDRAF/NIRAS., 2001. SAFIR 2: Safety Assessment and Feasibility Interim Report 2. ONDRAF/NIRAS.

Palandri, J.L., Kharaka, Y.K., 2004. A compilation of rate parameters of water-mineral interaction kinetics for application to geochemical modeling.

Pearson, F., 1998. Opalinus clay experimental water: A1 Type, Version 980318. PSI Internal report TM-44-98-07, Paul Scherrer Institut, Villigen PSI ….

Peretyazhko, T., Zachara, J.M., Heald, S.M., Jeon, B.-H., Kukkadapu, R.K., Liu, C., Moore, D., Resch, C.T., 2008. Heterogeneous reduction of Tc (VII) by Fe (II) at the solid–water interface. Geochimica et Cosmochimica Acta 72, 1521-1539.

Plymale, A.E., Fredrickson, J.K., Zachara, J.M., Dohnalkova, A.C., Heald, S.M., Moore, D.A., Kennedy, D.W., Marshall, M.J., Wang, C., Resch, C.T., 2011. Competitive reduction of pertechnetate (99TcO4−) by dissimilatory metal reducing bacteria and biogenic Fe (II). Environmental Science & Technology 45, 951-957.

Poineau, F., Rodriguez, E., Weck, P., Sattelberger, A., Forster, P., Hartmann, T., Mausolf, E., Silva, G., Jarvinen, G., Cheetham, A., 2009. Review of technetium chemistry research conducted at the University of Nevada Las Vegas. Journal of radioanalytical and nuclear chemistry 282, 605-609.

radioactifs, S.c.n.p.l.e.d.d., Johnson, L., 2002. Project Opalinus Clay: safety report: demonstration of disposal feasibility for spent fuel, vitrified high-level waste and long-lived intermediate-level waste (Entsorgungsnachweis). Nagra.

Shi, K., Hou, X., Roos, P., Wu, W., 2012. Determination of technetium-99 in environmental samples: a review. Analytica chimica acta 709, 1-20.

Tachi, Y., Ochs, M., Suyama, T., 2014a. Integrated sorption and diffusion model for bentonite. Part 1: clay–water interaction and sorption modeling in dispersed systems. Journal of Nuclear Science and Technology 51, 1177-1190.

Tachi, Y., Yotsuji, K., 2014. Diffusion and sorption of Cs+, Na+, I− and HTO in compacted sodium montmorillonite as a function of porewater salinity: Integrated sorption and diffusion model. Geochimica et Cosmochimica Acta 132, 75-93.

Tachi, Y., Yotsuji, K., Suyama, T., Ochs, M., 2014b. Integrated sorption and diffusion model for bentonite. Part 2: porewater chemistry, sorption and diffusion modeling in compacted systems. Journal of Nuclear Science and Technology 51, 1191-1204.

Tagami, K., 2003. Technetium-99 Behavior in the Terrestrial Environment Field Observations and Radiotracer Experiments. Journal of Nuclear and Radiochemical Sciences 4, A1-A8.

Tsai, T.-L., Tsai, S.-C., Shih, Y.-H., Chen, L.-C., Lee, C.-P., Su, T.-Y., 2017. Diffusion characteristics of HTO and 99TcO4− in compacted Gaomiaozi (GMZ) bentonite. Nuclear Science and Techniques 28, 1-8.

Van Loon, L., Eikenberg, J., 2005. A high-resolution abrasive method for determining diffusion profiles of sorbing radionuclides in dense argillaceous rocks. Applied Radiation and Isotopes 63, 11-21.

Van Loon, L., Soler, J., Bradbury, M., 2003. Diffusion of HTO, 36Cl− and 125I− in Opalinus Clay samples from Mont Terri: Effect of confining pressure. Journal of Contaminant Hydrology 61, 73-83.

Van Loon, L.R., Soler, J.M., 2003. Diffusion of HTO, 36 Cl-, 125 I-and 22 Na+ in Opalinus Clay: Effect of confining pressure, sample orientation, sample depth and temperature. Paul Scherrer Institute (PSI).

Wang, Z., Zhang, J., Chen, J., Zhang, Z., Zheng, Q., Li, J., Wu, T., 2017. Diffusion behavior of Re (VII) in compacted illite-, hematite-and limonite-montmorillonite mixtures. Journal of Radioanalytical and Nuclear Chemistry 311, 655-661.

Wharton, M., Atkins, B., Charnockab, J., Livens, F., Pattrick, R., Collison, D., 2000. An X-ray absorption spectroscopy study of the coprecipitation of Tc and Re with mackinawite (FeS). Applied Geochemistry 15, 347-354.

Wu, T., Amayri, S., Drebert, J., Loon, L.R.V., Reich, T., 2009. Neptunium (V) sorption and diffusion in Opalinus Clay. Environmental science & technology 43, 6567-6571.

Wu, T., Wang, H., Zheng, Q., Zhao, Y.L., Li, J.Y., 2014. Effect of EDTA on the diffusion behavior of 99TcO4− and ReO4− in GMZ bentonite. Journal of Radioanalytical and Nuclear Chemistry 299, 2037-2041.

Yuan-Hui, L., Gregory, S., 1974. Diffusion of ions in sea water and in deep-sea sediments. Geochimica et cosmochimica acta 38, 703-714.

Zachara, J.M., Heald, S.M., Jeon, B.-H., Kukkadapu, R.K., Liu, C., McKinley, J.P., Dohnalkova, A.C., Moore, D.A., 2007. Reduction of pertechnetate [Tc (VII)] by aqueous Fe (II) and the nature of solid phase redox products. Geochimica et Cosmochimica Acta 71, 2137-2157.

5 Summary, conclusions and suggestions for future work

5.1 Conclusions

In this thesis, technetium (^{99}Tc) retention and migration in clays was investigated by experiments and simulations and the mechanisms could be revealed step by step. The most stable form of Tc under oxic conditions is pertechnetate (TcO_4^-). In this form, ^{99}Tc hardly reacts with negatively charged clay minerals and is therefore expected to diffuse unretarded through it. However, when pertechnetate undergoes redox reactions with e.g. Fe(II) from canister corrosion or pyrite during its migration in clay, it will be reduced to Tc(IV) and will be immobilized. Because the redox potential of Fe(II) depends strongly on its speciation, the sorption behaviour of Fe(II) on illite was studied in a first step. Illite was taken as a model clay mineral because it is one of the main clay minerals in clay rocks. It could be shown that Fe(II) sorbs on strong and weak edge sites and on planar sites, depending on its concentration in the pore water and depending on the pH of the pore water. It could also be demonstrated that sorbed Fe(II) readily oxidizes to Fe(III) by electron transfer with structurally Fe(III). The sorption behaviour of Fe(II) could be described with the 2SPNE SC/CE model that was extended with a surface oxidation process. Below pH 6.5 surface complexed Fe(II) oxidizes on the surface. Above pH 6.5 the oxidized Fe reacts with water to form hydrolysed species and/or precipitates such as hematite.

In a second step, the diffusion of ^{99}Tc in compacted illite was studied in presence and absence of Fe(II), employing the a through-diffusion technique. In absence of Fe(II), ^{99}Tc diffuses as TcO_4^- and behaves as other anions such as $^{36}Cl^-$, showing anion exclusion effects and no retardation. Both the accessible porosity and the effective diffusion coefficients were calculated from the experimental data, taking the diffusion properties of the confining filters into account. Both the accessible porosity and effective diffusion coefficients are smaller than those of (uncharged) tritiated water (HTO). In presence of Fe(II), the diffusion behaviour is different. Fe(II) was added as sorbed Fe(II) and as pyrite. The Fe-loaded illite was sandwiched between two layers of natural illite. Independent of the speciation of Fe(II), the concentration of ^{99}Tc in the source reservoir of the diffusion setup quickly decreased. A break-through of ^{99}Tc could be observed, but the observed flux was much lower than in the reference case without Fe(II). Moreover, analysis of the diffusion profile showed almost no Tc present in the illite, neither in the natural illite, nor in the Fe(II)-loaded illite, and the majority of ^{99}Tc was located in the filter in contact with the source reservoir of the diffusion set-up. Because the diffusion cells were constructed from stainless steel, a possible explanation of the observed Tc distribution is a delocalized reduction of ^{99}Tc: electrons from the oxidation of Fe(II) in the sandwiched illite plug can be transferred by the diffusion cell-walls towards the stainless steel filters where ^{99}Tc is reduced and precipitates. This would indicate that the use of stainless steel cells in this type of work is not optima.

In a third part of the study, the migration/retention behaviour of ^{99}Tc in Opalinus Clay (OPA) was investigated for both under oxic (air) and anoxic (argon) conditions. The investigation was performed in cooperation with the University of Mainz, where the experimental work was conducted. A reactive transport model coupling diffusion and chemical reactions was developed and implemented in PFLOTRAN. Some important parameters were obtained, such as the diffusion coefficient of TcO_4^-, reaction rate constants for pyrite oxidation-dissolution, and the equilibrium constant of Tc reacting with surface complexed Fe. Modelling results showed that the final Tc distribution in OPA is a result of a series of complex processes, in which diffusion of TcO_4^- and dissolved O_2, redox reactions, and pyrite oxidation-dissolution are coupled. Under argon atmosphere,

TcO_4^- diffusive transport in OPA is retarded due to its reduction to surface complexing Tc(IV) by Fe(II) coming from the dissolution of pyrite. The oxidation-dissolution of pyrite and available surface sites determine the amount of ^{99}Tc that is reduced and immobilized. Under air atmosphere, Fe(II) is more prone to react with oxygen than to reduce TcO_4^-. Oxygen competitively consumed the dissolved Fe(II) from pyrite or oxidized the surface complexed Fe(II), leading to almost no Tc is reduced/immobilized in OPA close to the source reservoir, where oxygen is available, compare to experiment under argon atmosphere. At further distances, TcO_4^- is then reduced and complexed in OPA. The implemented model was able to describe the Tc retention/migration behaviour in OPA in a semi quantitative manner.

5.2 Suggestions for future work

This project provides a good basis for the understanding of technetium migration and retention in complex clay rocks. Although a relatively simple reactive transport model, in which diffusion and redox reactions were considered, could fit the transport behaviour of Tc in Opalinus clay, there are still many aspects left out in the model, such as other iron sources or other reducing agents and porosity changes. These open questions need to be addressed in order to become a complete picture of the migration/retention behaviour of ^{99}Tc in clay rocks.

The iron sorption mechanism on illite needs further investigation. The sorbed and/or surface complexed iron can reduce technetium into sparingly mobile species and may significantly influence the transport of technetium in clay rocks. It was found in this study that most of the sorbed Fe(II) will be oxidized at pH below 6.5, but the speciation of oxidized Fe at high pH could not be confirmed. According to the modelling, it could be surface-complexed Fe(III) or a precipitate of iron. Further experiments are necessary to validate the speciation. Spectroscopic studies using Mössbauer or X-ray photoelectron spectroscopy could be used to reveal the speciation of adsorbed Fe. Also X-ray absorption spectroscopy, which is applied to explore the local binding environment of ions, could be used to distinguish between adsorption and precipitation processes. In such studies special care should be taken to avoid the oxidation of the sample during the sample preparation or during measurements. Because the amount of sorbed iron is small, tiny changes in its oxidation state might make a big difference.

A second aspect is related to the diffusion of Tc in Fe-loaded illite. Although pre-loaded Fe(II) is observed to play a key role in Tc diffusion in illite, the observed behaviour was unexpected and it was not possible to differentiate between the two iron species. Moreover, it was shown that steel diffusion cells are not appropriate because they can induce delocalized reduction of ^{99}Tc. For future studies, it is advised to use a steel-free diffusion set-up for studying the migration/retention behaviour of redox sensitive elements. For instance, as observed in Chapter 3, the flux and accumulated mass in low side reservoir is different between cell 3 and cell 4, in which the cell is pre-loaded with same protocol and the diffusions are carried out in the same conditions. It is the same for cell 5 and cell 6. It is worth to note that breakthrough of Tc was observed in 1 cm long Fe-loaded illite after one week, while no breakthrough was observed for Tc diffusion in 1 cm Opalinus Clay even after more than one year. It is unresolved what make the different observation between Tc diffusion in illite and Opalinus Clay. Therefore, Tc diffusion experiments in Fe(II)-loaded illite would validate the observations and may help to unravel the contradictions in the different diffusion experiments. It is also highly recommended to measure the speciation and/or oxidation state of Tc in the solution reservoirs during diffusion and in the clay phase after finishing diffusion experiments. The speciation of Tc in clay could be measured by the X-ray absorption spectroscopy,

which was mentioned to be able to explore the local environment of an element. Since Opalinus Clay is a polymineral rock, experiments with illite loaded with other iron sources or reducing agents might help to understand the difference between illite and Opalinus Clay. Other iron sources or reducing agents might be more redox active or might be more accessible to technetium.

The reactive transport model presented in this study to describe the migration behaviour of ^{99}Tc in OPA is the simplest model, in which pyrite is considered as the only reducing agent and all surface sites are assigned to illite. In natural environment, there are several alternative reducing agents such as siderite, organic matters and others that may participate into redox reactions. These reducing agents should also be taken into account in the model. Also, the precise surface site capacity needs further characterized, which means the clay minerals component and the site density of each component. Last but not least, the effect of temperature was not considered in this model. The temperature on one hand affects the diffusion coefficient, but the activation energy is unknown for Tc species. On the other hand, temperature affect the equilibrium constant for redox reaction with surface sites. More information is available to confirm whether these reactions are exothermic or endothermic. The temperature effect would be a good aspect to improve the reactive transport model. These and other processes could make the model move closer to the real physical process taking place in clay.

CURRICULUM VITAE

Ping Chen

Born on 20.05.1991

Citizen of Ganzhou, Jiangxi, China

2018.11-	Doctoral studies at University of Bern Accomplished at PSI
2014.09- 2017.06	Master of nuclear science and technology Sun Yat-sen University
2010.09- 2014.06	Bachelor of radiation protection and environmental engineering East China University of Technology
2017.06-2018.11	Intern at Sun Yat-sen University

Declaration of consent

on the basis of Article 18 of the PromR Phil.-nat. 19

Name/First Name: Chen ping

Registration Number: 18-125-666

Study program: Earth Science

Bachelor ☐ Master ☐ Dissertation ☑

Title of the thesis: Technetium retention and migration in clay systems in presence of iron

Supervisor: Sergey Churakov

I declare herewith that this thesis is my own work and that I have not used any sources other than those stated. I have indicated the adoption of quotations as well as thoughts taken from other authors as such in the thesis. I am aware that the Senate pursuant to Article 36 paragraph 1 litera r of the University Act of September 5th, 1996 and Article 69 of the University Statute of June 7th, 2011 is authorized to revoke the doctoral degree awarded on the basis of this thesis.

For the purposes of evaluation and verification of compliance with the declaration of originality and the regulations governing plagiarism, I hereby grant the University of Bern the right to process my personal data and to perform the acts of use this requires, in particular, to reproduce the written thesis and to store it permanently in a database, and to use said database, or to make said database available, to enable comparison with theses submitted by others.

Place/Date: Baltzerstrasse 3, 3012 Bern/02.Oct.2023

Signature: